









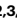





Identification of a non-canonical chemokine-receptor pathway suppressing regulatory T cells to drive atherosclerosis

Received: 29 March 2022

Accepted: 14 December 2023

 Check for updates

Yvonne Döring ^{1,2,3,15} ✉, Emiel P. C. van der Vorst ^{2,3,4,5,6,15}, Yi Yan ^{2,3,7,15}, Carlos Neideck^{2,15}, Xavier Blanchet ², Yvonne Jansen², Manuela Kemmerich², Soyolmaa Bayasgalan², Linsey J. F. Peters^{2,4,5,6}, Michael Hristov², Kiril Bidzhakov², Changjun Yin ^{2,3,8}, Xi Zhang², Julian Leberzammer ^{2,3}, Ya Li², Inhye Park⁹, Maria Kral^{2,3}, Katrin Nitz², Laura Parma ^{2,3}, Selin Gencer², Andreas J. R. Habenicht ^{2,3}, Alexander Faussner ², Daniel Teupser¹⁰, Claudia Monaco ⁸, Lesca Holdt¹⁰, Remco T. A. Megens ^{2,3,11}, Dorothee Atzler^{2,3,12}, Donato Santovito ^{2,3,13}, Philipp von Hundelshausen ² & Christian Weber ^{2,3,8,14} ✉

CCL17 is produced by conventional dendritic cells, signals through CCR4 on regulatory T (T_{reg}) cells and drives atherosclerosis by suppressing T_{reg} functions through yet undefined mechanisms. Here we show that conventional dendritic cells from CCL17-deficient mice display a pro-tolerogenic phenotype and transcriptome that is not phenocopied in mice lacking its cognate receptor CCR4. In the plasma of CCL17-deficient mice, CCL3 was the only decreased cytokine/chemokine. We found that CCL17 signaled through CCR8 as an alternate high-affinity receptor, which induced CCL3 expression and suppressed T_{reg} functions in the absence of CCR4. Genetic ablation of CCL3 and CCR8 in $CD4^+$ T cells reduced CCL3 secretion, boosted $FoxP3^+$ T_{reg} numbers and limited atherosclerosis. Conversely, CCL3 administration exacerbated atherosclerosis and restrained T_{reg} differentiation. In symptomatic versus asymptomatic human carotid atheroma, CCL3 expression was increased, whereas $FoxP3$ expression was reduced. Together, we identified a non-canonical chemokine pathway whereby CCL17 interacts with CCR8 to yield a CCL3-dependent suppression of atheroprotective T_{reg} cells.

Atherosclerosis is a lipid-driven chronic inflammatory disease of the arterial wall, underlying most cardiovascular diseases (CVDs)¹. Dendritic cells (DCs) have been identified in healthy and inflamed arterial intima of mice and humans^{2–4} and advanced human plaques contain an increased number of DCs in clusters with T cells⁵. The chemokine CCL17 (TARC/thymus and activation-regulated chemokine) was found to be elevated in patients with CVD⁶ and atopic dermatitis, who are

prone to develop CVD^{7,8}. An intronic single-nucleotide polymorphism (*rs223828*) is associated with higher serum CCL17 and elevated CVD risk in humans⁹ and mouse studies revealed a proinflammatory role of CCL17 in atherosclerosis¹⁰ and colitis¹¹. CCL17 is primarily expressed by a subset of antigen-presenting MHCII⁺ conventional DCs (cDCs), which migrates to draining lymph nodes (LNs) to prime naive T cells and plays a crucial role in the migration of various T cell subsets, including $CD4^+$

T cells and T_{reg} cells^{12–14}. T_{reg} cells use multiple effector mechanisms to modulate immune responses and to guard the balance between immune activation and tolerance toward self-antigens¹⁵. Naturally arising CD4⁺CD25⁺ T_{reg} cells limit atherosclerosis development and have been implicated in the regression of established atherosclerotic lesions by licensing pro-resolving macrophage functions^{16,17}. We found that CCL17 controls T_{reg} homeostasis, restraining their expansion and thereby promoting atherosclerosis¹⁰. Accordingly, genetic deficiency or antibody blockade of CCL17 reduced atheroprotection by facilitating T_{reg} expansion and survival in lymphoid organs, leading to T_{reg} expansion¹⁰; however, the precise mechanisms, by which DC-derived CCL17 controls T_{reg} homeostasis, remain to be elucidated, namely the relevant soluble mediators or the receptors involved.

To date, CCR4 is the only cognate signaling receptor for CCL17 identified and known to contribute to the recruitment and in vivo functions of T_{reg} cells¹⁸. Yet, CCR4 deficiency did not phenocopy the effects on T_{reg} cells and protection from atherosclerosis seen in CCL17-deficient mice¹⁰. Analogous findings were obtained in a model of atopic dermatitis, where the inflammatory burden was reduced in mice lacking CCL17 but not CCR4 (ref. 19). Consistently, deficiency in DC-derived CCL17 was protective against intestinal inflammation in a mouse model of colitis by creating a cytokine milieu that facilitated T_{reg} expansion and, likewise, did not require CCR4 (ref. 11). In conjunction, these results suggest the existence of an alternative CCR4-independent receptor pathway triggered by CCL17. Here, we provide unequivocal evidence that CCL17 signals via CCR8 as an alternative high-affinity receptor expressed on T cell and DC subsets, harnessing the autocrine and paracrine release of CCL3 to mediate suppression of atheroprotective T_{reg} cells via its receptor CCR1.

Results

CCR4 does not mediate the effects of CCL17 on atherosclerosis

Mice with a targeted replacement of the *Ccl17* gene by the enhanced green fluorescent protein gene (*eGFP*; *Apoe*^{-/-}*Ccl17*^{+/e} mice) displayed a reduced atherosclerotic lesion size in the aortic root, thoraco-abdominal aorta and aortic arch but unchanged lesional macrophage, smooth muscle cell (SMC) and collagen content after 12 weeks of western-type diet (WD), when compared to *Apoe*^{-/-} littermate controls (Extended Data Fig. 1a–g). This was related to a higher frequency of CD25⁺Foxp3⁺CD3⁺CD4⁺ T_{reg} cells in para-aortic LNs, spleen, axillary and inguinal LNs of *Apoe*^{-/-}*Ccl17*^{+/e} mice, compared to controls (Extended Data Fig. 1h–l). In contrast, mice lacking the canonical CCL17 receptor CCR4 did not phenocopy the effects observed in CCL17-deficient mice. Neither hematopoietic *Ccr4* deficiency¹⁰ nor systemic deletion in *Apoe*^{-/-}*Ccr4*^{-/-} mice altered atherosclerotic lesion size, composition or T_{reg} frequencies after 12 weeks of WD, compared to controls, and the decrease in apoptotic T_{reg} cells in LNs of CCL17-deficient mice¹⁰ was

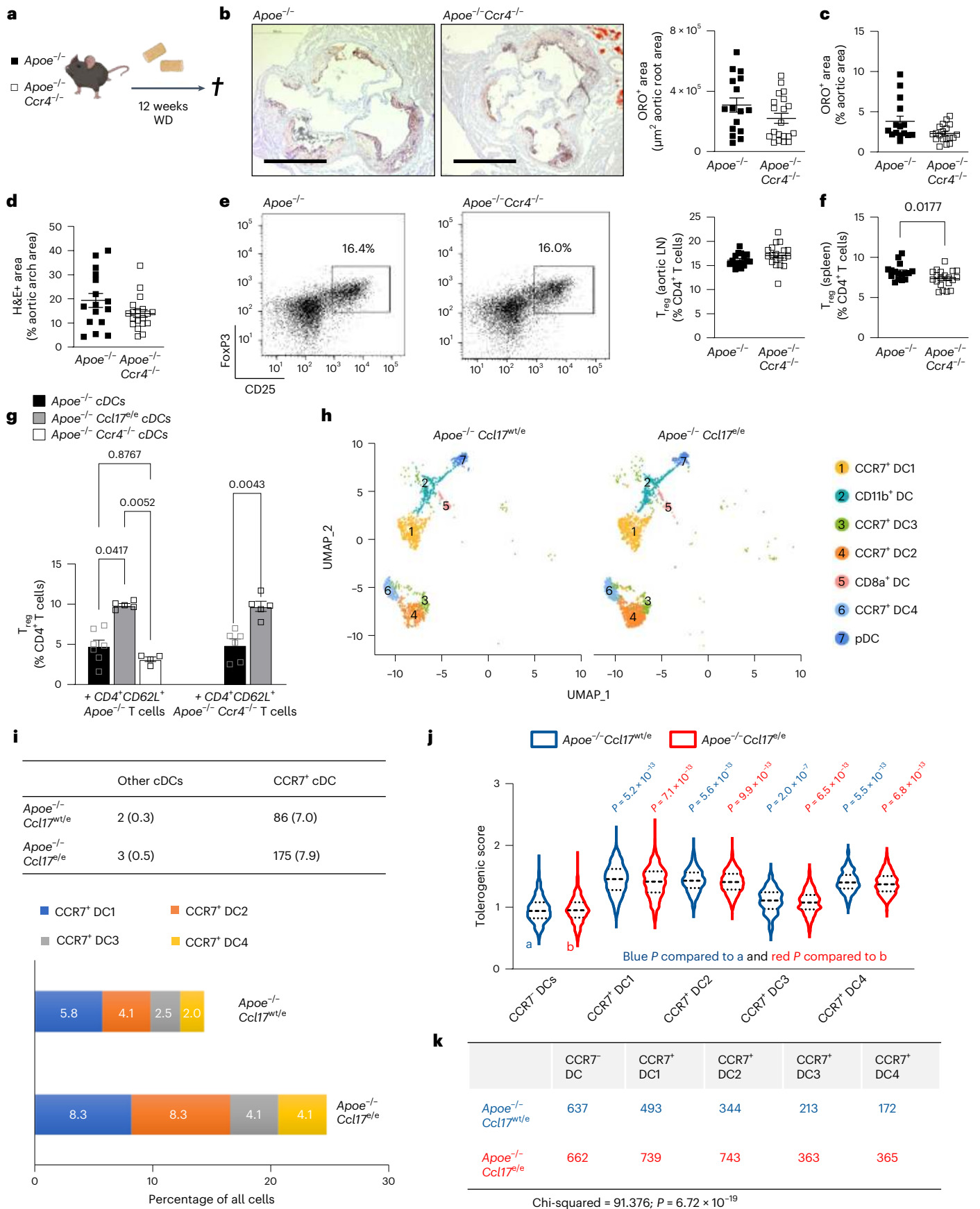
not found in LNs of CCR4-deficient mice (Fig. 1a–f and Extended Data Fig. 2a–g). Lipid levels, circulating leukocyte and thrombocyte counts did not differ between *Apoe*^{-/-}*Ccl17*^{+/e}, *Apoe*^{-/-}*Ccr4*^{-/-} and respective control mice (Supplementary Tables 1 and 2) and thus did not explain the observed phenotype. Using recombinant CCL17, CCL22 and the CCR4 inhibitor CO21 in Transwell assays, we confirmed CCR4-dependent chemotaxis of CD4⁺ T cells isolated from *Apoe*^{-/-} mice and from human peripheral blood mononuclear cells (PBMCs) in vitro, as CO21 abrogated CCL22-induced migration and inhibited CCL17-induced migration (Extended Data Fig. 2h,i). Together, these data indicate that an alternative signaling pathway is involved in mediating the effects of CCL17, a notion reinforced by investigating T_{reg} homeostasis. Co-culturing CD4⁺CD62L⁺ T cells from *Apoe*^{-/-} and *Apoe*^{-/-}*Ccr4*^{-/-} mice with ex vivo isolated cDCs revealed an increased differentiation of CD4⁺CD25⁺Foxp3⁺ T_{reg} cells in the presence of *Apoe*^{-/-}*Ccl17*^{+/e} cDCs but not *Apoe*^{-/-}*Ccr4*^{-/-} or *Apoe*^{-/-} cDCs (Fig. 1g). To explore whether CCL17-deficient cDCs differentially express putative mediators of this effect, we sorted CD45⁺CD11c⁺CD3⁻CD19⁻ cells from LNs of *Apoe*^{-/-}*Ccl17*^{+/e} or *Apoe*^{-/-}*Ccl17*^{+/e} mice and performed single-cell RNA sequencing (scRNA-seq) (GSE200862). Our analysis identified seven different DC clusters, with CCL17-expressing eGFP⁺ cells almost exclusively located among CCR7⁺ cDCs (Fig. 1h and Extended Data Fig. 3a–g). In CCL17-deficient samples, CCR7⁺ cDCs were enriched and had a higher tolerogenic score compared to other DC clusters (Fig. 1i). A tolerogenic profile was defined by high expression of *Aldh1a2*, *Cd83* and *Cd274* in CCR7⁺ cDCs (Fig. 1j and Extended Data Fig. 3d–g) and analysis of a gene set defining immunogenic and tolerogenic cell properties (Supplementary Table 3). While the tolerogenic score was similar in hetero- and homozygous samples, the number of CCR7⁺ tolerogenic cDCs was higher in CCL17-deficient mice (Fig. 1j,k), showing that more cDCs acquire a tolerogenic phenotype in the absence of CCL17. Accordingly, flow cytometry of cDCs in aortic LNs of *Apoe*^{-/-} and *Apoe*^{-/-}*Ccl17*^{+/e} mice uncovered a higher percentage of CD83⁺, CCR7⁺ and CD83⁺CCR7⁺ cDCs (Extended Data Fig. 3h–j). Deletion of CD83 in cDCs confers a proinflammatory DC phenotype driving antigen-dependent T cell proliferation, type 17 helper T (T_H17) cell commitment but impairing T_{reg} suppressive capacity and resolving mechanisms²⁰. Gene set variation analysis (GSVA) further revealed an enrichment of proinflammatory pathways in CCL17-competent cDCs (Extended Data Fig. 3k–m), in line with an atheroprotective role of CCR7 found in *Apoe*^{-/-} mice²¹.

CCL17 induces CCL3 release independent of CCR4 expression

Because CCL17-deficient mice displayed increased numbers of tolerogenic cDCs, we performed an unbiased screen for differentially regulated inflammatory mediators. A multiplex bead array for cytokines and chemokines identified only CCL3 to be substantially reduced in plasma of *Apoe*^{-/-}*Ccl17*^{+/e} mice versus *Apoe*^{-/-} controls after 12 weeks

Fig. 1 | CCR4 does not affect atherosclerosis or T_{reg} cells, while CCL17-deficiency increases tolerogenic DCs. **a**, Experimental scheme of WD feeding. **b**, Representative sections and quantification of lesion area after Oil-Red-O staining (ORO) for lipid deposits in the aortic root of *Apoe*^{-/-} (*n* = 16) or *Apoe*^{-/-}*Ccr4*^{-/-} (*n* = 20) mice. Scale bar, 500 μm. **c**, Quantification of lesion area after ORO in the thoraco-abdominal aorta of *Apoe*^{-/-} (*n* = 5) or *Apoe*^{-/-}*Ccr4*^{-/-} (*n* = 19) mice. **d**, Atherosclerotic lesion size quantified by hematoxylin and eosin (H&E) staining in the aortic arches of *Apoe*^{-/-} (*n* = 16) or *Apoe*^{-/-}*Ccr4*^{-/-} (*n* = 19) mice. **e, f**, Representative dot plots and flow cytometric quantification of CD45⁺CD3⁺CD4⁺CD25⁺Foxp3⁺ T_{reg} cells in para-aortic LNs (**e**) and spleen (**f**) of *Apoe*^{-/-} (**e**, *n* = 16; **f**, *n* = 16) or *Apoe*^{-/-}*Ccr4*^{-/-} (**e**, *n* = 19; **f**, *n* = 20) mice. **g**, Co-culture of CD45⁺CD11c⁺MHCII⁺ DCs sorted from *Apoe*^{-/-}, *Apoe*^{-/-}*Ccl17*^{+/e} or *Apoe*^{-/-}*Ccr4*^{-/-} mice with splenic CD4⁺CD62L⁺ T cells isolated from *Apoe*^{-/-} or *Apoe*^{-/-}*Ccr4*^{-/-} mice. After 72 h, the abundance of CD45⁺CD3⁺CD4⁺CD25⁺Foxp3⁺ T_{reg} cells was determined by flow cytometry (individual number of experiments per bar from left to right *n* = 7, 5, 4, 6 and 5). Besides the cells, no other factors were added to the culture. **h–j**, CD45⁺CD3⁻CD19⁻CD11c⁺ cells were sorted from pooled

LNs of *Apoe*^{-/-}*Ccl17*^{+/e} or *Apoe*^{-/-}*Ccl17*^{+/e} mice on chow diet. Uniform Manifold Approximation and Projection (UMAP) projection of 4,731 single cells colored by inferred cell types consisting of seven distinct DC clusters (**h**). Depicted are eGFP⁺ cell counts in CCR7⁺ DCs or other (CCR7⁻) DCs (percentage of total numbers) and proportions of four distinct CCR7⁺ DC clusters among all single cells (CD45⁺CD3⁻CD19⁻CD11c⁺) (bottom) (**i**). **j, k**, Tolerogenic score calculated for four distinct CCR7⁺ DC clusters and other (CCR7⁻) DC clusters based on the top 20 genes differentially expressed between the groups (top) as (1 + mean (top 20 upregulated tolerogenic genes))/(1 + mean (top 20 upregulated immunogenic genes)) (**j**). **k**, Table depicts cell counts of four CCR7⁺ DC and other DC clusters. LNs for scRNA-seq were obtained from *Apoe*^{-/-}*Ccl17*^{+/e} (*n* = 8) and *Apoe*^{-/-}*Ccl17*^{+/e} (*n* = 6). Data represent mean ± s.e.m. (**a–k**). Two-sided *P* values as indicated and as analyzed by unpaired Student's *t*-test (**b, e, f**), Mann–Whitney *U*-test (**c, d**) or Kruskal–Wallis *H* with Dunn's post hoc test (**g, j**). Differences in proportion in DC clusters between *Apoe*^{-/-}*Ccl17*^{+/e} and *Apoe*^{-/-}*Ccl17*^{+/e} were computed by Pearson's chi-squared test (**k**).



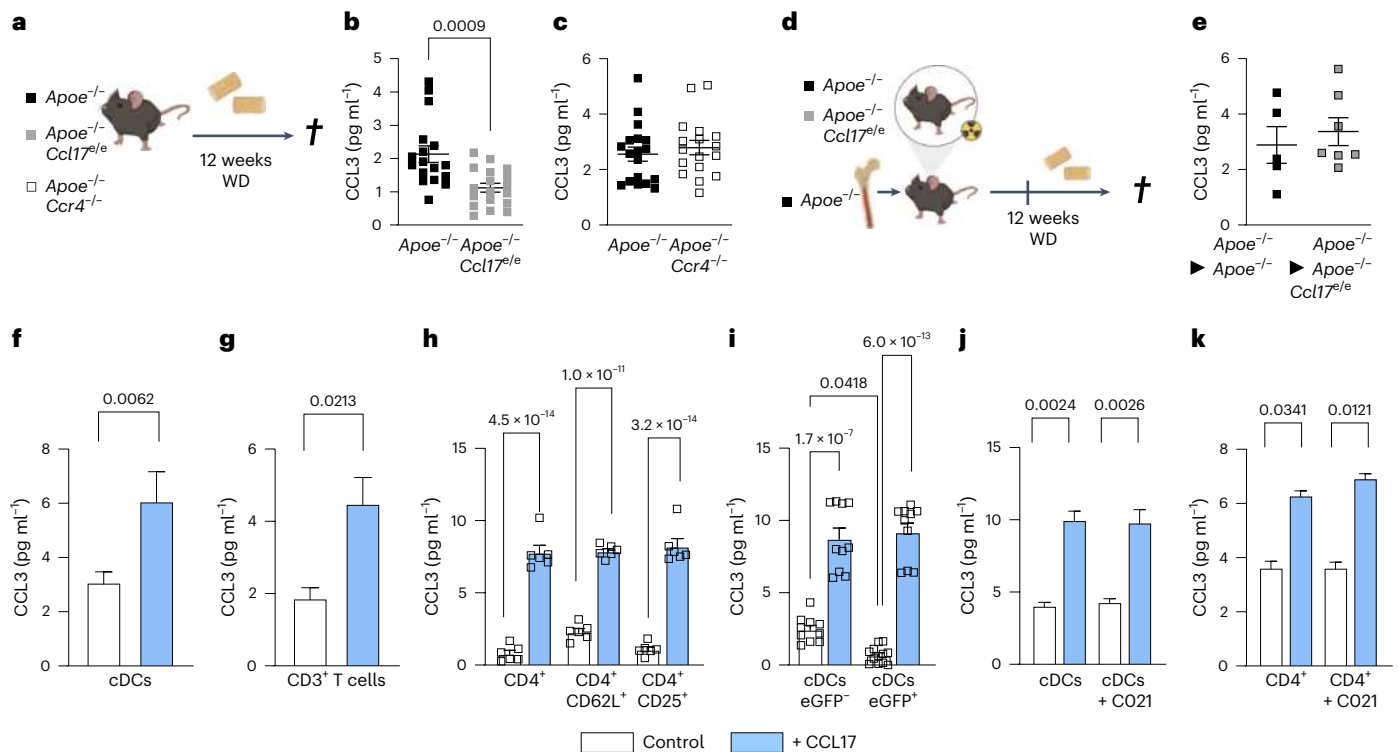


Fig. 2 | CCL3 induction by CCL17 does not require CCR4 but inversely correlates with T_{reg} numbers. **a**, Experimental scheme of $Apoe^{-/-}$, $Apoe^{-/-} Ccl17^{e/e}$ and $Apoe^{-/-} Ccr4^{-/-}$ mice fed a WD. **b, c**, CCL3 plasma concentrations in $Apoe^{-/-}$ ($n = 17$) and $Apoe^{-/-} Ccl17^{e/e}$ ($n = 18$) mice (**b**) or $Apoe^{-/-}$ ($n = 18$) and $Apoe^{-/-} Ccr4^{-/-}$ ($n = 17$) mice (**c**), as measured by ELISA. **d**, Experimental scheme of reconstituting irradiated $Apoe^{-/-}$ or $Apoe^{-/-} Ccl17^{e/e}$ mice with $Apoe^{-/-}$ BM before WD feeding. **e**, CCL3 concentrations in plasma of $Apoe^{-/-} \rightarrow Apoe^{-/-}$ ($n = 5$) or $Apoe^{-/-} \rightarrow Apoe^{-/-} Ccl17^{e/e}$ ($n = 7$) mice were measured by ELISA. **f, g**, Sorted CD11c⁺MHCII⁺ cDCs (control, $n = 17$ replicates over 11 independent experiments; CCL17, $n = 23$ replicates over 12 independent experiments) (**f**) or CD3⁺ T cells (control and CCL17, $n = 17$ replicates over six independent experiments) were cultured for 4 h with or without recombinant mouse CCL17 (**g**). CCL3 concentrations in the supernatant were measured by multiplex bead array. **h**, Isolated T cell subsets from LN suspensions of $Apoe^{-/-}$ mice were stimulated for 4 h in the presence or absence of CCL17. CCL3 concentrations in supernatants were measured by ELISA ($n = 6$ for each bar). **i**, Sorted CD11c⁺MHCII⁺eGFP⁺ cDCs (CCL17-competent, control and CCL17, $n = 10$) or CD11c⁺MHCII⁺eGFP⁺ cDCs

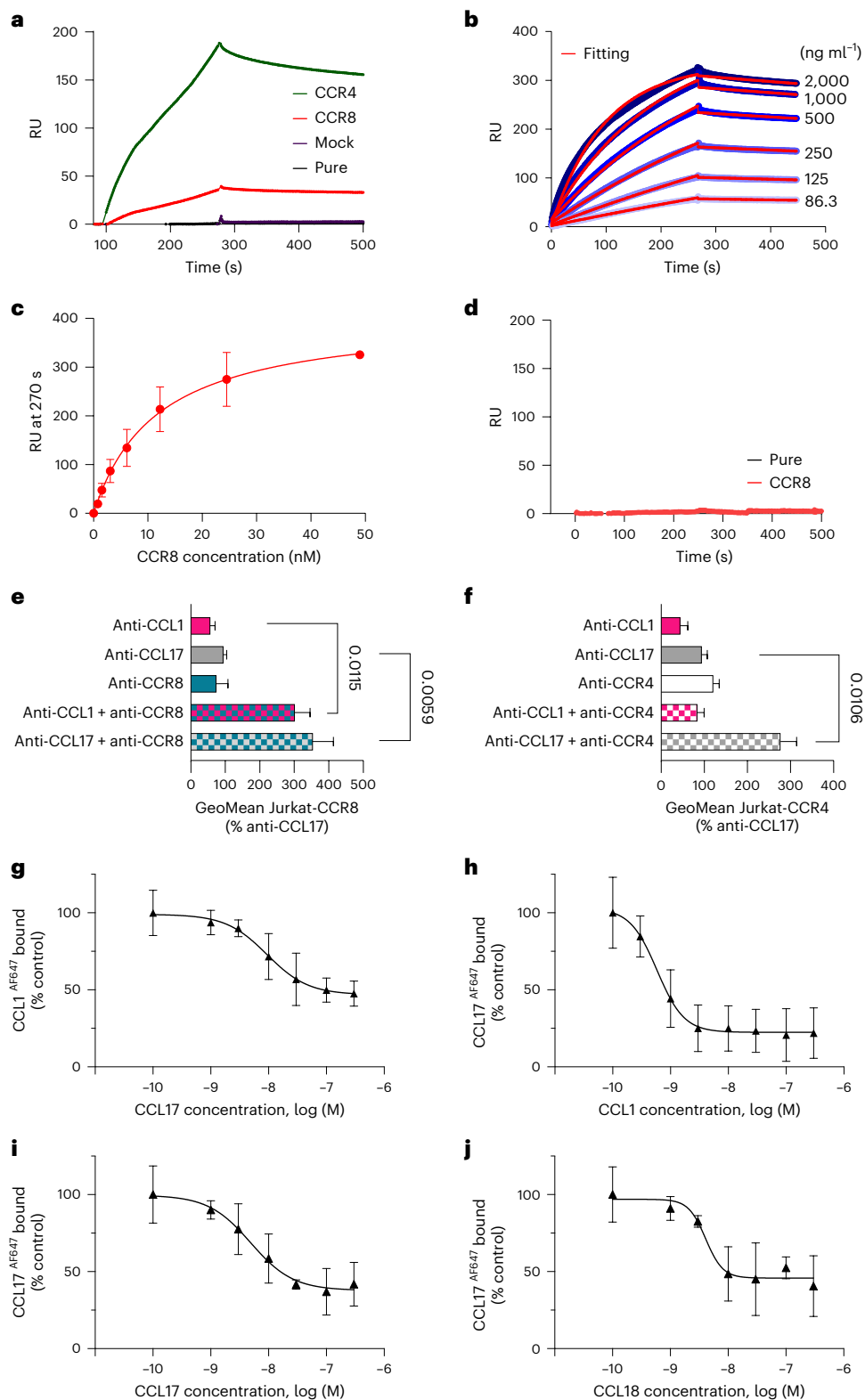
(CCL17-deficient, control $n = 12$; CCL17 $n = 10$) from $Apoe^{-/-} Ccl17^{e/e}$ mice were cultured for 4 h in the presence or absence of CCL17. CCL3 concentrations in supernatants were measured by ELISA. **j**, Sorted CD11c⁺MHCII⁺ cDCs from LNs of $Apoe^{-/-}$ mice were cultured for 4 h in the presence or absence of CCL17 with or without the CCR4 inhibitor CO21, and CCL3 concentrations in supernatants of isolated cDCs were measured by multiplex bead array ($n = 20$ replicates across six independent experiments for all conditions). **k**, Isolated T cell subsets from LN suspensions of $Apoe^{-/-}$ mice were stimulated with or without CCL17 in the presence or absence of the CCR4 inhibitor CO21 for 4 h and CCL3 concentrations in supernatants were measured by ELISA (control, $n = 39$ replicates; CO21, $n = 38$ replicates; CCL17, 42 replicates; CCL17 + CO21, $n = 40$ replicates; all distributed over nine independent experiments). Data represent mean \pm s.e.m. (**a–k**). Two-sided P values as indicated versus control/ $Apoe^{-/-}$ and as analyzed by unpaired Student's t -test (**b, c, e**), nested t -test (**f, g**), two-way analysis of variance (ANOVA) (**h**) or nested ANOVA (**j, k**) with Holm–Šidák's post hoc test and Kruskal–Wallis H with Dunn's post hoc test (**i**).

of WD (Fig. 2a,b and Extended Data Table 1), corresponding with decreased lesion size and increased T_{reg} numbers (Extended Data Fig. 1). In contrast, CCL3 plasma levels in $Apoe^{-/-} Ccr4^{-/-}$ mice were unaffected (Fig. 2a,c), consistent with unaltered atherosclerotic burden (Fig. 1a–f). Reconstituting $Apoe^{-/-} Ccl17^{e/e}$ mice with CCL17-sufficient bone marrow (BM) restored CCL3 plasma levels to those seen in $Apoe^{-/-}$ controls (Fig. 2d,e). Given that CCL3 was diminished in systemic circulation of CCL17-deficient mice, we assessed which cell types release CCL3 in response to CCL17 by sorting CD11c⁺MHCII⁺ cDCs, CD3⁺ T cells and CD19⁺B220⁺ B cells from LNs, monocytes and neutrophils from spleen and BM for in vitro treatment with CCL17. ELISA or multiplex bead array identified cDCs and T cells as the main source of CCL3 upon CCL17 stimulation, whereas CCL3 release from monocytes, B cells and neutrophils was less marked or negligible (Fig. 2f,g and Extended Data Fig. 3n). CCL3 release was induced by CCL17 in distinct T cell subsets, namely splenic CD4⁺ T helper cells, CD4⁺CD62L⁺ naive/memory T cells and CD4⁺CD25⁺ T_{reg} cells (Fig. 2h). Comparing sorted CCL17⁺ (eGFP⁺) with CCL17-deficient CD11c⁺MHCII⁺ cDCs (eGFP⁺), we found that baseline CCL3 secretion was lower in CCL17-deficient cDCs, whereas CCL17-stimulated CCL3 release was similar (Fig. 2i), implying that CCL17⁺ cDCs

can release CCL17 in an autocrine or paracrine fashion to induce CCL3 secretion. This effect was independent of CCR4 in cDCs and CD4⁺ T cells (Fig. 2j,k), indicating that CCL17 mediates CCL3 secretion through an alternative receptor.

CCL17 binds and activates CCR8 as a non-canonical receptor

Searching for alternative receptors, we revisited the notion that CCR8 could be a receptor for CCL17 (ref. 22) (findings subsequently contested²³), as CCR8 has also been implicated in controlling the migration and function of T_{reg} cells^{24,25}. To probe for binding of CCL17 to CCR8, we used surface plasmon resonance (SPR) to record the concentration-dependent binding of CCR8-carrying liposomes to biotinylated CCL17 immobilized on a BIAcore C1 sensor chip, using CCR4-carrying, mock protein-carrying or pure liposomes as positive or negative controls (Fig. 3a–d). CCR8-bearing liposomes displayed saturable binding with a K_d (k_{off}/k_{on}) of 1.1 ± 0.4 nM, indicating a high-affinity interaction between CCL17 and CCR8 (Fig. 3b,c). While CCR4-bearing liposomes showed even stronger binding, irrelevant protein-bearing or empty liposomes did not support binding to CCL17 (Fig. 3a). A CCL5-chip used as a negative control did not support binding of CCR8-bearing



liposomes (Fig. 3d). We next used a proximity-ligation assay in CCR4- or CCR8-transfected Jurkat cells or in adherent cDCs from LNs of *ApoE*^{-/-} mice treated with CCL17 or the cognate CCR8 ligand CCL1 and subsequently with non-blocking antibodies to CCL17 or CCL1 and to CCR4, CCR8 or CCR5 to yield signals reporting receptor interactions of CCL17 or CCL1. Proximity-ligation signals and their quantification revealed an interaction of CCL17 with both CCR4 and CCR8, whereas CCL1 interacted with CCR8 but not with CCR4 (Fig. 3e,f and Extended Data Fig. 4a,b). We further performed receptor binding competition

studies using fluorescently labeled CCL1 and CCL17 in CCR8-expressing HEK293 transfectants (Extended Data Fig. 4c). Inhibition of CCL1^{AF647} binding to CCR8-transfectants with increasing concentrations of unlabeled CCL17 yielded a half-maximum inhibitory concentration (IC_{50}) of 9.4 ± 4.4 nM. Inhibition of CCL17^{AF647} binding to CCR8-transfectants with increasing concentrations of unlabeled CCL1 yielded an IC_{50} of 0.58 ± 0.24 nM, and with unlabeled CCL18 yielded an IC_{50} of 4.1 ± 1.7 nM, similar to unlabeled CCL17 (IC_{50} 4.9 ± 2.4 nM) (Fig. 3g-j). Using primary CD4⁺ T cells from thymus or LNs of tamoxifen-inducible

Fig. 3 | CCL17 binds to CCR8 with high affinity in human and mouse cells. **a–d**, SPR to detect CCL17–CCR8 interactions. RU, response unit. Human biotinylated CCL17 was immobilized on CI sensor chips and sensorgrams of human CCR8-, CCR4-, mock protein-carrying or pure liposomes perfused at $0.5 \mu\text{g ml}^{-1}$ were recorded (**a**). Binding kinetics of CCR8-carrying liposomes perfused at indicated concentrations on immobilized CCL17 were determined after fitting (red) of curves (blue) with a 1:1 interaction model (**b**). Concentration-independent dissociation was low ($k_{\text{off}} 4.2 \pm 0.8 \times 10^{-4} \text{ s}^{-1}$), indicating high stability. Calculating the $k_{\text{off}}/k_{\text{on}}$ ratio using the theoretical molecular weight of CCR8 (40.2 kD) yielded an apparent K_d of $1.1 \pm 0.4 \text{ nM}$. Shown is one representative of five experiments. Saturation binding of experiments from **b** was fitted with one-site-specific binding, yielding a K_d of $11.7 \pm 2.1 \text{ nM}$ (**c**). Data represent mean \pm s.d. ($n = 5$ independent experiments). Sensorgrams of CCR8-carrying (red) or pure liposomes (black) perfused at $0.5 \mu\text{g ml}^{-1}$ on biotinylated human CCL5 immobilized as a negative control (**d**). **e, f**, Interactions of mouse CCL17 or CCL1 with CCR4 and CCR8 were analyzed in stably transfected Jurkat cells using Duolink proximity-ligation assays. Signals generated by close proximity of non-blocking antibodies bound to ligands or receptors on

CCR8- (**e**, all $n = 9$ replicates over four independent experiments) or CCR4-transfectants (**f**, anti-CCL1, anti-CCL17 + anti-CCR4, $n = 19$ replicates each over six independent experiments; anti-CCL17, $n = 22$ replicates; anti-CCR4, $n = 18$ replicates; anti-CCL1 + anti-CCR4, $n = 22$ replicates over seven independent experiments) were quantified by flow cytometry. For anti-CCL17 and anti-CCL1 incubation, recombinant CCL17 (100 ng ml^{-1}) or CCL1 (50 ng ml^{-1}) was added, respectively. **g–j**, HEK293 cells stably transfected with human CCR8 were incubated with CCL1 or CCL17 labeled with Alexa-Fluor 647 (AF467) at the C terminus (10 nM). Background binding to mock-transfected HEK293 cells was subtracted; data were normalized to binding without unlabeled chemokine (control) and subjected to nonlinear fitting. Data represent mean \pm s.d. ($n = 3$ independent experiments). Inhibition of CCL1^{AF647} binding to CCR8-transfectants with increasing concentrations of unlabeled CCL17; IC_{50} $9.4 \pm 4.4 \text{ nM}$ (**g**). Inhibition of CCL17^{AF647} binding to CCR8-transfectants with increasing concentrations of unlabeled CCL1 (**h**, IC_{50} $0.58 \pm 0.24 \text{ nM}$), CCL17 (**i**, IC_{50} $4.9 \pm 2.4 \text{ nM}$) or CCL18 (**j**, IC_{50} $4.1 \pm 1.7 \text{ nM}$). Data represent mean \pm s.e.m. (**e, f**). Two-sided P values versus respective controls were analyzed by nested ANOVA.

CCR8-competent $\text{Uni}^{\text{CreErt2}} \text{Ccr8}^{\text{fllox/fllox}}$ ($\text{Ccr8}^{\text{WT}} \text{Apoe}^{-/-}$) or CCR8-deficient $\text{Uni}^{\text{CreErt2}} \text{Ccr8}^{\text{fllox/fllox}}$ ($\text{Ccr8}^{\text{KO}} \text{Apoe}^{-/-}$) $\text{Apoe}^{-/-}$ mice, we found CCR8 internalization upon CCL17 treatment in CCR8-expressing but not CCR8-deficient T cells (Fig. 4a,b). The expression of CCR4 was unaltered in CCR8-deficient T cells and CCR4 internalization by CCL17 was preserved, while CCR8 internalization by CCL1 and CCL17 was dose-dependent in these cells (Extended Data Fig. 4d–f). In addition, human CD4^+ T cells exhibited both CCR4 and CCR8 internalization upon CCL17 treatment, whereas CCL1 only internalized CCR8 and CCL22 only internalized CCR4 (Fig. 4c,d). These experiments indicate that CCL17 binds to CCR8.

To test whether CCL17 can elicit G_i -protein-coupled signaling via CCR8, we determined downstream cAMP levels in Glosensor-HEK293 cells transfected with CCR4 or CCR8 (Extended Data Fig. 4c,g) and stimulated with recombinant human CCL17, CCL1 or CCL20 (Fig. 4e,f). Dose–response curves revealed a near maximal CCR8 activation by CCL1 at a concentration of $\approx 1.2 \text{ nM}$, corresponding to the IC_{50} for receptor binding competition, whereas CCL17 and CCL18 were less effective (Extended Data Fig. 4h). Previous studies reported CCL17 binding to CCR8 but lack of subsequent calcium signaling²². In contrast, our results revealed that CCL17 induced G_i -mediated signaling both in CCR4- and CCR8-transfectants. CCL1 induced G_i -signaling in CCR8- but not CCR4-transfectants, whereas CCL20, as a negative control, had no effect (Fig. 4e,f). We next performed Transwell migration assays with CD4^+ T cells from $\text{Ccr8}^{\text{WT}} \text{Apoe}^{-/-}$ or $\text{Ccr8}^{\text{KO}} \text{Apoe}^{-/-}$ mice. CCL17-induced migration of CD4^+ T cells lacking CCR8 was lower than that of wild-type cells, and more markedly reduced than by a CCR8 antibody in human T cells, whereas migration toward CCL1 was abolished and that toward CCL22 was unaffected (Fig. 4g and Extended Data Fig. 4i). The migration

of $\text{Apoe}^{-/-} \text{CD4}^+$ T cells induced by CCL1, CCL17 and CCL22 followed a bell-shaped dose–response curve mediated by CCR8 and CCR4, respectively, as shown by receptor blockade (Extended Data Fig. 4j–l) and was chemotactic, as evident by a checkerboard analysis applying CCR8-competent and -deficient CD4^+ T cells with CCL17 in the upper chamber (Fig. 4h). Together, our data demonstrate that CCL17 activates CCR8 to induce G_i -signaling and functional responses.

CCL17–CCR8–CCL3 axis interferes with T_{reg} differentiation

Having established the interaction of CCL17 with CCR8, we assessed which cell types express CCR8. Screening the Human Protein Atlas (<https://www.proteinatlas.org>; ref. 26) we found CCR8 mostly expressed on T cell subsets with an enrichment in T_{reg} cells (Extended Data Fig. 5a,b). Accordingly, scRNA-seq of aortic LNs from CCL17-competent and CCL17-deficient mice revealed a prominent expression of CCR8 in CD4^+ T cells, mainly in T_{reg} cells and follicular T helper cells, and detectable CCR8 expression in a cDC subset (Extended Data Fig. 5c,d). We next assessed whether the CCL17–CCR8 pathway directly mediates CCL3 secretion by culturing CD4^+ T cells from $\text{Apoe}^{-/-}$ mice with or without CCL17 and an antibody to CCR8 for 4 h. ELISA revealed an increase in CCL3 release induced by CCL17 alone but not when CCR8 was blocked (Extended Data Fig. 5e). Likewise, $\text{CD4}^+ \text{CD62L}^+$ T cells sorted from $\text{Ccr8}^{\text{WT}} \text{Apoe}^{-/-}$ or $\text{Ccr8}^{\text{KO}} \text{Apoe}^{-/-}$ mice were co-cultured with CCR8-competent cDCs with or without CCL17 addition for 3 d to quantify CCL3 release and T_{reg} differentiation (Fig. 5a). CCL3 secretion was induced by CCL17 in CCR8-competent but not CCR8-deficient CD4^+ T cell/DC co-cultures (Fig. 5b). Correspondingly, the number of T_{reg} cells in co-cultures of cDCs with CCR8-deficient CD4^+ T cells was higher than in CCR8-bearing controls, even after addition of CCL17

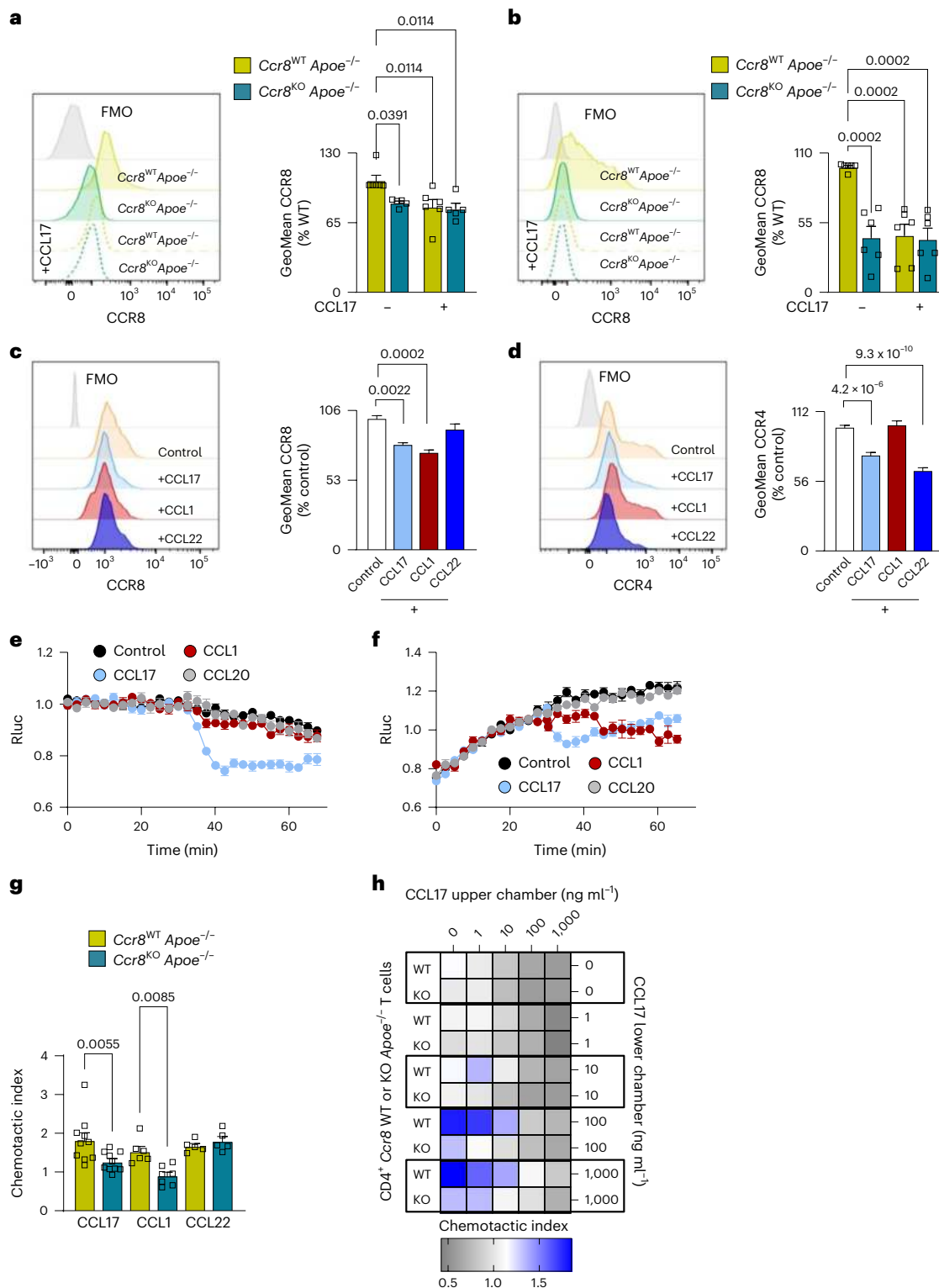
Fig. 4 | CCL17–CCR8 interaction induces G-protein-coupled signaling and T cell chemotaxis. **a, b**, Representative histogram and quantification of CCR8 surface availability and internalization upon stimulation with recombinant mouse CCL17 (100 ng ml^{-1}) on CD4^+ T cells isolated from thymus (**a**) and LNs (**b**) of $\text{Uni}^{\text{CreErt2}} \text{Ccr8}^{\text{fllox/fllox}} \text{Apoe}^{-/-}$ ($\text{Ccr8}^{\text{WT}} \text{Apoe}^{-/-}$, **a, b**, $n = 6$ for all conditions) or CCR8-deficient $\text{Uni}^{\text{CreErt2}} \text{Ccr8}^{\text{fllox/fllox}} \text{Apoe}^{-/-}$ ($\text{Ccr8}^{\text{KO}} \text{Apoe}^{-/-}$, **a, b**, $n = 5$ for both, **b**, $n = 6$ for both) mice. FMO, fluorescence minus one. **c, d**, Representative histogram and quantification of CCR8 (**c**) and CCR4 (**d**) surface expression and internalization upon stimulation with recombinant human CCL17 (100 ng ml^{-1}), CCL1 (50 ng ml^{-1}) or CCL22 (50 ng ml^{-1}) on CD4^+ T cells isolated from human PBMCs (number of replicates in parentheses over number of independent experiments per bar from left to right for **c**, $n = (59) 12, (28) 6, (29) 6$ and $(23) 6$ and **d**, $n = (56) 12, (27) 6, (23) 6$ and $(27) 6$). **e, f**, Glosensor-HEK293 cells transfected with either CCR4 (**e**) or CCR8 (**f**). Cells were stimulated with recombinant human CCL17, CCL1 and CCL20 (all 100 ng ml^{-1}) or PBS as vehicle control after 25 min of equilibration. Shown is one of four representative experiments. **g**, Transwell migration of CD4^+

T cells isolated from $\text{Ccr8}^{\text{WT}} \text{Apoe}^{-/-}$ or $\text{Ccr8}^{\text{KO}} \text{Apoe}^{-/-}$ mice toward recombinant murine chemokines. Migrated cells were quantified by flow cytometry; chemotactic index induced by the chemokines CCL17 (100 ng ml^{-1}), CCL1 (50 ng ml^{-1}) and CCL22 (50 ng ml^{-1}) was calculated as the ratio of chemokine-stimulated to unstimulated migration (number of independent experiments per bar from left to right, $n = 10, 10, 6, 7, 5$ and 5). **h**, Transwell migration of CD4^+ T cells isolated from $\text{Ccr8}^{\text{WT}} \text{Apoe}^{-/-}$ or $\text{Ccr8}^{\text{KO}} \text{Apoe}^{-/-}$ mice toward recombinant murine CCL17 displayed in a checkerboard heat map format. Columns indicate CCL17 concentrations (ng ml^{-1}) in the upper chamber; rows indicate CCL17 concentrations (ng ml^{-1}) in the lower chamber. While blue represents enhanced, gray indicates reduced migration toward CCL17 in the bottom chamber. Each box represents a mean value of three independent experiments. Data represent mean \pm s.e.m. (**a–d, g**). Two-sided P values as indicated versus $\text{Ccr8}^{\text{WT}} \text{Apoe}^{-/-}$ (**a, b, g**) or control (**c, d**) and as analyzed by two-way (**a, b, g**) or univariate (**c, d**) ANOVA with Holm–Šidák's post hoc test.

(Fig. 5c). This indicates that CCL17-induced signaling via CCR8 on CD4⁺ T cells and a subsequent autocrine CCL3 release are important for restraining T_{reg} differentiation, whereas cDC-derived paracrine production of CCL3 seems rather redundant.

Next, CD4⁺CD62L⁺ T cells sorted from *Ccr8*^{WT}*Apoe*^{-/-} or *Ccr8*^{KO}*Apoe*^{-/-} mice were co-cultured with CCL17-competent or CCL17-deficient cDCs for 3 d (Fig. 5d). Combining CCR8-competent naive T cells with CCL17-deficient compared to CCL17-competent cDCs reduced CCL3 levels, whereas co-cultures with CCR8-deficient naive T cells showed lower CCL3 levels with either CCL17-competent or

CCL17-deficient cDCs (Fig. 5e). This was accompanied by inverse changes in T_{reg} numbers, which were elevated in the presence of CCL17-deficient cDCs or using CCR8-deficient CD4⁺ T cells independent of CCL17 (Fig. 5f). To verify the requirement for T cell-derived CCL3, we co-cultured CD4⁺CD62L⁺ T cells from CCL3-competent or CCL3-deficient mice with CCR8-competent cDCs in the absence and presence of CCL17 for 3 d (Fig. 5g). CCL3 release was induced by CCL17 compared to baseline in CCL3-competent T cells and abolished in co-cultures with CCL3-deficient CD4⁺ T cells, where background CCL3 secretion from cDC was less sensitive to CCL17 (Fig. 5h). The number of T_{reg} cells



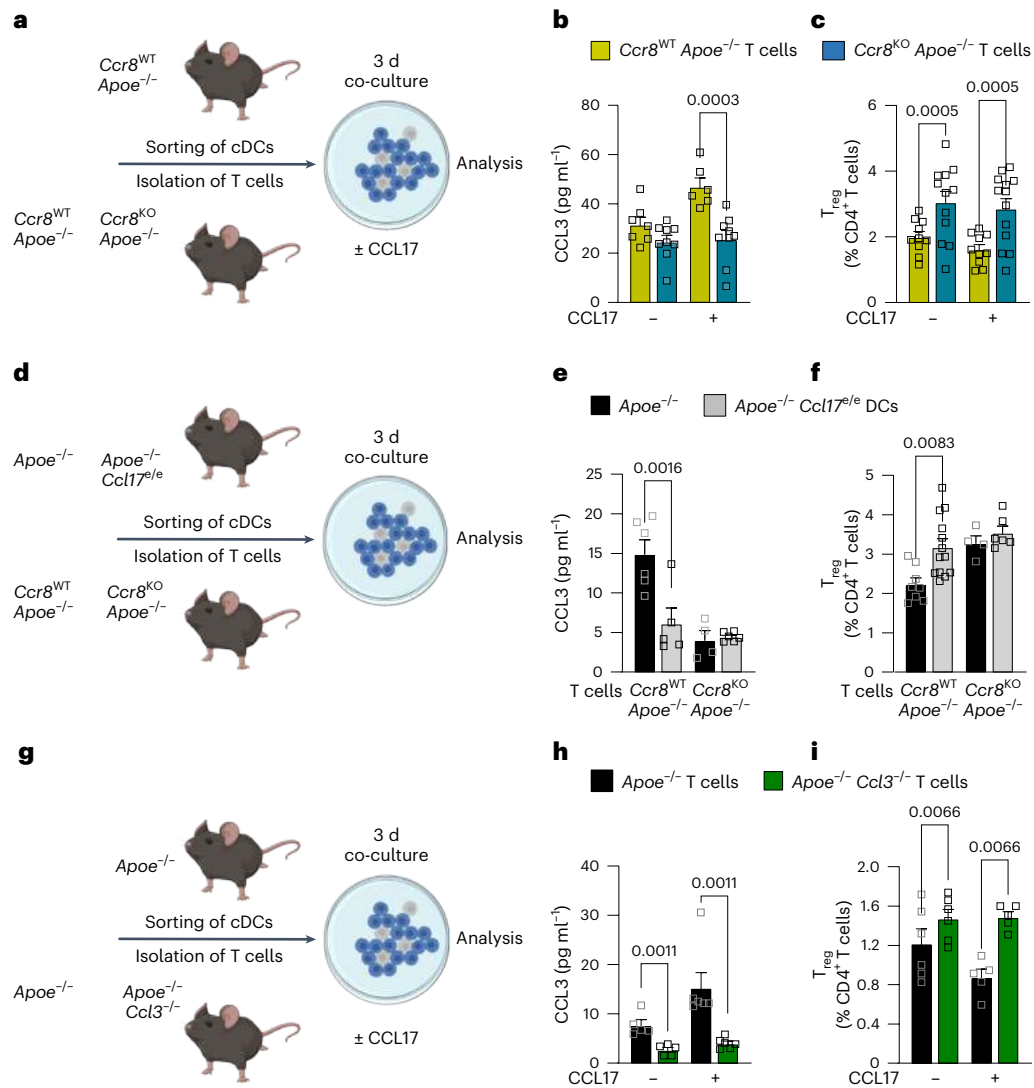


Fig. 5 | CCL17-CCR8-CCL3 axis critically interferes with T_{reg} differentiation.

a, Schematic of co-culture experiment, where isolated splenic $CD4^+CD62L^+$ T cells from *Ccr8*^{WT}*Apoe*^{-/-} or *Ccr8*^{KO}*Apoe*^{-/-} mice were combined with sorted $CD11c^+MHCII^+$ cDCs from LN of *Ccr8*^{WT}*Apoe*^{-/-} mice and cultured for 3 d in the absence or presence of recombinant murine CCL17 (100 ng ml⁻¹). **b**, CCL3 concentrations were measured in cell supernatants by ELISA (number of independent experiments per bar from left to right, $n = 7, 9, 6, 9$). **c**, $CD4^+CD25^+Foxp3^+$ T_{reg} cells were quantified using flow cytometry analysis (number of independent experiments per bar from left to right: $n = 10, 12, 10$ and 13). **d**, Scheme of co-culture experiment, where isolated splenic $CD4^+CD62L^+$ T cells from *Ccr8*^{WT}*Apoe*^{-/-} or *Ccr8*^{KO}*Apoe*^{-/-} mice were combined with sorted $CD11c^+MHCII^+$ cDCs from LN of *Apoe*^{-/-} or *Apoe*^{-/-}*Ccl17*^{e/e} mice and cultured for 3 d. **e**, CCL3 concentrations in the supernatant were determined by ELISA

(number of independent experiments per bar from left to right, $n = 6, 5, 4$ and 6). **f**, $CD4^+CD25^+Foxp3^+$ T_{reg} cells were quantified by flow cytometry (number of independent experiments per bar from left to right, $n = 8, 13, 4$ and 6). **g**, Scheme of co-culture experiment, where splenic $CD4^+CD62L^+$ T cells isolated from *Apoe*^{-/-} or *Apoe*^{-/-}*Ccl3*^{-/-} mice were combined with sorted $CD11c^+MHCII^+$ cDCs from LN of *Apoe*^{-/-} mice and cultured for 3 d. **h**, CCL3 concentrations in the supernatant were determined by ELISA (number of independent experiments per bar from left to right, $n = 5, 6, 5$ and 6). **i**, $CD4^+CD25^+Foxp3^+$ T_{reg} cells were quantified by flow cytometry (number of independent experiments per bar from left to right, $n = 6, 5, 6$ and 5). Data represent mean \pm s.e.m. (**a–i**). Two-sided P values as indicated versus respective controls and as analyzed by two-way ANOVA (**b, c, e, f, h, i**) with Holm-Šidák's post hoc test.

in co-cultures of cDCs with CCL3-deficient $CD4^+$ T cells was increased, as compared to controls, and remained higher and not diminished upon addition of CCL17 (Fig. 5i). Together, our data demonstrate that CCL17 interaction with CCR8, particularly on $CD4^+$ T cells, is critical in mediating CCL3 secretion and restraining T_{reg} differentiation.

Atheroprotection by blockade or $CD4$ -specific deletion of CCR8

To test whether CCR8 inhibition affects in vivo T_{reg} numbers and atherosclerosis, we injected a blocking antibody to CCR8 or isotype control three-times weekly into *Apoe*^{-/-} mice receiving WD for 4 weeks (Fig. 6a). The atherosclerotic lesion size in the aortic roots and arches

was reduced (Fig. 6b,c), whereas lesional macrophage, SMC and collagen content was unaltered in anti-CCR8-treated mice (Extended Data Fig. 5f–i). Accordingly, CCL3 expression was reduced, whereas $Foxp3^+CD25^+$ T_{reg} numbers were elevated in para-aortic LNs and spleens of anti-CCR8-treated mice (Fig. 6d–f) and lipid levels, circulating leukocyte and thrombocyte counts remained unaltered (Supplementary Table 4). Atherosclerotic lesion size in aortic root, thoracic-abdominal aorta and aortic arch was decreased in *Ccr8*^{KO}*Apoe*^{-/-} versus *Ccr8*^{WT}*Apoe*^{-/-} mice fed a WD for 12 weeks (Extended Data Fig. 6a–d). Because our in vitro data indicated a role of CCR8 on $CD4^+$ T cells in controlling T_{reg} differentiation, we generated *CD4*^{Cre}*Ccr8*^{fllox/fllox}*Apoe*^{-/-} mice (*CD4**Ccr8*^{KO}*Apoe*^{-/-}) lacking CCR8 in $CD4^+$ T cells (Fig. 6g). Compared

to $CD4^{Cre-} Ccr8^{fllox/fllox} Apoe^{-/-}$ ($CD4Ccr8^{WT} Apoe^{-/-}$) controls, we found a reduced atherosclerotic lesion burden in the aortic arch and thoraco-abdominal aorta after 12 weeks of WD (Fig. 6h,i). Lesional content of macrophages, SMCs and collagen was unaltered (Extended Data Fig. 6e–j), CCL3 expression in LNs was reduced, whereas T_{reg} numbers were increased in para-aortic LNs and spleens but not in blood and thymus of $CD4Ccr8^{KO} Apoe^{-/-}$ mice (Fig. 6k,l and Supplementary Table 5). As Helios is a marker distinguishing thymic-derived from peripherally induced $Foxp3^{+} T_{reg}$ cells²⁷, we quantified $CD4^{+} FoxP3^{+} Helios^{+} T_{reg}$ cells in aortic LNs, blood and thymus of $CD4Ccr8^{KO} Apoe^{-/-}$ and $CD4Ccr8^{WT} Apoe^{-/-}$ mice but did not observe any differences (Supplementary Table 5). Yet, flow cytometry analysis of aortic cell suspensions revealed increased $CD4^{+} FoxP3^{+} T_{reg}$ numbers in the aorta of $CD4Ccr8^{KO} Apoe^{-/-}$ versus control mice after 12 weeks of WD (Fig. 6m), whereas the suppression capacity of CCR8-deficient T_{reg} cells was reduced compared to CCR8-competent T_{reg} cells (Fig. 6n,o). These data indicate that the CCL17–CCR8–CCL3–CCR1 axis affects T_{reg} numbers directly at sites of inflammation (Fig. 6m) and in aortic LNs (Fig. 6k) rather than in blood and thymus. Lipid levels, circulating leukocyte and platelet counts, other T cell subsets in blood, spleen, aortic and axillary LNs did not differ in $CD4Ccr8^{KO} Apoe^{-/-}$ versus control mice (Supplementary Table 6), except a reduction of naive $CD44^{-} CD62L^{+}$ T cells in aortic LNs, reciprocating increased T_{reg} frequencies (Supplementary Table 7 and Fig. 6k). This corroborates a crucial role for CCR8 on $CD4^{+}$ T cells in conferring atherogenic effects of CCL17 via CCL3 release and T_{reg} suppression.

CCL17-driven CCL3 release limits T_{reg} differentiation via CCR1

To explore which CCL3 receptor (CCR1 or CCR5) expressed on $CD4^{+}$ T cells (Extended Data Fig. 6k,l) mediates the effects of CCL17-induced CCL3 release, we cultured $CD4^{+} CD62L^{+}$ T cells from spleens of $Apoe^{-/-}$, $Apoe^{-/-} Ccr1^{-/-}$ or $Apoe^{-/-} Ccr5^{-/-}$ mice under T_{reg} -polarizing conditions with or without CCL3 (Fig. 7a). Flow cytometry analysis revealed a decrease in $CD4^{+} CD25^{+} Foxp3^{+} T_{reg}$ frequencies among $CD4^{+}$ T cells, when comparing CCL3-treated $Apoe^{-/-}$ or $Apoe^{-/-} Ccr5^{-/-}$ T cell cultures to controls (TGf β only), whereas this did not occur in $Apoe^{-/-} Ccr1^{-/-}$ T cells (Fig. 7b), indicating that CCL3 restrains $CD4^{+} CD25^{+} Foxp3^{+} T_{reg}$ differentiation via CCR1. Evaluating the frequency of $CD4^{+} FoxP3^{+} Tbet^{+}$ cells (as a subset with pro-atherogenic functions²⁸) in LNs of CCL17- and CCL3-deficient mice, we observed a reduction of these cells in absence of CCL17 or CCL3 (Extended Data Fig. 6m). To confirm a role of the CCL3–CCR1 axis in mediating effects of CCL17, we sorted eGFP⁺ cDCs from $Apoe^{-/-} Ccl17^{wt/e}$ (CCL17-competent) or $Apoe^{-/-} Ccl17^{e/e}$ (CCL17-deficient) mice for co-culture with naive $CD4^{+} CD62L^{+}$ T cells from $Apoe^{-/-}$, $Apoe^{-/-} Ccr1^{-/-}$ or $Apoe^{-/-} Ccr5^{-/-}$ mice (Fig. 7c). $Apoe^{-/-} Ccl17^{wt/e}$ cDCs reduce $CD4^{+} CD25^{+} Foxp3^{+} T_{reg}$ frequencies in co-culture with $Apoe^{-/-}$ or $Apoe^{-/-} Ccr5^{-/-}$ but not $Apoe^{-/-} Ccr1^{-/-}$ T cells,

establishing the importance of a CCL17-instructed CCL3–CCR1 axis in restraining T_{reg} differentiation (Fig. 7d). As compared to controls, lesion size in the aortic root, arch and thoraco-abdominal aorta was reduced, lesional SMC content was increased, macrophage and collagen content were unaltered in $Apoe^{-/-} Ccr1^{-/-}$ mice (Fig. 7e–h and Extended Data Fig. 7a–d). While $CD3^{+} CD4^{+} CD25^{+} Foxp3^{+} T_{reg}$ cells were elevated in para-aortic, axillary and inguinal LNs and spleen of $Apoe^{-/-} Ccr1^{-/-}$ mice, CCL3 plasma levels (Fig. 7i,j and Extended Data Fig. 7e–g), lipid levels and blood cell counts were unaltered (Supplementary Table 8). Our data are in line with reduced lesion size in $Apoe^{-/-} Ccr1^{-/-}$ mice after 4 weeks of WD²⁹.

CCL3 confers atherosclerosis and reduced T_{reg} numbers in vivo

Under steady-state conditions, we found an increase in $CD4^{+} CD25^{+} Foxp3^{+} T_{reg}$ cells among $CD4^{+}$ T cells in para-aortic, axillary and inguinal LNs and spleen of $Ccl3^{-/-}$ mice compared to wild-type controls (Extended Data Fig. 7h–k). A pro-atherogenic role of hematopoietic CCL3 was evidenced by protection in $Ldlr^{-/-}$ mice bearing CCL3-deficient BM cells³⁰. Similar to CCL17-deficient mice, $Apoe^{-/-} Ccl3^{-/-}$ mice displayed a marked reduction in lesion size in the aortic root, arch and thoraco-abdominal aorta (Fig. 8a–d), elevated $FoxP3^{+}$ cells in aortic root lesions (Fig. 8e) and an increase in T_{reg} numbers in aortic, axillary or inguinal LNs and spleen, when compared to controls (Fig. 8f,g and Extended Data Fig. 7l,m). The suppression capacity of $Apoe^{-/-} Ccl3^{-/-} T_{reg}$ cells in a 3-d assay with $CD4^{+}$ effector T cells from $Apoe^{-/-}$ mice was enhanced (Fig. 8h,i). The lesional content of macrophages, SMCs and collagen (Extended Data Fig. 7n–p), body weight, lipid levels and blood cell counts (Supplementary Table 9) were unaltered in $Apoe^{-/-} Ccl3^{-/-}$ versus control mice.

To establish that the atheroprotective effects of CCL3 deficiency were mediated by T_{reg} cells, we depleted $CD25^{+}$ cells in $Apoe^{-/-} Ccl3^{-/-}$ mice using an antibody to CD25. As compared to isotype control, treatment of $Apoe^{-/-} Ccl3^{-/-}$ mice with anti-CD25 antibody increased lesion size in the aortic root and decreased T_{reg} frequencies in aortic LNs, restoring the levels to those observed in isotype control-treated $Apoe^{-/-}$ mice (Fig. 8j–l). Body weight, lipid levels and blood cell counts were unaltered in these mice (Supplementary Table 10). We next tested whether supplementing $Apoe^{-/-} Ccl17^{e/e}$ mice with CCL3 would reinstate the phenotype of CCL17-competent mice (Fig. 8m). Injection of CCL3 (three-times weekly) into $Apoe^{-/-} Ccl17^{e/e}$ mice during 4 weeks of WD increased aortic root lesion size and reduced axillary and splenic T_{reg} numbers to levels seen in $Apoe^{-/-}$ controls (Fig. 8n–p). Body weight, lipid levels and blood cell counts were unaltered (Supplementary Table 11). Our data demonstrate the importance of CCL3 in restraining T_{reg} cells and promoting atherosclerosis.

Proof-of-principle analysis in human gene expression datasets revealed higher CCL3 levels in atherosclerotic carotid artery

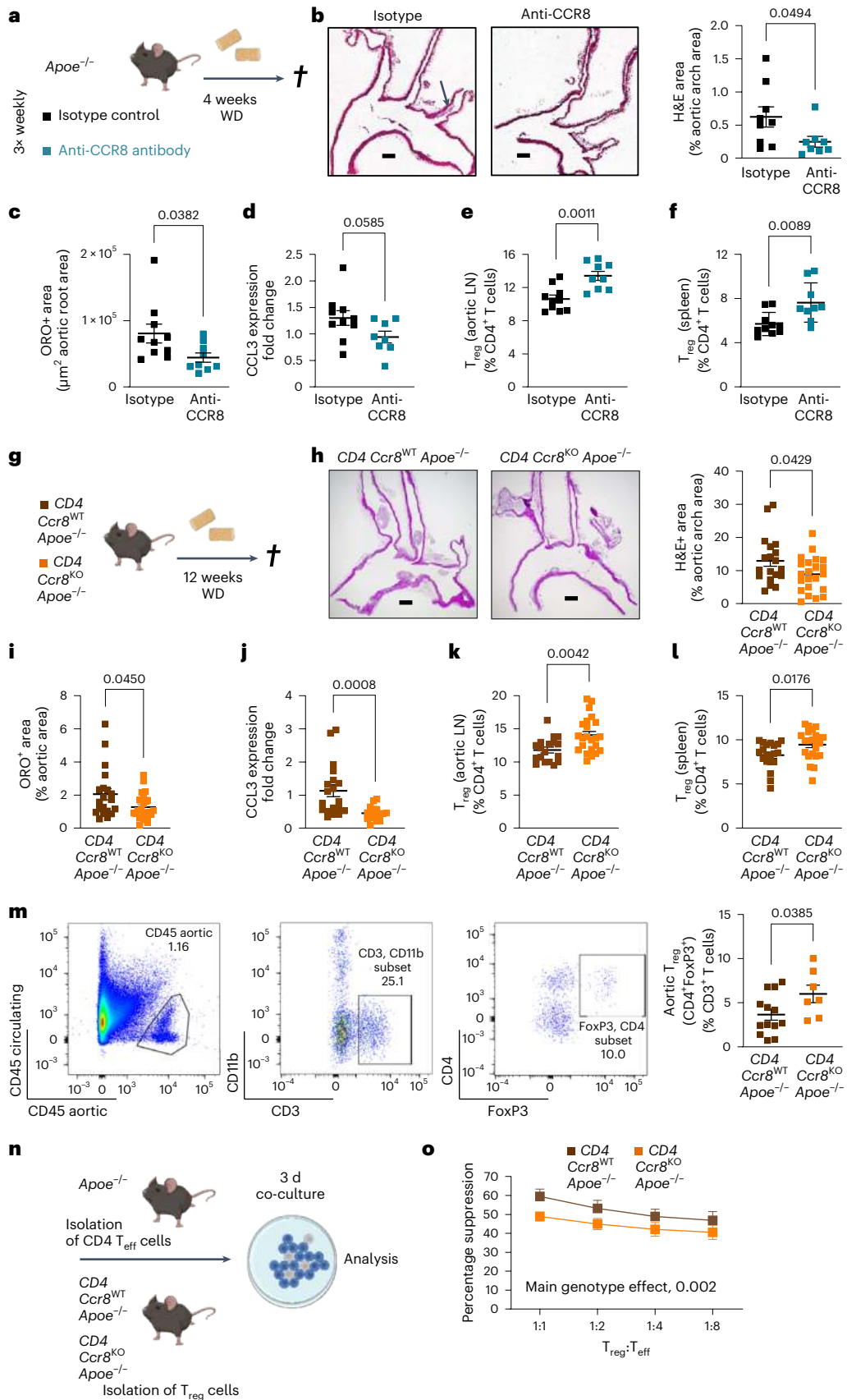
Fig. 6 | CCR8 blocking or $CD4^{+}$ T cell-specific CCR8 deficiency reduces atherosclerosis and increases T_{reg} cells.

a, Experimental scheme of $Apoe^{-/-}$ mice fed a WD and injected three-times weekly with a blocking antibody to CCR8 or isotype control. **b**, Representative images and quantification of atherosclerotic lesion size after H&E staining in aortic arches of $Apoe^{-/-}$ mice (isotype, $n = 9$; anti-CCR8, $n = 8$). Scale bar, 200 μ m. **c**, Lesion area after ORO in aortic roots of $Apoe^{-/-}$ mice (isotype, $n = 10$; anti-CCR8, $n = 9$). **d**, CCL3 mRNA expression levels in LNs of $Apoe^{-/-}$ mice. 18S rRNA was used as a housekeeping gene and changes in expression are given as fold change calculated with the $2^{-\Delta\Delta Ct}$ method (isotype, $n = 10$; anti-CCR8, $n = 8$). **e, f**, Flow cytometry analysis of $CD45^{+} CD3^{+} CD4^{+} CD25^{+} Foxp3^{+} T_{reg}$ cells in para-aortic LNs (**e**) and spleens (**f**) of $Apoe^{-/-}$ mice (isotype, $n = 10$; anti-CCR8, $n = 9$). **g**, Experimental scheme of $CD4^{Cre-} Ccr8^{fllox/fllox} Apoe^{-/-}$ ($CD4Ccr8^{WT} Apoe^{-/-}$) and $CD4^{Cre-} Ccr8^{fllox/fllox} Apoe^{-/-}$ ($CD4Ccr8^{KO} Apoe^{-/-}$) mice fed a WD. **h**, Representative images and quantification of lesion area after H&E staining in the aortic arches of $CD4Ccr8^{WT} Apoe^{-/-}$ ($n = 19$) or $CD4Ccr8^{KO} Apoe^{-/-}$ ($n = 22$) mice. Scale bar, 200 μ m. **i**, Atherosclerotic lesion size after ORO in aortas of $CD4Ccr8^{WT} Apoe^{-/-}$ ($n = 20$) or $CD4Ccr8^{KO} Apoe^{-/-}$ ($n = 22$) mice. **j**, CCL3 mRNA

expression levels in LNs of $CD4Ccr8^{WT} Apoe^{-/-}$ ($n = 19$) or $CD4Ccr8^{KO} Apoe^{-/-}$ ($n = 16$) mice. 18S rRNA was used as a housekeeping gene and changes in expression are given as fold change calculated with the $2^{-\Delta\Delta Ct}$ method. **k, l**, Flow cytometry analysis of $CD45^{+} CD3^{+} CD4^{+} CD25^{+} Foxp3^{+} T_{reg}$ cells in para-aortic LNs ($n = 18$ or 23) (**k**) and spleen ($n = 20$ or 23) (**l**) of $CD4Ccr8^{WT} Apoe^{-/-}$ (**k**, $n = 18$; **l**, $n = 20$) or $CD4Ccr8^{KO} Apoe^{-/-}$ (**k, l**, $n = 23$ each) mice. **m**, Flow cytometry analysis of $CD45^{+} CD4^{+} FoxP3^{+} T_{reg}$ cells in aortic cell suspensions from $CD4Ccr8^{WT} Apoe^{-/-}$ ($n = 13$) or $CD4Ccr8^{KO} Apoe^{-/-}$ ($n = 7$) mice fed a WD. **n**, Experimental scheme of a T_{reg} suppression assay conducted with $Apoe^{-/-}$ $CD4^{+}$ effector T cells or T_{reg} cells from $CD4Ccr8^{WT} Apoe^{-/-}$ or $CD4Ccr8^{KO} Apoe^{-/-}$ mice. **o**, Capacity of $CD4Ccr8^{WT} Apoe^{-/-}$ or $CD4Ccr8^{KO} Apoe^{-/-} T_{reg}$ cells to suppress $CD4^{+}$ effector T cell proliferation at varying $T_{reg}:T_{eff}$ ratios ($n = 2$ replicates for each dilution over six independent experiments). Data represent mean \pm s.e.m. (**a–o**). Two-sided P values as indicated and as analyzed by Mann–Whitney U -test (**b, i, j, m**), unpaired Student's t -test (**c, d–f, h, k, l**) or a generalized linear model and Wald test for main model effects (**o**).

segments with advanced (thick or thin fibrous cap atheroma) versus early lesions (intimal thickening or xanthoma) (Extended Data Fig. 8a; [GSE28829](#)) or in carotid atheroma specimens (stage IV) containing plaque core and shoulders versus remote, macroscopically

intact tissue (stages I/II) (Extended Data Fig. 8b; [GSE43292](#)). We found increased CCL3 expression in human coronary arteries with atherosclerotic lesions from symptomatic compared to asymptomatic patients with coronary artery disease (Extended Data Fig. 8c;



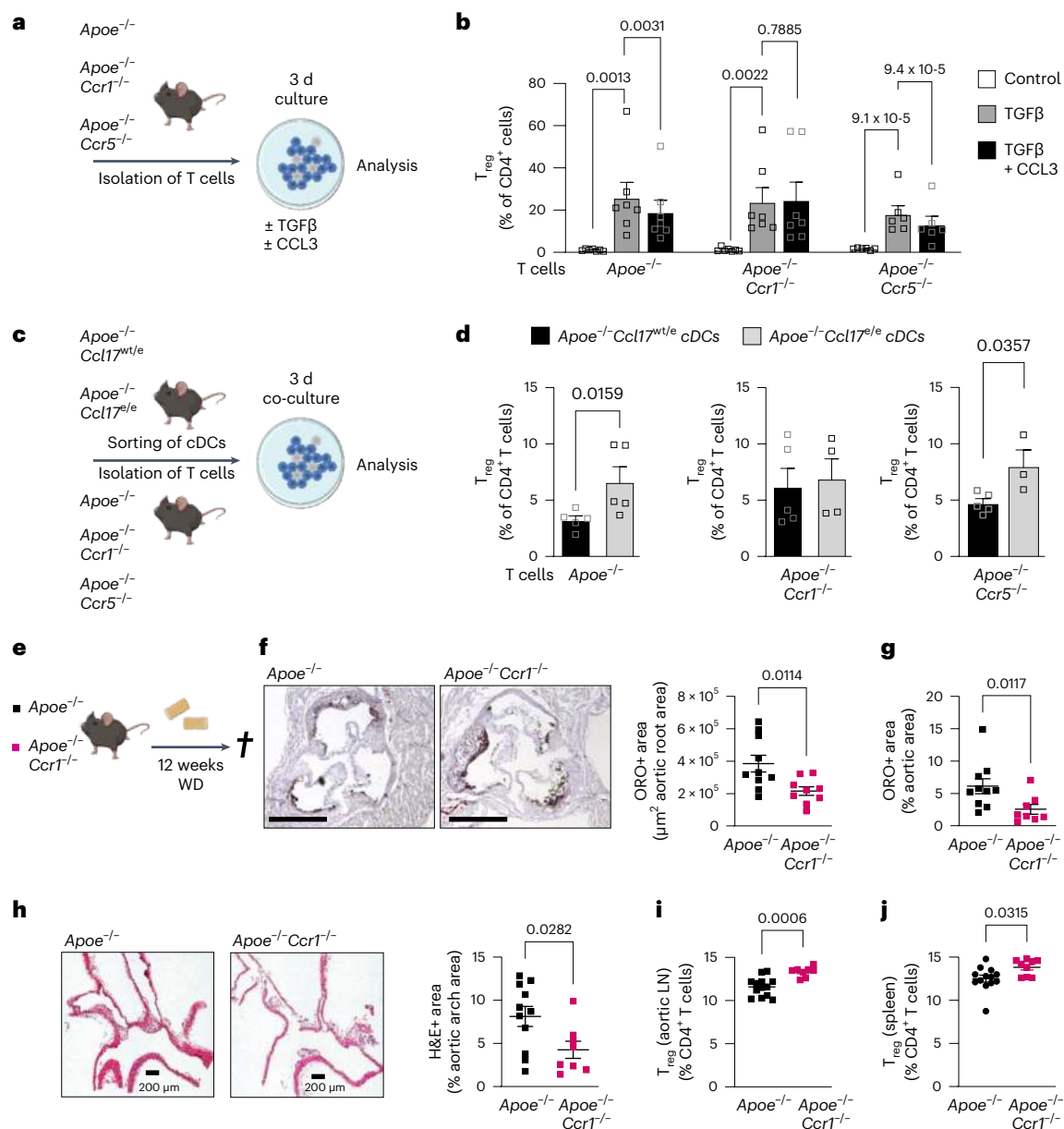


Fig. 7 | CCL17-dependent CCL3 release controls T_{reg} differentiation via CCR1. **a**, Experimental scheme wherein CD4⁺CD62L⁺ T cells isolated from spleens of *Apoe*^{-/-}, *Apoe*^{-/-} *Ccr1*^{-/-} or *Apoe*^{-/-} *Ccr5*^{-/-} mice were cultured for 3 d under T_{reg}-polarizing conditions (TGFβ at 100 ng ml⁻¹) in the presence or absence of recombinant mouse CCL3 (100 ng ml⁻¹). **b**, Quantification of CD45⁺CD4⁺CD25⁺FoxP3⁺ T_{reg} cells (number of independent experiments per bar from left to right, *n* = 7, 7, 7, 7, 7, 6, 6 and 6) using flow cytometry. **c**, Scheme of co-culture experiment wherein CD4⁺CD62L⁺ T cells isolated from spleens of *Apoe*^{-/-}, *Apoe*^{-/-} *Ccr1*^{-/-} or *Apoe*^{-/-} *Ccr5*^{-/-} mice were combined with sorted CD45⁺CD11c⁺MHCII⁺eGFP⁺ cDCs from LNs of *Apoe*^{-/-} *Ccl17*^{wt/e} or *Apoe*^{-/-} *Ccl17*^{e/e} mice and cultured for 3 d. **d**, Quantification of CD45⁺CD4⁺CD25⁺FoxP3⁺ T_{reg} cells (number of independent experiments per bar from left to right, *n* = 5, 5, 5, 4, 5 and 3) using flow cytometry. **e**, Experimental scheme of *Apoe*^{-/-} or *Apoe*^{-/-} *Ccr1*^{-/-}

mice fed a WD for 12 weeks (**e–j**). **f**, Representative images and quantification of lesion area after ORO staining for lipid deposits in the aortic root of *Apoe*^{-/-} (*n* = 10) or *Apoe*^{-/-} *Ccr1*^{-/-} (*n* = 9) mice. Scale bar, 500 μm. **g**, Quantification of lesion area after ORO staining for lipid deposits in the thoraco-abdominal aorta of *Apoe*^{-/-} (*n* = 10) or *Apoe*^{-/-} *Ccr1*^{-/-} (*n* = 8) mice. **h**, Representative images and quantification of atherosclerotic lesion size in aortic arches of *Apoe*^{-/-} (*n* = 11) or *Apoe*^{-/-} *Ccr1*^{-/-} (*n* = 8) mice after H&E staining. **i, j**, Flow cytometric quantification of CD45⁺CD3⁺CD4⁺CD25⁺FoxP3⁺ T_{reg} cells in para-aortic LNs (**i**) and spleen (**j**) of *Apoe*^{-/-} (**i, j**, *n* = 13 each) or *Apoe*^{-/-} *Ccr1*^{-/-} (**i**, *n* = 8; **j**, *n* = 9) mice. Data represent mean ± s.e.m. (**a–j**). Two-sided *P* values as indicated and as analyzed by a mixed-effects regression model followed by pairwise contrasts for fixed factors corrected by a Holm–Šidák’s procedure (**b**), unpaired Student’s *t*-test (**d, f, i**) or Mann–Whitney *U*-test (**g, h, j**).

GSE11138). Likewise, CCL3 transcript levels were higher in carotid atherectomy specimens from symptomatic patients (characteristics in Extended Data Table 2) with ipsilateral neurological events, for example, transient ischemic attacks (*n* = 16), than in those from asymptomatic patients (*n* = 13) (Extended Data Fig. 8d). This was mirrored by lower FoxP3 expression indicative of reduced T_{reg} abundance (Extended Data Fig. 8e). These data confirm increased CCL3 levels in

progressing human lesions and imply a role in suppressing T_{reg} differentiation in humans.

Discussion

Our quest to disambiguate the mechanisms underlying effects of CCL17 in an atherogenic context uncovered that aortic LNs of CCL17-deficient mice contain more tolerogenic cDCs, which license atheroprotective

T_{reg} maintenance. In turn, mice lacking the canonical CCL17 receptor CCR4 failed to phenocopy the effects of CCL17 deficiency. Instead, we could identify CCR8 as a functional high-affinity CCL17 receptor expressed by cDCs, $CD4^+$ T cells and T_{reg} cells. Further analysis established that CCL17–CCR8 interactions on $CD4^+$ T cells facilitate CCL3 release, thereby suppressing T_{reg} differentiation. Accordingly, interference with CCR8 by antibody blockade or $CD4^+$ T cell-specific deletion blunted CCL3 levels and atherosclerotic lesion formation. Likewise, CCL3 deficiency attenuated lesion development and increased T_{reg} numbers, whereas CCL3 applied in CCL17-deficient mice worsened atherosclerosis and hindered T_{reg} differentiation, an effect that was dependent on CCR1. We found increased CCL3 expression and reduced FoxP3 levels in human plaques versus healthy arteries and in symptomatic versus asymptomatic plaques.

CCR7 is a key receptor guiding cDCs into T cell rich regions of lymphatic organs, enabling them to stimulate or suppress T cell immunity³¹. CCR7 has also been implicated in mediating egress of antigen-presenting cells from atherosclerotic lesions³². We provide evidence that the CCR7-expressing DCs cluster in aortic LNs harbors both CCL17⁺ and CCL17-deficient cDC populations. In LNs from CCL17-deficient mice, the number of CCR7-expressing DCs with a tolerogenic gene expression profile was twofold higher than in controls. Hence, an increased number of tolerogenic cDCs together with locally decreased CCL3 levels might explain higher T_{reg} frequencies in lymphoid organs of CCL17-deficient mice. This is consistent with the hypothesis that CCL17⁺ DCs regulate the homeostatic mechanisms of T cells, including T_{reg} differentiation in lymphoid tissues, and are thereby able to affect the development of atherosclerosis¹⁰. The involvement of T_{reg} cells in limiting chronic inflammation and immune responses in mouse models of atherosclerosis^{17,33} and in alleviating atherosclerosis-related diseases in humans^{34–36} is well documented.

It is notable that a deficiency of CCR4, conventionally considered as the sole CCL17 receptor, failed to recapitulate any experimental features associated with CCL17 deficiency in our models. These findings mirrored related reports in experimental models of atopic dermatitis¹⁹ and colitis¹¹, where reduced inflammation was observed in CCL17-deficient but not CCR4-deficient mice. A similar discrepancy was evident in models of allograft tolerance, where CCR4-deficient mice fail to develop tolerance due to diminished T_{reg} recruitment, whereas CCL17-deficient mice show prolonged allograft survival^{13,37}. Hence, we revisited the previously proposed but later contested concept^{22,25,38} that CCR8 may serve as an alternate CCL17 receptor and unequivocally establish that CCR8 indeed acts as a functional high-affinity receptor for CCL17. CCR8 is mainly expressed on $CD4^+$ T cells and specifically on T_{reg} cells^{39,40} but also present on monocytes, natural killer (NK) cells, group 2 innate lymphoid cells and DCs, depending on disease context and tissue location^{41–43}. While the role of CCR8 in

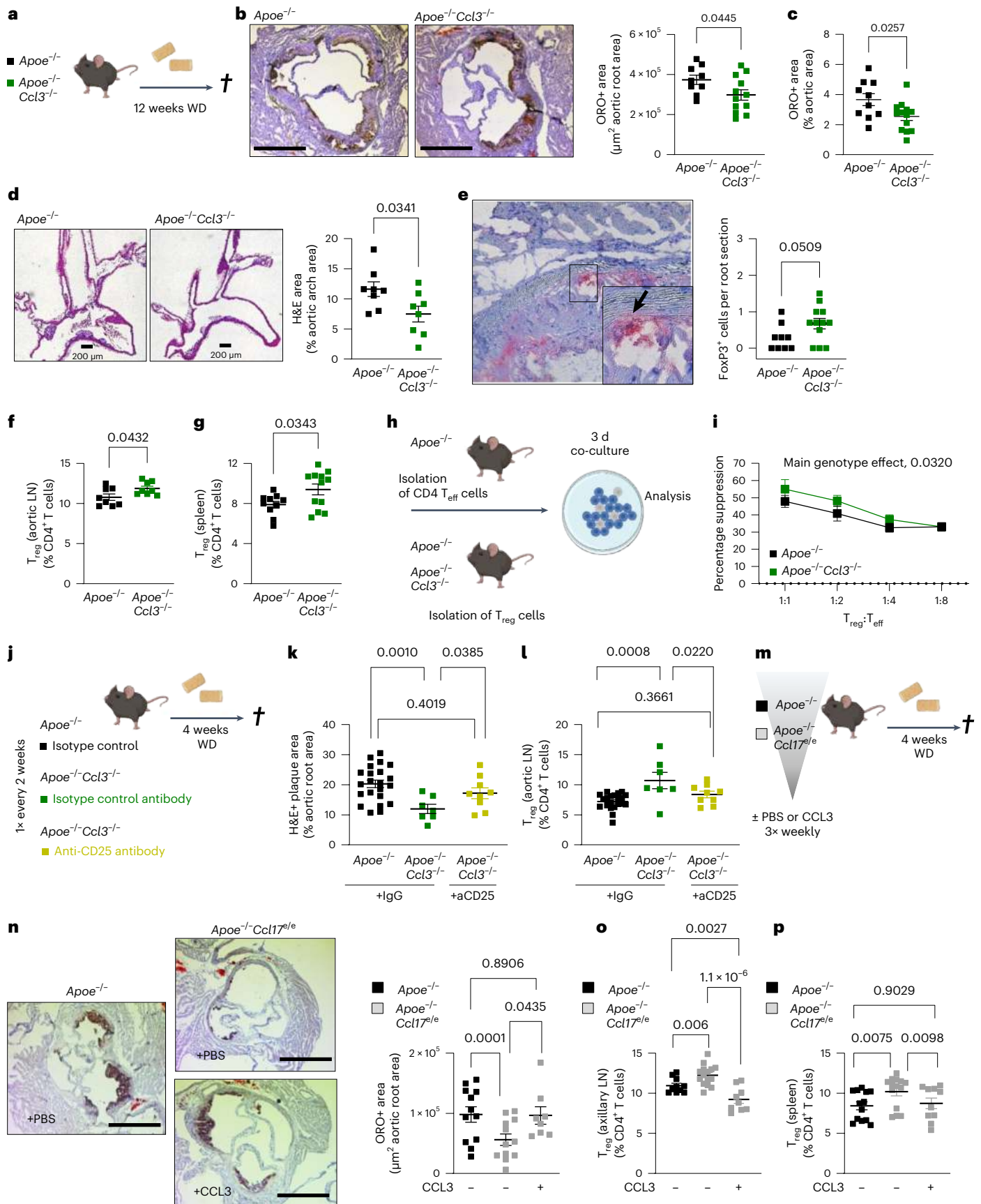
cancer has received great attention^{44,45}, reports on its contributions to chronic inflammation remain scarce. CCR8 has been implicated in airway inflammation⁴⁶ and in promoting pathogenic functions of interleukin (IL)-5⁺ T_H2 cells during atopic dermatitis⁴⁷. The role of CCR8 in atherosclerosis has been addressed in a study showing that genetic deletion of CCL1 in *Apoe*^{-/-} mice reduced T_{reg} recruitment to inflamed arteries and increased lesion formation⁴⁸. In *Ldlr*^{-/-} mice reconstituted with BM cells expressing FoxP3-driven red fluorescent protein, treatment with a CCR8-blocking antibody increased lesion size⁴⁸, contrasting our findings likely due to different experimental setups. Whereas we used *Apoe*^{-/-} mice for CCR8 blocking studies, the *Ldlr*^{-/-} mice were subjected to BM transplantation⁴⁸ and fed a cholesterol-rich diet for 1 week, an unusually short time span for evaluating the pathogenic role of adaptive immune cells in atherosclerosis. Yet, CCR8-expressing T_{reg} cells interacting with CCL1 have been identified as key drivers of suppressive immunity in models of autoimmune encephalomyelitis²⁴. We cannot exclude that CCL1–CCR8 interactions driving T_{reg} recruitment contribute to atheroprotective effects in CCL17-deficient mice, nor that differences in receptor affinity or local availability of its ligands or biased signaling may shape anti- versus proinflammatory immune responses mediated by CCR8. In fact, both CCR8 ligands may be involved and differential levels in a given pathology may determine functional outcomes.

Expression of CCR8 was initially identified on human monocytes and lymphocytes⁴⁹. Mouse pre-B cell transfectants (4DE4) expressing CCR8 dose-dependently migrated and exhibited specific calcium transients in response to CCL1 but not other chemokines tested (albeit not including CCL17)⁴⁹. Subsequently, CCL17 was suggested to act as a functional CCR8 ligand, evidenced by a dose-dependent migration of Jurkat CCR8-transfectants toward CCL17 (ref. 22). This was supported by a study revealing CCR8 expression and dose-dependent migration of human IL-2-activated NK cells (IANK) in response to CCL17 (ref. 36). While CCL1 induced a CCR8-dependent calcium flux in IANK cells, partially inhibiting CCL17-induced calcium flux, CCL17 fully desensitized the calcium response to CCL1. This discrepancy was explained by the expression of CCR4 on IANK cells, which cannot be desensitized by CCL1 (ref. 41). Accordingly, other groups were unable to show migration, calcium flux or receptor internalization in CCR8-transfected 4DE4 cells in response to CCL17 (refs. 38,50). This may be related to the fact that 4DE4 transfectants are a suboptimal model for signaling studies, whereas primary human IANK⁴¹ cells such as $CD4^+$ T cells used herein represent more physiological CCR8-bearing cell types. Still, calcium flux induced by CCL17 in IANK cells was predominantly mediated by CCR4 (ref. 41). Given these inconsistencies, we applied assays beyond migration and receptor internalization, both of which documented CCL17 activity for CCR8, to confirm a functional high-affinity CCL17 interaction with CCR8. Proximity ligation in DCs or Jurkat

Fig. 8 | CCL3 drives atherosclerosis and mediates reduced T_{reg} numbers in vivo. **a**, Experimental scheme. **b**, Representative images and quantification of lesion area after ORO staining in aortic roots of *Apoe*^{-/-} ($n = 9$) or *Apoe*^{-/-} *Ccl3*^{-/-} ($n = 12$) mice. Scale bar, 500 μ m. **c**, Quantification of lesion area after ORO in the thoraco-abdominal aorta of *Apoe*^{-/-} ($n = 10$) or *Apoe*^{-/-} *Ccl3*^{-/-} ($n = 12$) mice. **d**, Representative images (scale bar, 200 μ m) and quantification of lesion area after H&E staining of aortic arches from *Apoe*^{-/-} or *Apoe*^{-/-} *Ccl3*^{-/-} mice ($n = 8$ each). **e**, Representative image and immunohistochemical quantification of lesional FoxP3⁺ cell numbers in aortic roots of *Apoe*^{-/-} ($n = 9$) or *Apoe*^{-/-} *Ccl3*^{-/-} ($n = 12$) mice. **f, g**, Flow cytometry analysis of $CD45^+CD3^+CD4^+CD25^+FoxP3^+T_{reg}$ cells in para-aortic LNs (**f**) and spleen (**g**) of *Apoe*^{-/-} (**f**, $n = 8$; **g**, $n = 10$) or *Apoe*^{-/-} *Ccl3*^{-/-} (**f**, $n = 8$; **g**, $n = 12$) mice. **h**, Experimental scheme of T_{reg} suppression assays with *Apoe*^{-/-} $CD4^+$ effector T cells. **i**, Capacity of *Apoe*^{-/-} or *Apoe*^{-/-} *Ccl3*^{-/-} T_{reg} cells to suppress $CD4^+$ T cell proliferation at varying $T_{reg}:T_{eff}$ ratios ($n = 6$ each). **j**, Experimental scheme of *Apoe*^{-/-} or *Apoe*^{-/-} *Ccl3*^{-/-} mice injected twice with isotype control or anti-CD25 antibody for T_{reg} depletion. **k**, Lesion quantification in aortic roots of isotype control-treated *Apoe*^{-/-} ($n = 22$), *Apoe*^{-/-} *Ccl3*^{-/-} ($n = 7$) or

anti-CD25-treated *Apoe*^{-/-} *Ccl3*^{-/-} mice ($n = 9$). **l**, Flow cytometry analysis of $CD45^+CD3^+CD4^+CD25^+FoxP3^+T_{reg}$ cells in para-aortic LNs of isotype control-treated *Apoe*^{-/-} ($n = 21$), *Apoe*^{-/-} *Ccl3*^{-/-} ($n = 7$) or anti-CD25-treated *Apoe*^{-/-} *Ccl3*^{-/-} mice ($n = 9$). **m**, Experimental scheme of *Apoe*^{-/-} or *Apoe*^{-/-} *Ccl17*^{+/e} mice injected three-times weekly with PBS or recombinant mouse CCL3 (20 μ g i.p. injection), i.p., intraperitoneal. **n**, Representative images and quantification of lesion area after ORO in aortic roots of PBS-treated *Apoe*^{-/-} or *Apoe*^{-/-} *Ccl17*^{+/e} ($n = 12$ each) or CCL3-treated *Apoe*^{-/-} *Ccl17*^{+/e} ($n = 8$) mice. Scale bar, 500 μ m. **o, p**, Flow cytometry analysis of $CD45^+CD3^+CD4^+CD25^+FoxP3^+T_{reg}$ cells in para-aortic LNs (**o**) and spleen (**p**) of PBS-treated *Apoe*^{-/-} (**o**, $n = 10$; **p**, $n = 13$) or *Apoe*^{-/-} *Ccl17*^{+/e} (**o**, $n = 15$; **p**, $n = 14$) or CCL3-treated *Apoe*^{-/-} *Ccl17*^{+/e} mice (**o**, $n = 9$; **p**, $n = 10$). Data represent mean \pm s.e.m. (**a–p**). Two-sided *P* values were analyzed by unpaired Student's *t*-test or Mann–Whitney *U*-test (**b–g**), a generalized linear model and Wald test for main model effects (**i**) or a generalized linear model with mixed effects and post hoc pairwise contrasts within fixed factors corrected by a step-down Holm–Šidák's procedure (**k–p**).

CCR8-transfectants, SPR and binding competition revealed binding of CCL17 to CCR8 with apparent affinities ranging from 1.1 nM (K_d SPR) to 9.4 nM (IC_{50} CCL1 competition), thus equivalent to that for CCL18 (K_d 1.9 nM) but lower than that found for CCL1 by us (IC_{50} 0.58 nM) and others (K_i/IC_{50} 0.11–0.22 nM)^{30,31}. Determining cAMP levels in CCR4- or CCR8-transfected HEK293 cells confirmed that CCL17 induced



G_i-signaling via both receptors. This extends findings that CCR8 mediates chemotactic migration toward CCL17, unequivocally establishing that CCR8 as a signaling high-affinity receptor for CCL17. Our data can be reconciled with a report that CCL17 induced chemotaxis of Jurkat CCR8-transfectants, albeit without eliciting calcium mobilization²². Findings disputing the assignment of CCL17 as a CCR8 ligand may have been due to insufficient bioactivity, as no positive controls were provided²². A role of CCR8 in mediating the restraint of T_{reg} homeostasis may thus serve to complement or counter-balance functions of CCR4 in T_{reg} recruitment during inflammation and cancer^{52,53}. Preliminary evidence that CCR4 and CCR8 can engage in a heterodimeric interaction may further imply alternative mechanisms of modulation that will be subject of future studies. For instance, CCL17 inhibited T_{reg} recruitment through biased activation of CCR4, activating G_q-signaling but inhibiting CCL22-stimulated β-arrestin signaling to explain the abundance of T_{reg} cells in injured myocardium of CCL17-deficient mice⁵⁴, an effect possibly attributable to CCL17 activity mediated by CCR8.

It is tempting to speculate that only chronic inflammatory conditions, as present in atherosclerosis, atopic dermatitis¹⁹ or colitis¹¹, foster the development of CCL17-expressing cDCs, which then trigger T_{reg} restraint by inducing CCL3 release through CCR8 in lymphoid organs. Notably, our data show that it is primarily CCR8 on CD4⁺ T cells, which orchestrates the restraint of T_{reg} cells by upregulating CCL3 in response to CCL17, as evident by decreased lesion size and increased T_{reg} numbers in *Apoe*^{-/-} mice lacking CCR8 on CD4⁺ T cells. Because CCR8 is prominently expressed in T_{reg} cells, it is conceivable that at sites of inflammation or in T cell rich areas of LNs CCL17 directs T_{reg} trafficking but also prevents T_{reg} differentiation through induction of CCL3. This mechanism would explain why isolated CD25⁺CD4⁺ T cells secreted CCL3 in response to CCL17. Under chronic inflammatory conditions like atherosclerosis, however, CCL17⁺ cDCs are continuously present and skewing CD4⁺ T cell responses toward a proinflammatory type. This concept is corroborated by mechanistic studies in psoriasis as a chronic inflammatory autoimmune disease. The transcription factor Grainyhead-like 3 is crucial for maintaining barrier integrity of the skin, whereas its knockdown upregulates CCL17 in keratinocytes, driving their proliferation and an inflammatory T cell infiltration pattern resembling psoriasis⁵⁵. Moreover, elevated CCL3 inversely correlates with FoxP3 levels in T_{reg} cells of psoriatic patients and CCL3 interferes with FoxP3 stability by promoting ubiquitination-dependent degradation⁵⁶. Psoriatic disease may thus be prompted by CCL17-induced CCL3 expression to impair FoxP3 stability and reduce T_{reg} numbers. It will be intriguing to dissect whether CCL3 induction by CCL17 is restricted to cell types expressing CCR8, whether additional cell types are licensed by CCR8 expression to enact this mechanism of T_{reg} control and which specific signaling pathways couple CCR8 to CCL3 release.

Previous evidence on the role of CCL3 in atherosclerosis, despite not pinpointing the cellular sources of CCL3, lends support to our findings. In *Ldlr*^{-/-} mice reconstituted with *Ccl3*^{-/-} BM, aortic lesion formation and inflammatory neutrophil adhesion was reduced; however, an involvement of T cell subsets was not examined³⁰. Atorvastatin inhibits the 5-lipoxygenase pathway in *Apoe*^{-/-} mice, thereby downregulating CCL3 expression and attenuating lesion development, to implicate CCL3 as a therapeutic target in atherosclerosis⁵⁷. Mice lacking CCL3 are also protected from aortic inflammation and aneurysm formation⁵⁸. Here we show that genetic deletion of CCL3 in *Apoe*^{-/-} mice reduced lesion size and increased T_{reg} numbers and depletion studies indicated that atheroprotection was mediated by T_{reg} cells. Probing CCL3 receptors, CCR5 deficiency conferred a protective phenotype in different mouse models of atherosclerosis⁵⁹, whereas results on CCR1 deficiency were more ambiguous^{29,59}. Our data demonstrate that T_{reg} restraint by CCL3 is afforded by CCR1 and that CCR1 deficiency in *Apoe*^{-/-} mice decreased lesion development and enhanced T_{reg} numbers. Nevertheless, findings may be reconciled depending on the mouse model

and disease phenotype, as CCR1 engages multiple other chemokine ligands. Thus, cell subsets interacting in the vicinity and the local tissue environment may determine the availability of CCR1 ligands and how CCL3 shapes the immune response at relevant interfaces.

In synopsis, our data establish that CCL17 binds to CCR8 as its second functional high-affinity receptor besides CCR4, and introduce CCL17 to the unique ligand spectrum of CCR8, including its major ligand CCL1, CCL8 (ref. 47), a chemokine responsible for pathogenic circuits in atopic dermatitis and the widely expressed inflammatory chemokine CCL18 (ref. 50). The functional relevance in primary cells (T_{reg} cells), unfolds another facet within the remarkable versatility of the chemokine-receptor family⁶⁰. Our data show that CCL17 signaling via CCR8 on CD4⁺ T cells triggers CCL3 secretion, which engages CCR1 and suppresses T_{reg} differentiation to drive atherogenic effects of CCL17 (Extended Data Fig. 8f). We propose that the specific instruction of CD4⁺ T cells by CCL17⁺ cDCs dictating a CCL3-dependent restraint of T_{reg} cells may constitute a broadly relevant mechanism in chronic inflammatory disease and identify the sequential CCL17–CCR8–CCL3–CCR1 pathway as a target for multilayered therapeutic intervention.

Methods

Mice

All experiments were approved by local authorities and complied with German animal protection law (Regierung von Oberbayern; ROB-55.2-2532.Vet_02-14-189, ROB-55.2-2532.Vet_02-18-96 and ROB-55.2-2532.Vet_02-20-26). Every effort was made to minimize suffering. *Ccr4*^{-/-} mice⁶¹ were kindly provided by K. Pfeffer (Heinrich-Heine-Universität) and *Ccl17*^{wt/e} (GFP reporter knock-in) mice¹³ were kindly provided by I. Förster (Universität Bonn). *Ccl3*^{-/-} mice were purchased from the Jackson Laboratories. *Ccr1*^{-/-} mice and *Ccr5*^{-/-} mice were kindly provided by P.M. Murphy and W.A. Kuziel, respectively, and have been previously characterized^{59,62}. *Ccr4*^{-/-}, *Ccr1*^{-/-}, *Ccr5*^{-/-}, *Ccl17*^{wt/e} and *Ccl3*^{-/-} mice were crossed with *Apoe*^{-/-} mice purchased from the Jackson Laboratories. *Ccr8*^{flox/flox} mice were generated at Ozgene, backcrossed into a C57BL/6 background and crossed with C57BL/6 *Apoe*^{-/-} mice in house. *Apoe*^{-/-} *Unj*^{CreErt2} (ubiquitous inducible Cre expression), described previously⁶³, and *CD4*^{Cre} (purchased from Jackson laboratory) bred to *Apoe*^{-/-} were crossed in house with *Apoe*^{-/-} *Ccr8*^{flox/flox} mice to generate whole body or T cell-specific *Ccr8* knockout mice, respectively. To induce *Ccr8* deletion in *Unj*^{CreErt2} mice the mice received an i.p. injection with tamoxifen (50 mg kg⁻¹ body weight, from Sigma-Aldrich and dissolved in Miglyol, Caelo) for five consecutive days. All strains were backcrossed for at least ten generations to the C57BL/6 background. All mice were housed under specific-pathogen-free conditions in 12-h light–dark cycles at 21 °C and 50% humidity with ad libitum food and water. Depending on the type of study, mice were either fed a normal chow diet (steady state) or WD (for atherosclerosis studies) containing 21% fat and 0.15–0.2% cholesterol (Altromin 132010, Sniff TD88137) starting at 8–10 weeks of age for 4 or 12 weeks before being killed. For the rescue experiment using CCL3 injections, mice were injected 3× weekly with 20 μg recombinant mouse CCL3 or PBS control by i.p. injection. For depletion of CD25⁺ cells, including T_{reg} cells, *Apoe*^{-/-} or *Apoe*^{-/-} *Ccl3*^{-/-} mice were fed a WD for 4 weeks and injected twice (every second week) with isotype control or anti-CD25 antibody (each 250 μg antibody per i.p. injection). For the experiment using anti-CCR8 blocking antibody, mice were injected 3× weekly with 5 μg anti-CCR8 antibody or isotype control by i.p. injection. For scRNA-seq, male *Ccl17*^{wt/e} *Apoe*^{-/-} and *Ccl17*^{wt/e} *Apoe*^{-/-} mice were fed a normal chow diet or 6 weeks of WD. All experimental mice were sex- and age-matched.

Histology and immunofluorescence

Atherosclerotic lesion size was assessed by analyzing cryosections of the aortic root by staining for lipid depositions with ORO. In brief, hearts with the aortic root were embedded in Tissue-Tek O.C.T. compound (Sakura) for cryosectioning. ORO⁺ atherosclerotic lesions were

quantified in 4- μm transverse sections and averages were calculated from three sections. The thoraco-abdominal aorta was fixed with 4% paraformaldehyde and opened longitudinally, mounted on glass slides and stained enface with ORO. Aortic arches with the main branch points (brachiocephalic artery, left subclavian artery and left common carotid artery) were fixed with 4% paraformaldehyde and embedded in paraffin. Lesion size was quantified after H&E staining of 4- μm transverse sections and averages were calculated from 3–4 sections. For analysis of the cellular composition or inflammation of atherosclerotic lesions, aortic root sections were stained with antibodies to Mac2 (Cedarline), smooth muscle actin (Dako) or FoxP3 (Abcam). Nuclei were counterstained by 4',6'-diamidino-2-phenylindol (DAPI). After incubation with a secondary FITC- or Cy3-conjugated antibody (Life Technologies) for 30 min at room temperature, sections were embedded with VectaShield Hard Set Mounting Medium (Vector Laboratories) and analyzed using a Leica DM4000B LED fluorescence microscope and charge-coupled device camera. For FoxP3 staining, an Avidin/Biotin Blocking kit, VECTASTAIN ABC-AP and Vector Red Substrate kit were applied (all from Vector Laboratories). Blinded image analysis was performed using Diskus, Leica Qwin Imaging (Leica) or ImageJ software. For each mouse and staining, two to three root sections were analyzed and the average was taken.

Laboratory blood parameters and flow cytometry

Whole blood from the mice was collected in EDTA-buffered tubes. Thrombocyte counts were determined using a Celltac Automated Hematology Analyzer (Nihon Kohden). Afterwards, samples were subjected to red-blood-cell lysis for further analysis using flow cytometry. Spleen and LNs were mechanically crushed and passed through a 30- μm cell strainer (Cell-Trics, Partec) using Hank's medium (HBSS + 0.3 mmol l⁻¹ EDTA + 0.1% BSA; Gibco by Life Technologies) to obtain single-cell suspensions. Leukocyte subsets were analyzed using the following surface marker combinations: neutrophils (CD45⁺CD11b⁺CD115⁺Gr1^{high}), classical (CD45⁺CD11b⁺CD115⁺GR1^{high}) and non-classical (CD45⁺CD11b⁺CD115⁺GR1^{low}) monocytes, B cells (CD45⁺B220⁺), T cells (CD45⁺CD3⁺), T_{reg} cells were classified as CD45⁺CD3⁺CD4⁺CD25⁺FoxP3⁺ (the gating strategy used to identify T_{reg} cells throughout the manuscript is depicted in Extended Data Fig. 1j) and its subpopulation as CD45⁺CD3⁺CD4⁺FoxP3⁺Tbet⁺. Foxp3 transcription factor was stained using the Foxp3/Transcription Factor Staining Buffer Set (eBioscience). Annexin-V⁺ cells were analyzed using the Dead Cell Apoptosis kit (Thermo Fisher Scientific). Cell populations and marker expression were analyzed using a FACSCanto II, FACSDiva software v.8.0 (BD Biosciences) and the FlowJo analysis program v.10 (Tree Star).

All aortas, including the aortic root, aortic arch and thoracic portions were subjected to a house-made enzymatic digestion and post-digestion protocol⁶⁴. Single-cell suspensions were obtained by mashing aortas through a 70- μm cell strainer. Live/dead staining was performed with Zombie Violet Fixable Viability kit (BioLegend, 423113) followed by surface staining with antibodies: anti-CD45-APC-Cy7 (BioLegend, clone 30-F11, 1:300 dilution), anti-CD11b-PerCP-Cy5.5 (BioLegend, clone M1/70, 1:300 dilution), anti-CD3e-FITC (BioLegend, clone 145-2C11, 1:300 dilution) and anti-CD4-PE-Cy7 (BioLegend, clone RM4-5; 1:500 dilution) including unconjugated anti-CD16/32 (BioLegend, clone 93, 1:500 dilution). Intracellular staining for FoxP3 was performed using anti-FoxP3-PE antibody (eBiosciences, clone FJK-16s, 1:50 dilution) and FoxP3/Transcription Factor Staining Buffer Set (eBiosciences, 00-5523-00) according to the manufacturer's protocol. Data were acquired using flow cytometry (BD FACSCanto II, BD Biosciences) and analyzed using FlowJo v.10 (FlowJo).

Plasma lipid levels

Cholesterol and triglyceride levels were analyzed using mouse EDTA-buffered plasma and quantified using enzymatic assays (c.f.a.s. Cobas, Roche Diagnostics) according to the manufacturer's protocol.

Fluorescence-activated cell sorting and tolerogenic DC analysis

For the isolation of DCs, LNs were mechanically crushed and passed through a 30- μm cell strainer (Cell-Trics, Partec) using Hank's medium (HBSS + 0.3 mmol l⁻¹ EDTA + 0.1% BSA; Gibco by Life Technologies) to obtain single-cell suspensions. cDCs were isolated from this suspension by fluorescence-activated cell sorting (BD FACSAria), by gating for CD45⁺CD11c⁺MHCII⁺ cells. Furthermore, eGFP⁺Ccl17^{wt/e} and eGFP⁺Ccl17^{e/e} DCs were isolated by gating for the endogenous eGFP signal in the FITC channel (pre-gating, CD45⁺CD11c⁺MHCII⁺). Flow cytometric analysis of tolerogenic DCs in aortic LNs was performed by pre-gating for CD45⁺CD11c⁺MHCII⁺ followed by evaluation of CD83, CCR7, IDO and CD274 on pre-gated cDCs^{20,65–67}.

For the isolation of T and B cells, spleens were mechanically crushed and passed through a 30- μm cell strainer (Cell-Trics, Partec) using Hank's medium (HBSS + 0.3 mmol l⁻¹ EDTA + 0.1% BSA; Gibco by Life Technologies) to obtain single-cell suspensions. Cell subsets were isolated by fluorescence-activated cell sorting (BD FACSAria), by gating for CD45⁺CD3⁺ cells (T cells) or CD45⁺CD19⁺ cells (B cells). After sorting, all cells were cultured in 96-well round-bottom plates (1 × 10⁵ cells per well) (Corning Costar by Sigma-Aldrich/Merck) in RPMI-1640 medium supplemented with 10% (*v/v*) fetal calf serum, 2 mM L-glutamine and 1% penicillin/streptomycin (all Gibco by Life Technologies), unless stated otherwise and with/without specific stimuli as indicated for the individual experiments.

Immunomagnetic cell isolation

For the isolation of monocytes and neutrophils, BM cells were collected by flushing femurs with Hank's medium (HBSS + 0.3 mmol l⁻¹ EDTA + 0.1% BSA) (Gibco by Life Technologies). Monocytes are isolated using the mouse Monocyte Isolation kit and an LS separation column (all Miltenyi Biotec), according to the manufacturer's protocol. Neutrophils were isolated using the mouse Neutrophil Isolation kit and an LS separation column (all Miltenyi Biotec), according to the manufacturer's protocol. After isolation, all cells were cultured in 96-well round-bottom plates (1 × 10⁵ cells per well) (Corning Costar by Sigma-Aldrich/Merck) in RPMI-1640 medium supplemented with 10% (*v/v*) fetal calf serum, 2 mM L-glutamine and 1% penicillin/streptomycin (All Gibco by Life Technologies) unless stated otherwise, with/without specific stimuli as indicated for the individual experiments.

For the isolation of CD4⁺, CD4⁺CD62L⁺ and CD4⁺CD25⁺ T cells, spleens were mechanically crushed and passed through a 30- μm cell strainer (Cell-Trics, Partec) using Hank's medium (HBSS + 0.3 mmol l⁻¹ EDTA + 0.1% BSA; Gibco by Life Technologies) to obtain single-cell suspensions. CD4⁺ T cells were subsequently isolated using the mouse CD4⁺ T cell Isolation kit and an LS separation column (all Miltenyi Biotec), according to the manufacturer's protocol. CD4⁺CD62L⁺ T cells were subsequently isolated using the mouse CD4⁺CD62L⁺ T cell Isolation kit II and an LS separation column (all Miltenyi Biotec), according to the manufacturer's protocol. CD4⁺CD25⁺ T cells were subsequently isolated using the mouse CD4⁺CD25⁺ T cell Isolation kit and an LS separation column (all Miltenyi Biotec), according to the manufacturer's protocol. After isolation, cells were cultured in 96-well round-bottom plates (1 × 10⁵ cells per well) (Corning Costar by Sigma-Aldrich/Merck) in RPMI-1640 medium supplemented with 10% (*v/v*) fetal calf serum, 2 mM L-glutamine and 1% penicillin/streptomycin (all Gibco by Life Technologies), unless stated otherwise and with/without specific stimuli as indicated for the individual experiments.

For the isolation of human CD4⁺ T cells, 18 ml whole blood was collected from healthy volunteers and mixed with 2 ml citrate to avoid blood coagulation (approved by the local ethics committee, LMU Munich, no. 18–283). Whole blood was then diluted with same volume of T cell isolation buffer (phosphate-buffered saline + 2 mmol l⁻¹ EDTA + 0.1% BSA; Gibco by Life Technologies) and gently layered over twofold volume of Biocoll solution (1.077 g ml⁻¹; Bio&SELL), followed

by centrifugation for 25 min at 600g without brake. The top layer of plasma was removed and mononuclear cells in the middle layer were carefully collected and transferred to a new tube. The mononuclear cells were washed with T cell isolation buffer twice and centrifuged for 10 min at 300g. The supernatants were discarded and cell pellets were resuspended with T cell isolation buffer to reach a final density of 1×10^8 cells per ml. Human CD4⁺ T cells were isolated from this cell suspension with Dynabeads Untouched Human CD4 T Cells kit (Invitrogen) according to the manufacturer's protocol.

Transmigration assay

Mouse and human CD4⁺ T cells were isolated according to the manufacturer's protocols as detailed above. Transmigration assays were performed using HTS Transwell 96-well plates (3.0- μ m pore size with polycarbonate membrane; Corning). Murine or human recombinant CCL17 (BioLegend) was added to the bottom chambers at a concentration of 100 ng ml⁻¹ or as indicated in RPMI-1640 medium containing 0.5% BSA. Murine or human recombinant CCL1 or CCL22 (Peprotech) was added to the bottom chambers at a concentration of 50 ng ml⁻¹ or as indicated in RPMI-1640 medium containing 0.5% BSA. Mouse CD4⁺ T cells from *Apoe*^{-/-}, *Ccr8*^{WT}*Apoe*^{-/-} or *Ccr8*^{KO}*Apoe*^{-/-} mice or human CD4⁺ T cells (1×10^5) were added to the top chamber in the presence or absence of CCR4 receptor antagonist C021 dihydrochloride (Tocris) at a concentration of 0.5 μ M; or human CD4⁺ T cells (1×10^5) were pretreated with or without anti-CCR8 antibody (R&D Systems) and added to the top chamber and allowed to migrate for 3 h. The number of cells migrated was analyzed by flow cytometry (FACSCanto II, BD Biosciences) and FlowJo v.10 software (Tree Star). The chemotactic index was calculated as the ratio of chemokine-stimulated to unstimulated migration.

In another quantitative transmigration assay (checkerboard), HTS Transwell 96-well plates (3.0- μ m pore size with polycarbonate membrane; Corning) were also used. Isolated CD4⁺ T cells (1×10^5) were added to the upper chamber of each well in a total volume of 80 μ l of RPMI-1640 medium containing 0.5% BSA. Murine recombinant CCL17 (BioLegend) was used at concentrations of 1 μ g ml⁻¹, 100 ng ml⁻¹, 10 ng ml⁻¹, 1 ng ml⁻¹ or 0 ng ml⁻¹ in RPMI-1640 medium containing 0.5% BSA in the lower, upper or both lower and upper chambers of the Transwell to generate 'checkerboard' analysis matrix of positive, negative and the absent gradients of CCL17, respectively. Cells were collected from the lower chamber 3 h later and counted. The number of cells migrated was analyzed by flow cytometry (FACSCanto II, BD Biosciences) and FlowJo v.10 software (Tree Star). The chemotactic index was calculated as the ratio of migrated cell counts of each well to unstimulated migration without murine recombinant CCL17 in both lower and upper chamber.

T effector polarization assay

Splenic CD4⁺CD62L⁺ T cells were obtained by immunomagnetic cell isolation as described previously. CD4⁺CD62L⁺ T cells (1×10^5) were cultured in 96-well tissue round-bottom culture plates in the presence of anti-CD3e (pre-coated overnight, 5 μ g ml⁻¹), anti-CD28 (1 μ g ml⁻¹) and supplemented with TGF β (5 ng ml⁻¹) in the presence or absence of CCL17 (100 ng ml⁻¹) for 3 d. T_{reg} cells were classified as CD45⁺CD3⁺CD4⁺CD25⁺Foxp3⁺. The number of T_{reg} cells was analyzed by flow cytometry (FACSCanto II, BD Biosciences) and FlowJo v.10 software (Tree Star).

T_{reg} suppression assay

Splenic CD4⁺CD25⁻ T cells and CD4⁺CD25⁺ T_{reg} cells from *Apoe*^{-/-}, *Apoe*^{-/-}*Ccl3*^{-/-} or *Ccr8*^{KO}*Apoe*^{-/-} were isolated using CD4⁺CD25⁺ Regulatory T Cell Isolation kit (Miltenyi Biotec, 130-091-041) according to manufacturer's instructions. Isolated CD4⁺CD25⁻ T cells were labeled with 5 μ M Cell Proliferation Dye eFluor 670 dye (eBioscience, 65-0840-90) according to the manufacturer's instructions and co-cultured with different concentrations of CD4⁺CD25⁺ T_{reg} cells and with Dynabeads Mouse T-Activator CD3/CD28 (Thermo Fisher Scientific, 11456D)

for 72 h at 37 °C with 5% CO₂. Proliferation of CD4⁺CD25⁻ T cells was assessed by flow cytometry (BD FACSCanto II, BD Biosciences). Data were analyzed using FlowJo v.10 (Tree Star).

Co-culture experiments

DCs were isolated from cell suspension from LNs by fluorescence-activated cell sorting (BD FACS Aria), by gating for CD45⁺CD11c⁺MHCII⁺ cells as previously mentioned. Sorted DCs were subsequently co-cultured for 3 d in 96-well tissue flat-bottom culture plates with splenic naive CD4⁺CD62L⁺ T cells obtained by immunomagnetic cell isolation as described previously in a DC:T cell ratio of 1:2 (in general 2.5×10^4 to 5×10^4 cells), with/without specific stimuli as indicated for the individual experiments. The percentage of T_{reg} cells (CD45⁺CD3⁺CD4⁺CD25⁺Foxp3⁺ cells) relative to CD4⁺ T cells was analyzed by flow cytometry (FACSCanto II, BD Biosciences) and FlowJo v.10 software (Tree Star). Supernatants were collected for further ELISA or multiplex bead array analysis.

Cell culture experiments for CCL3 release

To measure CCL3 release of CD4⁺, CD4⁺CD62L⁺, CD4⁺CD25⁺, CD45⁺CD11c⁺MHCII⁺, eGFP⁺Ccl17^{wt/e}DCs, eGFP⁺Ccl17^{e/e}DCs CD45⁺CD3⁺ cells (T cells) or CD45⁺CD19⁺ B cells and monocytes as well as neutrophils cells were seeded at 1×10^5 into a 96-well round-bottom plate and incubated in the absence or presence of CCL17 (100 ng ml⁻¹) in combination with C021 (5 μ M) or anti-CCR8 antibody (2 μ g ml⁻¹) for 4 h. Thereafter, supernatants were collected and measured by CCL3 ELISA as detailed below.

Multiplex bead array

Cell culture supernatants and mouse plasma were analyzed for various cytokines using the 'Cytokine & Chemokine 26-Plex Mouse ProcartaPlex Panel 1' (Thermo Fisher Scientific, eBioscience), sample preparation and analysis were performed according to the manufacturer's protocol. The kit allows the simultaneous detection and quantification of soluble murine IFN γ ; IL-12p70; IL-13; IL-1 β ; IL-2; IL-4; IL-5; IL-6; TNF α ; granulocyte-macrophage colony-stimulating factor; IL-10; IL-17A; IL-18; IL-22; IL-23; IL-27; IL-9; GRO α (CXCL1); IP-10 (CXCL10); MCP-1 (CCL2); MCP-3 (CCL7); MIP-1 α (CCL3); MIP-1 β (CCL4); MIP-2 (CXCL2); RANTES (CCL5); eotaxin (CCL11). The bead-based assay followed the principles of a sandwich immunoassay. Fluorescent magnetic beads were coupled with antibodies specific to the analytes to be detected. Beads were differentiated by their sizes and distinct spectral signature (color-coded) by flow cytometry using Luminex xMAP, data were collected with xPONENT software (Thermo Fisher Scientific, v.4.2) and analyzed with ProcartaPlex Analyst software (Thermo Fisher Scientific, v.1.0).

ELISA

CCL3 plasma (EDTA-plasma of full blood) levels or CCL3 levels in cell culture supernatants were quantified by ELISA using a commercially available kit (CCL3 Mouse Uncoated ELISA kit with plates from Thermo Fisher Scientific or Mouse CCL3/MIP-1 alpha Quantikine ELISA kit by R&D System) following the manufacturer's protocol. The final measurement of absorbance was carried out using a plate reader (Tecan) set to 450 nm with a correction factor of 550 nm.

Cyclic AMP signaling

Levels of cyclic adenosine monophosphate (cAMP) were measured in confluent Flp-In system and Flp-In TREx-293 (HEK293) cells (Invitrogen). HEK293 cells were transfected using plasmids harboring sequences of CCR4 and CCR8 (Missouri S&T cDNA Resource Center; www.cdna.org). The sequence of the luciferase-cAMP binding site fusion protein from the pGloSensor-20F-vector (Promega) was amplified and ligated into a bicistronic pIRESneo vector (Clontech) to obtain the reporter gene plasmid. HEK293 cells were transfected with the

reporter gene vector using Eco-Transfect (OZBioscience), stable clones were selected as host cell lines for expressing receptor constructs using the Flp-In system⁶⁸ and reselected with G418 and hygromycin B. After incubation with luciferin-EF (2.5 mM, Promega) at room temperature for 2 h, cells were stimulated with CCL17, CCL1 or CCL20 (100 ng ml⁻¹ each) or left unstimulated (PBS control) and luminescence indicating the reduction of cAMP was recorded over time.

Proximity-ligation assay

Proximity ligation was carried out using the Duolink In Situ Red kit goat/rabbit (Sigma-Aldrich) on PFA-fixed mouse DCs cultured on collagen-coated coverslips that were pre-incubated with recombinant mouse CCL1 (Peprotech) and CCL17 (BioLegend) using primary polyclonal antibodies to mouse CCL17 (R&D systems), mouse CCL1 (Acris), mouse CCR4 (Thermo Scientific), mouse CCR5 (Santa Cruz Biotechnology) and mouse CCR8 (Abcam) according to the manufacturer's instructions. Imaging was performed using fluorescence microscopy (Leica DM4000) after which deconvolution algorithms for wide-field microscopy were applied to improve overall image quality (Huygens Professional 16.10; SVI). The number of Duolink-detected interactions was determined in the processed images using the Leica LAS 4.2 analyses software. To more accurately resolve the interactions detected with Duolink, representative DC samples of each condition were also visualized with a Leica SP8 3X microscope using a combination of 3D confocal microscopy (DAPI) and 3D STED nanoscopy (Duolink Red). Image processing and deconvolution of the resultant 3D datasets was performed using the Leica LAS X and Huygens professional software packages.

Proximity ligation was also carried out using the Duolink In Situ Probe anti-goat or anti-rabbit or anti-mouse kit (Sigma-Aldrich) on PFA-fixed CCR4-transfected or CCR8-transfected Jurkat cells (ATCC), which were pre-incubated with or without recombinant human CCL1 (Peprotech) and CCL17 (BioLegend) using primary polyclonal antibodies against human CCL17 (Thermo Fisher Scientific), human CCL1 (R&D Systems), human CCR4 (Thermo Fisher Scientific or BioLegend) and human CCR8 (Thermo Fisher Scientific). Cells were then treated with ligase and polymerase according to the manufacturer's instructions of Duolink flowPLA Detection Far Red kit (Sigma-Aldrich). The fluorescent signal was analyzed by flow cytometry (FACSCanto II, BD Biosciences) and FlowJo v.10 software (Tree Star).

Expression, purification and labeling of CCL17

The gene encoding native CCL17 was inserted into a pET-32a(+) vector between Kpn I and Xho I restriction sites. The expression of recombinant CCL17 in One Shot BL21(DE3)Star *E. coli* in LB medium was induced by 0.1 mM IPTG when the OD₆₀₀ reached 0.8–1.0. Inclusion bodies were isolated and resuspended in binding buffer (50 mM Tris, 500 mM NaCl, 4 M Gnd-HCl, 40 mM imidazole, 10 mM β-mercaptoethanol, pH 7.4). The extract was loaded on a HisTrap HP column (Cytiva Europe) equilibrated with equilibration buffer (50 mM Tris, 500 mM NaCl and 6 M Gnd-HCl, pH 7.4). After washing with 2% of elution buffer (50 mM Tris, 500 mM NaCl and 2 M imidazole, pH 7.4), the protein was eluted using a gradient of 2–50% elution buffer, followed by dialysis against acetic acid and lyophilization. The lyophilized was resuspended in 10 mM Tris (pH 8.0), 3 U EKMax protease (Thermo Fisher Scientific) was added and the solution was incubated for 16 h at 37 °C to remove the tag. The cleaved product was further purified using a 3-ml RESOURCE RPC column with an acetonitrile + 0.1% TFA gradient. After lyophilization, the protein was refolded in 50 mM Tris, 10 mM cysteine and 0.5 mM cystine (pH 8.0) for 24 h at 4 °C under gentle stirring, purified using a HiTrap Heparin HP column and HPLC. The correct mass and folding were verified by mass spectrometry and NMR, respectively.

CCL17 was labeled using 1-ethyl-3-(3-dimethylaminopropyl)carbodiimide (EDC) and Alexa-Fluor 647 Cadaverine (Thermo Fisher Scientific). Briefly, CCL17 was incubated in presence of tenfold molar

excess of EDC and dye in 10 mM MES (pH 6.0). After 10 min the labeled product was purified using Zeba Spin Desalting Columns (Life Technologies) and stored at 4 °C.

Surface plasmon resonance

SPR was performed on a BIAcore X100 instrument (Cytiva Europe) using neutravidin-modified C1 sensor chips⁶⁹ coated with biotinylated human recombinant CCL17 or CCL5 to 1,300 resonance units. Sensograms were obtained by injecting different concentrations of CCR8-carrying proteoliposomes or with CCR4-carrying liposomes (positive control), mock protein-carrying or pure liposomes (negative controls) in running buffer (62.5–2,000 ng ml⁻¹ in HBS-EP + buffer). Analytes were perfused over the chip for 270 s (at 20 μl min⁻¹) followed by a final dissociation phase of 180 s. The sensor chip was regenerated with two pulses of 60 s of NAS (30% acetonitrile, 100 mM NaOH and 0.1% SDS). Responses from analyte injections were overlaid with the fit of 1:1 interaction model (Langmuir) determined using BIACORE X100 evaluation 2.0 software.

Competitive chemokine receptor-ligand binding

HEK293 cells stably transfected with human CCR8 (HA-tagged to monitor expression) and mock HEK293 cells (10⁵ each) were incubated in binding buffer (HBSS supplemented with 20 mM HEPES and 0.2% BSA) with increasing concentrations of unlabeled human recombinant CCL1, CCL17 or CCL18. After 20 min at 4 °C, recombinant human CCL17 or synthetic human CCL1 (ALMAC) labeled with Alexa-Fluor 647 at the C terminus was added at a final concentration of 10 nM and further incubated for 30 min. After washing with binding buffer and fixation in 2% PFA/PBS, fluorescence intensity was measured by flow cytometry (FACSCanto II) and analyzed using FlowJo v.10 software (Ashland). Background binding to HEK293 mock-transfectants was subtracted and data were normalized to binding without unlabeled chemokine (control) and subjected to nonlinear fitting. Data represent mean ± s.d. from three independent experiments performed in duplicate or triplicate.

CCR8 and CCR4 internalization assay

For isolation of CD4⁺ T cells from *Ccr8*^{WT}*ApoE*^{-/-} or *Ccr8*^{KO}*ApoE*^{-/-} mice, thymus or LNs were mechanically crushed and passed through a 30-μm cell strainer (Cell-Trics, Partec) using Hank's medium (HBSS + 0.3 mmol l⁻¹ EDTA + 0.1% BSA; Gibco by Life Technologies) to obtain single-cell suspensions. Subsequently, CD4⁺ T cells were isolated using the mouse CD4⁺ T cell Isolation kit (Miltenyi Biotec). Cells (1 × 10⁵) were incubated with recombinant murine CCL17 (100 ng ml⁻¹), CCL1 (50 ng ml⁻¹) or CCL22 (50 ng ml⁻¹) at 37 °C for 1 h and surface stained with antibodies against CD4, CCR8 and CCR4 at 4 °C for 30 min. CCR8 fluorescence intensity of CD4⁺ T cells was analyzed by flow cytometry (FACSCanto II, BD Biosciences) and FlowJo v.10 software (Tree Star). Human CD4⁺ T cells were isolated from PBMCs with Dynabeads Untouched Human CD4 T Cells kit (Invitrogen) according to the manufacturer's protocol as previously mentioned. Cells (1 × 10⁵) were incubated with recombinant human CCL17 (100 ng ml⁻¹), CCL1 (50 ng ml⁻¹) or CCL22 (50 ng ml⁻¹, all Peprotech) at 37 °C for 20 min or 40 min and surface stained with antibodies against CD4, CCR8 and CCR4 at 4 °C for 30 min. Cells were then washed with PBS. CCR8 and CCR4 fluorescence intensity of CD4⁺ T cells was analyzed by flow cytometry (FACSCanto II, BD Biosciences) and FlowJo v.10 software (Tree Star).

RNA purification and real-time PCR

Total mRNA was isolated from frozen mouse axillary LNs with Trizol (Invitrogen). Isolated RNA was subsequently transcribed into cDNA using an iScript cDNA Synthesis kit (Bio-Rad) according to the manufacturer's instructions. Real-time PCR was then performed with QuantiNova Probe PCR kit (QIAGEN) in QuantStudio 6 Real-Time PCR system (Thermo Fisher). The threshold cycle (Ct) values of the target genes were normalized to that of the housekeeping gene (endogenous

control) encoding 18S ribosomal RNA (rRNA). All data were analyzed by adopting $2^{-\Delta\Delta Ct}$ method. Relative mRNA expression is shown, with the average from control samples set as 1. The TaqMan gene expression assays used in this study were Mm00441259_g1 (CCL3) and Mm03928990_g1 (Rn18S) (all Life Technologies).

Quantification of FoxP3 mRNA and CCL3 copy numbers in human plaque specimens was performed as described^{70–72} and correlated with the clinical phenotype, either defined by asymptomatic stable atherosclerosis or by symptomatic disease, as apparent by cerebral ischemic events, for example transient ischemic attacks or stroke. The following primers/probes were applied: FoxP3_h_fwd GCCCG-GATGTGAGAAGGCTTT, FoxP3_h_rev GCCCTGCCCTTCTCATCCAG, FoxP3_h_Probe 5'FAM-CTTCTCAAGCACTGCCAGGCGGAC-3'TAM; hCCL3-fwd: CTGCACCATGGCTCTCTGC; hCCL3-rev: CTGAAGCAGCAG-GCGGTC, hCCL3-Probe:CTCTGCATCACTTGCTGCTGACACGC. The use of human material was approved by the local ethics committee (LMU Munich, no. 18–296). The study procedure was in accordance with the Helsinki Declaration and all participants provided their written informed consent.

Microarray data acquisition and data processing of published datasets

For the *CCR8* mRNA expression in various human tissues and in different blood cell types, datasets were downloaded from the Human Protein Atlas (<https://www.proteinatlas.org>).

For the *CCL3*, *CCR8* and *FOXP3* mRNA expression in human plaques or T cells from patients with familial hypercholesterolemia, four microarray datasets (GSE43292 (ref. 73), GSE28829 (ref. 74), GSE11138 (ref. 75)) were downloaded from the Gene Expression Omnibus (<http://www.ncbi.nlm.nih.gov/geo>). The GSE43292 dataset contained 32 human atheroma plaques or 32 paired distant macroscopically intact tissue. The GSE28829 dataset consisted of 16 advanced atherosclerotic plaques and 13 early lesions. The GSE11138 dataset consisted of eight symptomatic and six asymptomatic patients with carotid and coronary plaque. Data preprocessing included transforming gene probes into gene symbols, data consolidation and normalization. Probes without gene symbols were deleted. Probes with maximal expression were retained for further analysis if the probes contained more than one probe.

Cell suspension preparation for scRNA-seq

For the scRNA-seq experiment of pooled lymph nodes (including mesenteric, para-aortic, inguinal, axillary, brachial and mandibular LNs), eight *Ccl17^{w/e}Apoe^{-/-}* and six *Ccl17^{e/e}Apoe^{-/-}* male mice (C57BL/6J background) were fed a normal chow diet. Perfusion was performed with 5 ml PBS through left ventricular puncture until the liver yielded a pale color. Pooled LNs from either *Ccl17^{w/e}Apoe^{-/-}* or *Ccl17^{e/e}Apoe^{-/-}* mice were mechanically crushed and passed through a 30- μ m cell strainer (Cell-Trics, Partec) using Hank's medium (HBSS + 0.04% BSA; Gibco by Life Technologies) to obtain single-cell suspensions, followed by B cell depletion using CD19 MicroBeads (Miltenyi Biotec) according to the manufacturer's instructions. B cell-depleted fractions were stained with Fixable Viability Dyes eFluor 660, anti-CD45, anti-CD3, anti-CD19 and anti-CD11c (All from eBioscience) at 4 °C for 20 min. After washing in PBS for 5 min, cells were resuspended in Hank's medium (HBSS + 0.04% BSA; Gibco by Life Technologies) and then isolated by fluorescence-activated cell sorting (BD FACSAria), by gating for live CD45⁺CD11c⁺CD3⁻CD19⁻ cells. The cell suspension with viability >80% was ready for subsequent single-cell capture and library preparation.

For the scRNA-seq experiment of para-aortic LNs, seven *Ccl17^{w/e}Apoe^{-/-}* and ten *Ccl17^{e/e}Apoe^{-/-}* male mice (C57BL/6J background) were fed a 6-week WD. Para-aortic LNs of same genotype were pooled and strained as previously mentioned. Cells were resuspended in Hank's medium (HBSS + 0.04% BSA; Gibco by Life Technologies), stained

and isolated by fluorescence-activated cell sorting (BD FACSAria), by gating for live CD45⁺CD19⁻MHCII⁺ cells. The cell suspension with viability > 80% was ready for subsequent single-cell capture and library preparation.

Single-cell RNA sequencing

Cell suspensions were loaded into a 10x Genomics Chromium Next GEM Chips and encapsulated with Single Cell 3' v.3.1 barcoded gel beads using the 10x Genomics Chromium controller, according to the manufacturer's instructions. Single-cell libraries were then constructed according to the manufacturer's instructions. Libraries from individual samples were sequenced on an Illumina NovaSeq 6000 platform. The sequencing depth was set to around 50,000 reads per cell for pooled LNs from various positions and around 65,000 reads per cell for para-aortic LNs.

Analysis of scRNA-seq data

Fastq files of sorted CD45⁺CD11c⁺CD3⁻CD19⁻ cells from LNs of *Ccl17^{w/e}Apoe^{-/-}* and *Ccl17^{e/e}Apoe^{-/-}* mice on a chow diet were aligned to the customized reference genome (eGFP was added to the mm10 reference) individually using Cell Ranger Software (v.3.0.0, 10x Genomics). Individual datasets were then aggregated using the Cell Ranger aggr command without subsampling normalization. The aggregated dataset was then analyzed using the R package Seurat (v.3.1.4)^{76,77}. The dataset was trimmed of cells expressing <200 or >5,000 genes for exclusion of non-cell or cell aggregates. Cells containing >10% mitochondrial genes were presumed to be of poor quality and were also discarded. A 'log-Normalize' method was employed to normalize the gene expression for each cell by the total expression, the resulting expression values were then multiplied by 10,000 and log-transformed. The most highly variable genes in the dataset were discovered with FindVariableFeatures function and used in principal-component analysis (PCA), followed by a linear transformation ('scaling') following the standard pipeline. PCA was used for dimensionality reduction and UMAP was then used for two-dimensional visualization of the clusters. Visualization of gene expression with feature plot was generated with Seurat function FeaturePlot. Marker genes of each cluster were found by FindAllMarkers function.

Similar alignment was performed in sorted CD45⁺CD19⁻MHCII⁺ cells from para-aortic LNs of *Ccl17^{w/e}Apoe^{-/-}* and *Ccl17^{e/e}Apoe^{-/-}* mice on a WD for 6 weeks individually using Cell Ranger Software (v.3.0.0., 10x Genomics). Individual datasets were then aggregated using the Cell Ranger aggr command without subsampling normalization. Cells expressing <200 or >4,000 genes were filtered out for the exclusion of non-cell or cell aggregates. Cells containing >5% mitochondrial genes were also discarded. Similar normalization, scaling, PCA, clustering and UMAP analysis were then performed.

Tolerogenic score

XCRI⁺ tolerogenic DCs undergo a continuous homeostatic maturation that is essential for central tolerance and that occurs irrespective of IFN-I according to previous study⁷⁸. The 82 specifically upregulated genes during thymic and peripheral homeostatic XCRI⁺ DC maturation in this study were listed as tolerogenic genes. Interferon-stimulated genes were among the few discriminators of immunogenic and tolerogenic XCRI⁺ DCs. The 31 interferon-stimulated genes from this study are listed as immunogenic genes (Supplementary Table 3). The tolerogenic score was then calculated using the top 20 genes that distinguished tolerogenic DCs and immunogenic DCs as follows: tolerogenic score = (1 + mean (top 20 upregulated tolerogenic genes)) / (1 + mean (top 20 upregulated immunogenic genes)).

Gene set variation analysis enrichment score

To generate a GSEA enrichment score of each eGFP-expressing CCL17-deficient cell from tolerogenic DCs of *Apoe^{-/-} Ccl17^{e/e}* mice and each

CCL17-expressing cell from tolerogenic DCs of *Apoe*^{-/-} *Ccl17*^{wt/e} mice fed on chow diet, the ontology gene sets v.7.1 were provided in MSigDB (<https://www.gsea-msigdb.org/gsea/msigdb>). The analysis was implemented using R package gsva.

Statistical analysis

Statistical analyses were performed with GraphPad Prism v.10 (GraphPad Software) and IBM SPSS Statistics v.29.0 (IBM). Data distribution and homogeneity of variance were tested by the Shapiro–Wilk and Levene’s tests, respectively. Data violating the assumption of Gaussian distribution were analyzed by Mann–Whitney *U*-test (two-group comparisons) or Kruskal–Wallis *H* test with Dunn’s post hoc test. For normally distributed data, unpaired Student’s *t*-test with Welch correction when appropriate (two-group comparisons) or univariate ANOVA with Holm–Šidák’s post hoc test (three or more groups) was performed. In analyses involving two or more factors, factorial (two-way) ANOVA with Holm–Šidák’s post hoc test for pairwise comparisons was applied. Data from multiple biological replicates over independent experiments were analyzed with a nested approach by fitting mixed-effect regression based on generalized linear models with nested data (within the independent experiment) as random factors and robust estimation of the covariance matrix to avoid the influence of violation of model assumptions (nested ANOVA). Pairwise contrasts within fixed factors were corrected by step-down Holm–Šidák’s procedure. Main model effects were tested by Wald chi-squared test. For models involving dependency of measurements, the assumption of sphericity was verified with Mauchly’s *W* test, and the Greenhouse–Geisser correction was applied in case of violation. Differences were considered significant for a two-tailed *P* value < 0.05. Data were reported as mean ± s.e.m., unless otherwise stated. For mouse experiments, a priori calculation of power based on a two-sample *t*-test design and previous data or pilot experiments was performed with the software Java Applets for Power and Sample Size (available at <http://www.stat.uiowa.edu/~rlenth/Power>) and aimed at 80% statistical power for detecting biological relevant changes (30%) with a two-tailed α -value of 5%. For in vitro experiments, group sample sizes were determined empirically based on pilot experiments.

Materials

A detailed overview of used materials is provided in the Major Resources Table (Supplementary Table 12).

Reporting summary

Further information on research design is available in the Nature Portfolio Reporting Summary linked to this article.

Data availability

All data associated with this study are presented within the paper and associated files. The scRNA-seq data of *Ccl17*^{wt/e} *Apoe*^{-/-} and *Ccl17*^{wt/e} *Apoe*^{-/-} mice fed on a chow diet or a WD for 6 weeks have been deposited in Gene Expression Omnibus and are available under accession code [GSE200862](https://www.ncbi.nlm.nih.gov/geo/query/acc.cgi?acc=GSE200862). The following publicly available datasets for human atherosclerosis were included: [GSE28829](https://www.ncbi.nlm.nih.gov/geo/query/acc.cgi?acc=GSE28829) (advanced atherosclerotic plaques or early lesions), [GSE43292](https://www.ncbi.nlm.nih.gov/geo/query/acc.cgi?acc=GSE43292) (human atheroma or paired distant macroscopically intact tissue) and [GSE11138](https://www.ncbi.nlm.nih.gov/geo/query/acc.cgi?acc=GSE11138) (symptomatic or asymptomatic patients with carotid and coronary plaques). Schematic panels in the figures were created using www.biorender.com. Source data are provided with this paper.

References

- Lutgens, E. et al. Immunotherapy for cardiovascular disease. *Eur. Heart J.* **40**, 3937–3946 (2019).
- Jongstra-Bilen, J. et al. Low-grade chronic inflammation in regions of the normal mouse arterial intima predisposed to atherosclerosis. *J. Exp. Med.* **203**, 2073–2083 (2006).
- Millonig, G. et al. Network of vascular-associated dendritic cells in intima of healthy young individuals. *Arter. Thromb. Vasc. Biol.* **21**, 503–508 (2001).
- Choi, J. H. et al. Identification of antigen-presenting dendritic cells in mouse aorta and cardiac valves. *J. Exp. Med.* **206**, 497–505 (2009).
- Gil-Pulido, J. & Zernecke, A. Antigen-presenting dendritic cells in atherosclerosis. *Eur. J. Pharmacol.* **816**, 25–31 (2017).
- Ye, Y. et al. Serum chemokine CCL17/thymus activation and regulated chemokine is correlated with coronary artery diseases. *Atherosclerosis* **238**, 365–369 (2015).
- Brunner, P. M. et al. The atopic dermatitis blood signature is characterized by increases in inflammatory and cardiovascular risk proteins. *Sci. Rep.* **7**, 8707 (2017).
- He, H. et al. Increased cardiovascular and atherosclerosis markers in blood of older patients with atopic dermatitis. *Ann. Allergy Asthma Immunol.* **124**, 70–78 (2020).
- Ye, Y. et al. Association between a CCL17 genetic variant and risk of coronary artery disease in a Chinese Han population. *Circulation* **82**, 224–231 (2017).
- Weber, C. et al. CCL17-expressing dendritic cells drive atherosclerosis by restraining regulatory T cell homeostasis in mice. *J. Clin. Investig.* **121**, 2898–2910 (2011).
- Heiseke, A. F. et al. CCL17 promotes intestinal inflammation in mice and counteracts regulatory T cell-mediated protection from colitis. *Gastroenterology* **142**, 335–345 (2012).
- Steinman, R. M. Decisions about dendritic cells: past, present, and future. *Annu. Review. Immunol.* **30**, 1–22 (2012).
- Alferink, J. et al. Compartmentalized production of CCL17 in vivo: strong inducibility in peripheral dendritic cells contrasts selective absence from the spleen. *J. Exp. Med.* **197**, 585–599 (2003).
- Saigusa, R., Winkels, H. & Ley, K. T cell subsets and functions in atherosclerosis. *Nat. Rev. Cardiol.* **17**, 387–401 (2020).
- Arce-Sillas, A. et al. Regulatory T cells: molecular actions on effector cells in immune regulation. *J. Immunol. Res.* **2016**, 1720827 (2016).
- Sharma, M. et al. Regulatory T cells license macrophage pro-resolving functions during atherosclerosis regression. *Circ. Res.* **127**, 335–353 (2020).
- Ait-Oufella, H. et al. Natural regulatory T cells control the development of atherosclerosis in mice. *Nat. Med.* **12**, 178–180 (2006).
- Imai, T. et al. The T cell-directed CC chemokine TARC is a highly specific biological ligand for CC chemokine receptor 4. *J. Biol. Chem.* **272**, 15036–15042 (1997).
- Stutte, S. et al. Requirement of CCL17 for CCR7- and CXCR4-dependent migration of cutaneous dendritic cells. *PNAS* **107**, 8736–8741 (2010).
- Wild, A. B. et al. CD83 orchestrates immunity toward self and non-self in dendritic cells. *JCI Insight* **4**, e126246 (2019).
- Wan, W., Lionakis, M. S., Liu, Q., Roffe, E. & Murphy, P. M. Genetic deletion of chemokine receptor Ccr7 exacerbates atherogenesis in ApoE-deficient mice. *Cardiovasc. Res.* **97**, 580–588 (2013).
- Bernardini, G. et al. Identification of the CC chemokines TARC and macrophage inflammatory protein-1 β as novel functional ligands for the CCR8 receptor. *Eur. J. Immunol.* **28**, 582–588 (1998).
- Garlisi, C. G. et al. The assignment of chemokine-chemokine receptor pairs: TARC and MIP-1 β are not ligands for human CC-chemokine receptor 8. *Eur. J. Immunol.* **29**, 3210–3215 (1999).
- Barsheshet, Y. et al. CCR8⁺FOXP3⁺ T_{reg} cells as master drivers of immune regulation. *PNAS* **114**, 6086–6091 (2017).
- Iellem, A. et al. Unique chemotactic response profile and specific expression of chemokine receptors CCR4 and CCR8 by CD4⁺CD25⁺ regulatory T cells. *J. Exp. Med.* **194**, 847–853 (2001).

26. Uhlen, M. et al. Proteomics. Tissue-based map of the human proteome. *Science* **347**, 1260419 (2015).
27. Thornton, A. M. et al. Expression of Helios, an Ikaros transcription factor family member, differentiates thymic-derived from peripherally induced Foxp3⁺ T regulatory cells. *J. Immunol.* **184**, 3433–3441 (2010).
28. Li, J. et al. CCR5^T-bet⁺FoxP3⁺ effector CD4 T cells drive atherosclerosis. *Circ. Res.* **118**, 1540–1552 (2016).
29. Soehnlein, O. et al. Distinct functions of chemokine receptor axes in the atherogenic mobilization and recruitment of classical monocytes. *EMBO Mol. Med.* **5**, 471–481 (2013).
30. de Jager, S. C. et al. Leukocyte-specific CCL3 deficiency inhibits atherosclerotic lesion development by affecting neutrophil accumulation. *Arter. Thromb. Vasc. Biol.* **33**, e75–e83 (2013).
31. Schneider, M. A., Meingassner, J. G., Lipp, M., Moore, H. D. & Rot, A. CCR7 is required for the in vivo function of CD4⁺ CD25⁺ regulatory T cells. *J. Exp. Med.* **204**, 735–745 (2007).
32. Worbs, T., Hammerschmidt, S. I. & Forster, R. Dendritic cell migration in health and disease. *Nat. Rev. Immunol.* **17**, 30–48 (2017).
33. Klingenberg, R. et al. Depletion of FOXP3⁺ regulatory T cells promotes hypercholesterolemia and atherosclerosis. *J. Clin. Investig.* **123**, 1323–1334 (2013).
34. Mor, A., Luboshits, G., Planer, D., Keren, G. & George, J. Altered status of CD4⁺CD25⁺ regulatory T cells in patients with acute coronary syndromes. *Eur. Heart J.* **27**, 2530–2537 (2006).
35. Zhang, W. C. et al. Impaired thymic export and increased apoptosis account for regulatory T cell defects in patients with non-ST segment elevation acute coronary syndrome. *J. Biol. Chem.* **287**, 34157–34166 (2012).
36. Albany, C. J., Trevelin, S. C., Giganti, G., Lombardi, G. & Scotta, C. Getting to the heart of the matter: the role of regulatory T-cells (Tregs) in cardiovascular disease (CVD) and atherosclerosis. *Front. Immunol.* **10**, 2795 (2019).
37. Lee, I. et al. Recruitment of Foxp3⁺ T regulatory cells mediating allograft tolerance depends on the CCR4 chemokine receptor. *J. Exp. Med.* **201**, 1037–1044 (2005).
38. Fox, J. M. et al. Structure/function relationships of CCR8 agonists and antagonists. Amino-terminal extension of CCL1 by a single amino acid generates a partial agonist. *J. Biol. Chem.* **281**, 36652–36661 (2006).
39. Freeman, C. M. et al. CCR8 is expressed by antigen-elicited, IL-10-producing CD4⁺CD25⁺ T cells, which regulate Th2-mediated granuloma formation in mice. *J. Immunol.* **174**, 1962–1970 (2005).
40. Sebastiani, S. et al. Chemokine receptor expression and function in CD4⁺ T lymphocytes with regulatory activity. *J. Immunol.* **166**, 996–1002 (2001).
41. Inngjerdigen, M., Damaj, B. & Maghazachi, A. A. Human NK cells express CC chemokine receptors 4 and 8 and respond to thymus and activation-regulated chemokine, macrophage-derived chemokine, and I-309. *J. Immunol.* **164**, 4048–4054 (2000).
42. Puttur, F. et al. Pulmonary environmental cues drive group 2 innate lymphoid cell dynamics in mice and humans. *Sci. Immunol.* **4**, eaav7638 (2019).
43. Sokol, C. L., Camire, R. B., Jones, M. C. & Luster, A. D. The chemokine receptor CCR8 promotes the migration of dendritic cells into the lymph node parenchyma to initiate the allergic immune response. *Immunity* **49**, 449–463 (2018).
44. De Simone, M. et al. Transcriptional landscape of human tissue lymphocytes unveils uniqueness of tumor-infiltrating T regulatory cells. *Immunity* **45**, 1135–1147 (2016).
45. Eruslanov, E. et al. Expansion of CCR8⁺ inflammatory myeloid cells in cancer patients with urothelial and renal carcinomas. *Clinical Cancer Res.* **19**, 1670–1680 (2013).
46. Mitsuyama, E., Kunori, Y., Kamimura, T. & Kaminuma, O. Functional chemokine receptors in allergic diseases: is CCR8 a novel therapeutic target? *Mini Rev. Med. Chem.* **6**, 463–466 (2006).
47. Islam, S. A. et al. Mouse CCL8, a CCR8 agonist, promotes atopic dermatitis by recruiting IL-5⁺ T(H)2 cells. *Nat. Immunol.* **12**, 167–177 (2011).
48. Vila-Caballer, M. et al. Disruption of the CCL1–CCR8 axis inhibits vascular Treg recruitment and function and promotes atherosclerosis in mice. *J. Mol. Cell. Cardiol.* **132**, 154–163 (2019).
49. Tiffany, H. L. et al. Identification of CCR8: a human monocyte and thymus receptor for the CC chemokine I-309. *J. Exp. Med.* **186**, 165–170 (1997).
50. Islam, S. A., Ling, M. F., Leung, J., Shreffler, W. G. & Luster, A. D. Identification of human CCR8 as a CCL18 receptor. *J. Exp. Med.* **210**, 1889–1898 (2013).
51. Liu, L. et al. Biological characterization of ligands targeting the human CC chemokine receptor 8 (CCR8) reveals the biased signaling properties of small molecule agonists. *Biochem. Pharmacol.* **188**, 114565 (2021).
52. Haas, J. et al. Specific recruitment of regulatory T cells into the CSF in lymphomatous and carcinomatous meningitis. *Blood* **111**, 761–766 (2008).
53. Oo, Y. H. et al. Distinct roles for CCR4 and CXCR3 in the recruitment and positioning of regulatory T cells in the inflamed human liver. *J. Immunol.* **184**, 2886–2898 (2010).
54. Feng, G. et al. CCL17 aggravates myocardial injury by suppressing recruitment of regulatory T cells. *Circulation* **145**, 765–782 (2022).
55. Goldie, S. J. et al. Loss of GRHL3 leads to TARC/CCL17-mediated keratinocyte proliferation in the epidermis. *Cell Death Dis.* **9**, 1072 (2018).
56. Chen, L., Wu, J., Pier, E., Zhao, Y. & Shen, Z. mTORC2-PKBα/Akt1 serine 473 phosphorylation axis is essential for regulation of FOXP3 stability by chemokine CCL3 in psoriasis. *J. Investig. Dermatol.* **133**, 418–428 (2013).
57. Yang, L.-X. et al. Atorvastatin inhibits the 5-lipoxygenase pathway and expression of CCL3 to alleviate atherosclerotic lesions in atherosclerotic ApoE knockout mice. *J. Cardiovasc. Pharmacol.* **62**, 205–211 (2013).
58. Ishida, Y. et al. Prevention of CaCl₂-induced aortic inflammation and subsequent aneurysm formation by the CCL3–CCR5 axis. *Nat. Commun.* **11**, 5994 (2020).
59. Braunersreuther, V. et al. Ccr5 but not Ccr1 deficiency reduces development of diet-induced atherosclerosis in mice. *Arterioscler. Thromb. Vasc. Biol.* **27**, 373–379 (2007).
60. Bachelierie, F. et al. International union of basic and clinical pharmacology. [corrected]. LXXXIX. Update on the extended family of chemokine receptors and introducing a new nomenclature for atypical chemokine receptors. *Pharmacol. Rev.* **66**, 1–79 (2014).
61. Huser, N. et al. CCR4-deficient mice show prolonged graft survival in a chronic cardiac transplant rejection model. *Eur. J. Immunol.* **35**, 128–138 (2005).
62. Zerneck, A. et al. Deficiency in CCR5 but not CCR1 protects against neointima formation in atherosclerosis-prone mice: involvement of IL-10. *Blood* **107**, 4240–4243 (2006).
63. Doring, Y. et al. CXCL12 derived from endothelial cells promotes atherosclerosis to drive coronary artery disease. *Circulation* **139**, 1338–1340 (2019).
64. Park, I. et al. C-type lectin receptor CLEC4A2 promotes tissue adaptation of macrophages and protects against atherosclerosis. *Nat. Commun.* **13**, 215 (2022).
65. Domogalla, M. P., Rostan, P. V., Raker, V. K. & Steinbrink, K. Tolerance through education: how tolerogenic dendritic cells shape immunity. *Front. Immunol.* **8**, 1764 (2017).

66. Vendelova, E. et al. Tolerogenic transcriptional signatures of steady-state and pathogen-induced dendritic cells. *Front. Immunol.* **9**, 333 (2018).
67. Kryczanowsky, F., Raker, V., Graulich, E., Domogalla, M. P. & Steinbrink, K. IL-10-modulated human dendritic cells for clinical use: identification of a stable and migratory subset with improved tolerogenic activity. *J. Immunol.* **197**, 3607–3617 (2016).
68. Feierler, J. et al. Helix 8 plays a crucial role in bradykinin B(2) receptor trafficking and signaling. *J. Biol. Chem.* **286**, 43282–43293 (2011).
69. von Hundelshausen, P. et al. Heterophilic interactions of platelet factor 4 and RANTES promote monocyte arrest on endothelium. *Blood* **105**, 924–930 (2005).
70. Holdt, L. M. et al. ANRIL expression is associated with atherosclerosis risk at chromosome 9p21. *Arterioscler. Thromb. Vasc. Biol.* **30**, 620–627 (2010).
71. Holdt, L. M. et al. Circular non-coding RNA ANRIL modulates ribosomal RNA maturation and atherosclerosis in humans. *Nat. Commun.* **7**, 12429 (2016).
72. El Housni, H., Heimann, P., Parma, J. & Vassart, G. Single-nucleotide polymorphism genotyping by melting analysis of dual-labeled probes: examples using factor V Leiden and prothrombin 20210A mutations. *Clin. Chem.* **49**, 1669–1672 (2003).
73. Ayari, H. & Bricca, G. Identification of two genes potentially associated in iron-heme homeostasis in human carotid plaque using microarray analysis. *J. Biosci.* **38**, 311–315 (2013).
74. Doring, Y. et al. Auto-antigenic protein-DNA complexes stimulate plasmacytoid dendritic cells to promote atherosclerosis. *Circulation* **125**, 1673–1683 (2012).
75. Cagnin, S. et al. Reconstruction and functional analysis of altered molecular pathways in human atherosclerotic arteries. *BMC Genomics* **10**, 13 (2009).
76. Satija, R., Farrell, J. A., Gennert, D., Schier, A. F. & Regev, A. Spatial reconstruction of single-cell gene expression data. *Nat. Biotechnol.* **33**, 495–502 (2015).
77. Stuart, T. et al. Comprehensive integration of single-cell data. *Cell* **177**, 1888–1902 (2019).
78. Ardouin, L. et al. Broad and largely concordant molecular changes characterize tolerogenic and immunogenic dendritic cell maturation in thymus and periphery. *Immunity* **45**, 305–318 (2016).

Acknowledgements

We are indebted to A. Rot (Queen Mary University) for thoughtful discussions. We thank L. Saroyan, O. Schengel and staff at the animal facility (all LMU Munich) for excellent technical assistance. We thank S. Michaelides (LMU Munich) for generously providing Jurkat CCR4- and CCR8-transfectants, K. Pfeffer (Heinrich-Heine-Universität) for kindly providing *Ccr4*^{-/-} mice and I. Förster (Universität Bonn) for generously providing *Ccl17*^{+/e} (GFP reporter knock-in) mice. This work was supported by Deutsche Forschungsgemeinschaft (DFG) SFB1123-A1/A10 to Y.D. and C.W., SFB1123-A2 to P.v.H., SFB1123-B1 to D.T. and L.H., SFB1123-Z1 to R.T.A.M., SFB1123-A5 to D.A., SFB1123-B5 to D.S. and 390857198-EXC 2145 to C.W.; by the European Research Council (AdG °692511 to C.W.); by the German Ministry of Education and Research (BMBF) and the German Center for Cardiovascular Research (DZHK) to Y.D., C.W., D.S. and E.P.C.v.d.V. (81X2600254, 81Z0600202 and 81Z0600203); by grants from the Interdisciplinary Center for Clinical Research within the faculty of Medicine at the RWTH Aachen University and NWO-ZonMw Veni (91619053) to E.P.C.v.d.V.; by the DFG YI 133/3-5 and Friedrich-Baur-Stiftung 39/20 to C.Y.; by the DFG HA 1083/15-4, HA 1083/15-5 and ERA-CVD (PLAQUEFIGHT) 01KL1808 to A.J.R.H. and ERA-CVD (Atheroinside) 01KL1908 to R.T.A.M. The position of L.P. was kindly supported by DZHK (81X2600271). C.W. is van der Laar-Professor of Atherosclerosis.

Author contributions

Y.D. conceived and supervised the study, designed experiments, provided funding performed experiments, analyzed data and wrote the manuscript. E.P.C.v.d.V. supervised the study, designed experiments, performed experiments, analyzed data and contributed to writing the manuscript. Y.Y. and C.N. designed experiments, performed experiments and analyzed the data. Y.J. performed and analyzed mouse experiments and data. X.B., J.L. and Y.L. performed and analyzed plasmon resonance and receptor binding assays. M.K., S.B., L.J.F.P., S.G., L.P. and R.T.A.M. contributed to the conduction of mouse experiments and data analysis. M.H. and K.B. performed cell culture and cell-sorting experiments; C.Y., X.Z. and A.J.R.H. contributed to scRNA-seq experiments and data analysis. A.F. helped to perform and analyze cAMP signaling assays and provided critical reagents. D.T. and L.H. provided human plaque material and analysis. C.M. and I.P. provided critical reagents, contributed to scRNA-seq experiments and data analysis and provided intellectual input. M.K., K.N. and D.A. contributed to T_{reg} suppression and T cell migration studies. D.S. provided critical revision of the manuscript, analyzed data and calculated statistics. P.v.H. contributed to receptor binding experiments, analyzed data, provided supervision and intellectual input, and contributed to writing the manuscript. C.W. conceived and supervised the study, designed experiments, provided funding and wrote the manuscript.

Competing interests

The authors declare no competing interests.

Additional information

Extended data is available for this paper at <https://doi.org/10.1038/s44161-023-00413-9>.

Supplementary information The online version contains supplementary material available at <https://doi.org/10.1038/s44161-023-00413-9>.

Correspondence and requests for materials should be addressed to Yvonne Döring or Christian Weber.

Peer review information *Nature Cardiovascular Research* thanks Christoph Binder, and the other, anonymous, reviewer(s) for their contribution to the peer review of this work.

Reprints and permissions information is available at www.nature.com/reprints.

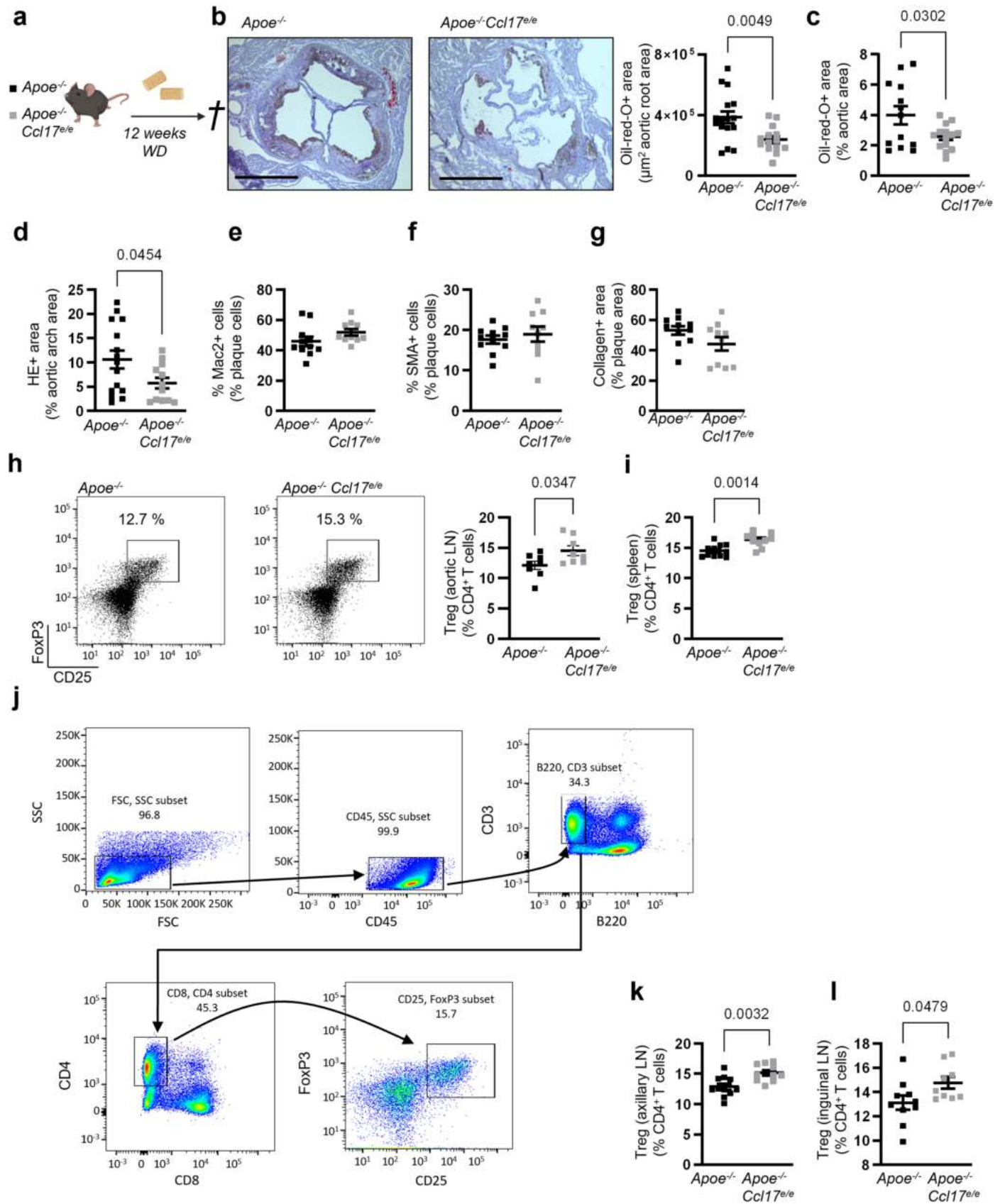
Publisher's note Springer Nature remains neutral with regard to jurisdictional claims in published maps and institutional affiliations.

Open Access This article is licensed under a Creative Commons Attribution 4.0 International License, which permits use, sharing, adaptation, distribution and reproduction in any medium or format, as long as you give appropriate credit to the original author(s) and the source, provide a link to the Creative Commons license, and indicate if changes were made. The images or other third party material in this article are included in the article's Creative Commons license, unless indicated otherwise in a credit line to the material. If material is not included in the article's Creative Commons license and your intended use is not permitted by statutory regulation or exceeds the permitted use, you will need to obtain permission directly from the copyright holder. To view a copy of this license, visit <http://creativecommons.org/licenses/by/4.0/>.

© The Author(s) 2024

¹Division of Angiology, Swiss Cardiovascular Center, Inselspital, Bern University Hospital, University of Bern, Bern, Switzerland. ²Institute for Cardiovascular Prevention (IPEK), LMU Munich, Munich, Germany. ³DZHK (German Centre for Cardiovascular Research), partner site Munich Heart Alliance, Munich, Germany. ⁴Interdisciplinary Center for Clinical Research (IZKF), RWTH Aachen University, Aachen, Germany. ⁵Institute for Molecular Cardiovascular Research (IMCAR), RWTH Aachen University, Aachen, Germany. ⁶Department of Pathology, Cardiovascular Research Institute Maastricht (CARIM), Maastricht University Medical Centre, Maastricht, the Netherlands. ⁷Pediatric Translational Medicine Institute and Shanghai Institute of Pediatric Congenital Heart Disease, Shanghai Children's Medical Center, School of Medicine, Shanghai Jiao Tong University, Shanghai, China. ⁸Munich Cluster for Systems Neurology (SyNergy), Munich, Germany. ⁹The Kennedy Institute of Rheumatology, Nuffield Department of Orthopedics, Rheumatology and Musculoskeletal Sciences, University of Oxford, Oxford, UK. ¹⁰Institute of Laboratory Medicine, University Hospital, LMU Munich, Munich, Germany. ¹¹Department of Biomedical Engineering, Cardiovascular Research Institute Maastricht (CARIM), Maastricht University, Maastricht, the Netherlands. ¹²Walther Straub Institute of Pharmacology and Toxicology, LMU Munich, Munich, Germany. ¹³Institute for Genetic and Biomedical Research (IRGB), Unit of Milan, National Research Council, Milan, Italy. ¹⁴Department of Biochemistry, Cardiovascular Research Institute Maastricht (CARIM), Maastricht University, Maastricht, the Netherlands. ¹⁵These authors contributed equally: Yvonne Döring, Emiel P. C. van der Vorst, Yi Yan, Carlos Neideck.

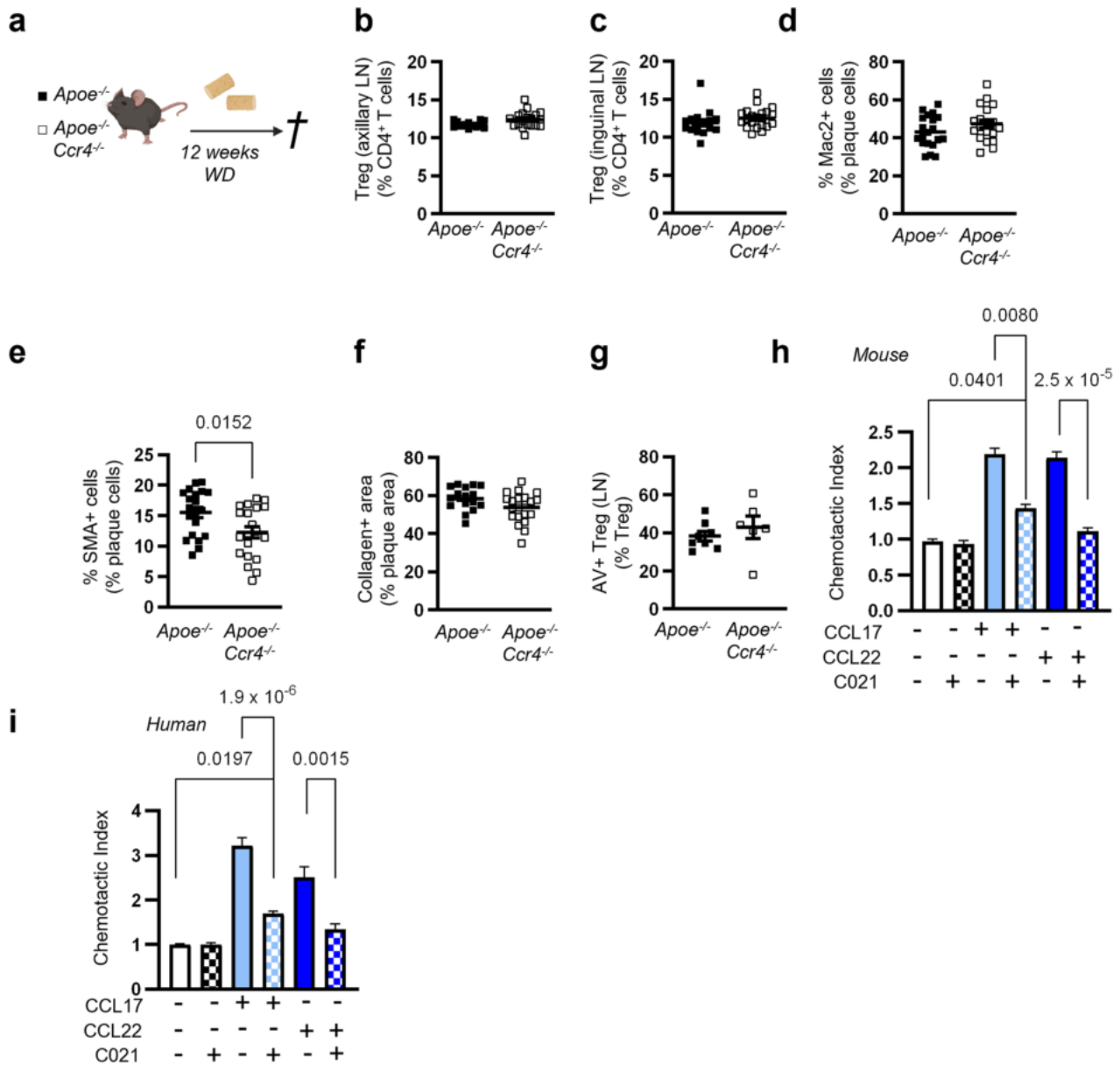
✉ e-mail: yvonne.doering@unibe.ch; chweber@med.lmu.de



Extended Data Fig. 1 | See next page for caption.

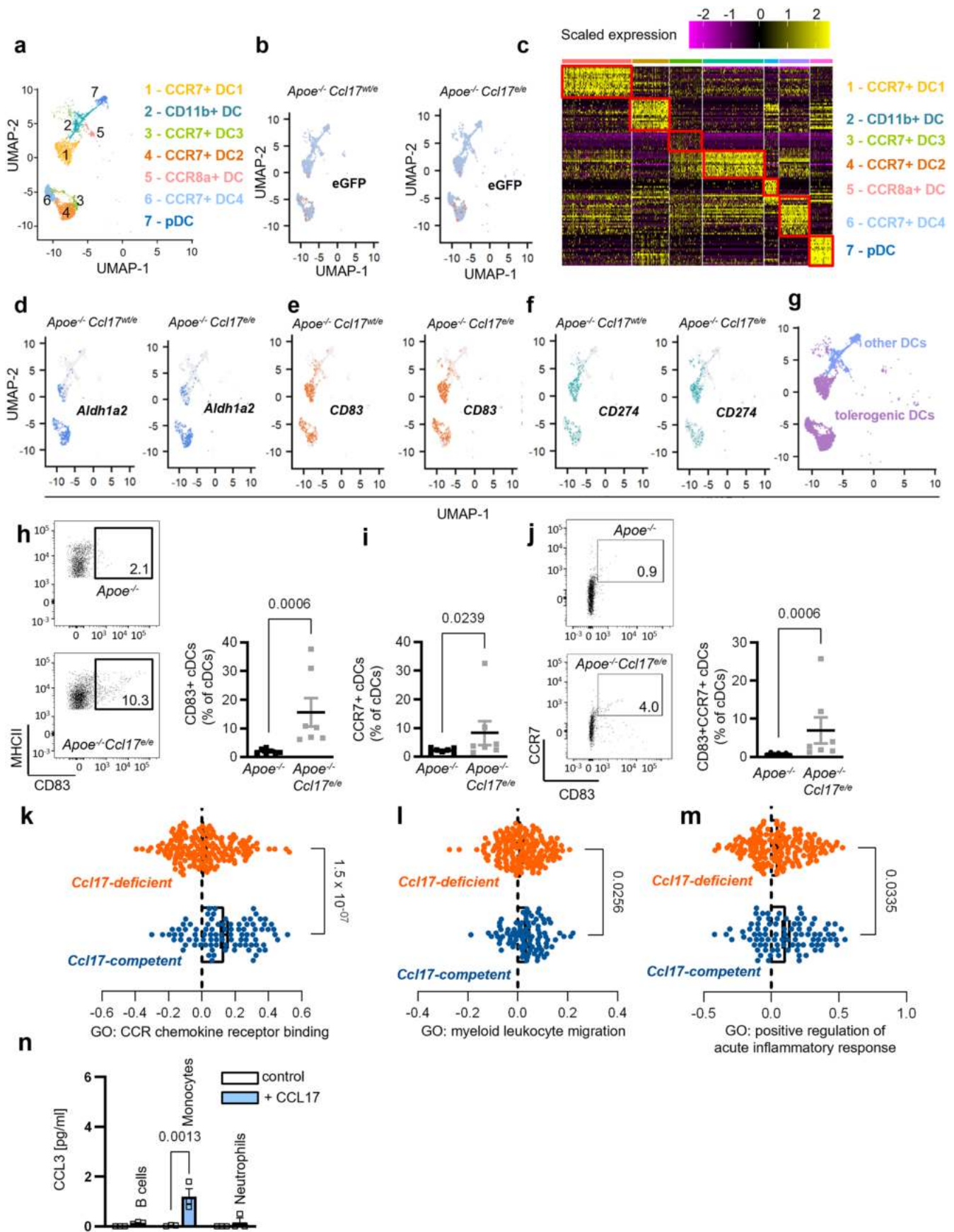
Extended Data Fig. 1 | Effects of CCL17 deficiency on atherosclerosis and Treg numbers. (a) Experimental scheme of *ApoE*^{-/-} or *ApoE*^{-/-}*Ccl17*^{+/e} mice fed a Western-diet (WD) for 12 weeks; (b) Representative images and quantification of lesion area of *ApoE*^{-/-} (n = 16) or *ApoE*^{-/-}*Ccl17*^{+/e} (n = 14) mice measured after Oil-Red-O staining (ORO) for lipid deposits in the aortic root. Scale bar = 500 μm; (c) Quantification of lesion area measured after ORO for lipid deposits in the thoraco-abdominal of *ApoE*^{-/-} (n = 13) or *ApoE*^{-/-}*Ccl17*^{+/e} (n = 14); (d) Atherosclerotic lesion size in aortic arches of *ApoE*^{-/-} (n = 15) or *ApoE*^{-/-}*Ccl17*^{+/e} (n = 12), as quantified after H&E staining; (e-g) Quantification of the percentage of lesional Mac2⁺ macrophages (e), smooth muscle α-actin

(SMA)⁺ smooth muscle cells (SMCs) (f) and collagen content (g) of *ApoE*^{-/-} (n = 11) or *ApoE*^{-/-}*Ccl17*^{+/e} (n = 10) mice fed a WD for 12 weeks; (h-i) Representative dot plots and flow cytometric quantification of CD45⁺CD3⁺CD4⁺CD25⁺FoxP3⁺ Tregs in para-aortic lymph nodes (LNs) (h) and spleen (i) of *ApoE*^{-/-} (h, n = 8; i, n = 11) or *ApoE*^{-/-}*Ccl17*^{+/e} (h, n = 8; i, n = 10) mice; (j) Gating strategy for CD45⁺CD3⁺CD4⁺CD25⁺FoxP3⁺ Tregs in lymphatic organs; (k-l) flow cytometric quantification of CD45⁺CD3⁺CD4⁺CD25⁺FoxP3⁺ Tregs in axillary (k) and inguinal LNs (l) of *ApoE*^{-/-} (k, n = 11; l, n = 10) or *ApoE*^{-/-}*Ccl17*^{+/e} (k, n = 10; l, n = 9) mice; (a-l) Data represent mean ± SEM. Two-sided *P* values as indicated and analyzed by unpaired Student's *t*-test.



Extended Data Fig. 2 | Effects of CCR4 deficiency on atherosclerosis and CCL17-induced migration via CCR4. (a) Experimental scheme of $Apoe^{-/-}$ or $Apoe^{-/-} Ccr4^{-/-}$ mice fed a Western-diet (WD) for 12 weeks; (b, c) Flow cytometric quantification of CD45⁺CD3⁺CD4⁺CD25⁺FoxP3⁺ Tregs, axillary (b) and inguinal LNs (c) of $Apoe^{-/-}$ (b, n = 13; c, n = 16) or $Apoe^{-/-} Ccr4^{-/-}$ (b, n = 18; c, n = 20) mice after 12 weeks of WD; (d-f) Quantification of the percentage of lesional Mac2⁺ macrophages (d), SMA⁺ SMCs (e) and collagen content (f) in $Apoe^{-/-}$ (d, e n = 20; f, n = 19) or $Apoe^{-/-} Ccr4^{-/-}$ (d, n = 19; e, n = 20; f = 16) mice fed a WD for 12 weeks; (g) Analysis of Annexin-V (AnnV) expression on Tregs (CD45⁺CD3⁺CD4⁺CD25⁺FoxP3⁺) from isolated LNs (para-aortic, axillary and inguinal combined) of $Apoe^{-/-}$ (n = 8) or $Apoe^{-/-} Ccl17^{fl/e}$ (n = 6); (h) Transwell migration assay with CD4⁺ T cells (isolated from $Apoe^{-/-}$ mice) towards recombinant mouse CCL17 (100 ng/ml) or CCL22 (50 ng/ml) in the presence or absence of the CCR4 inhibitor

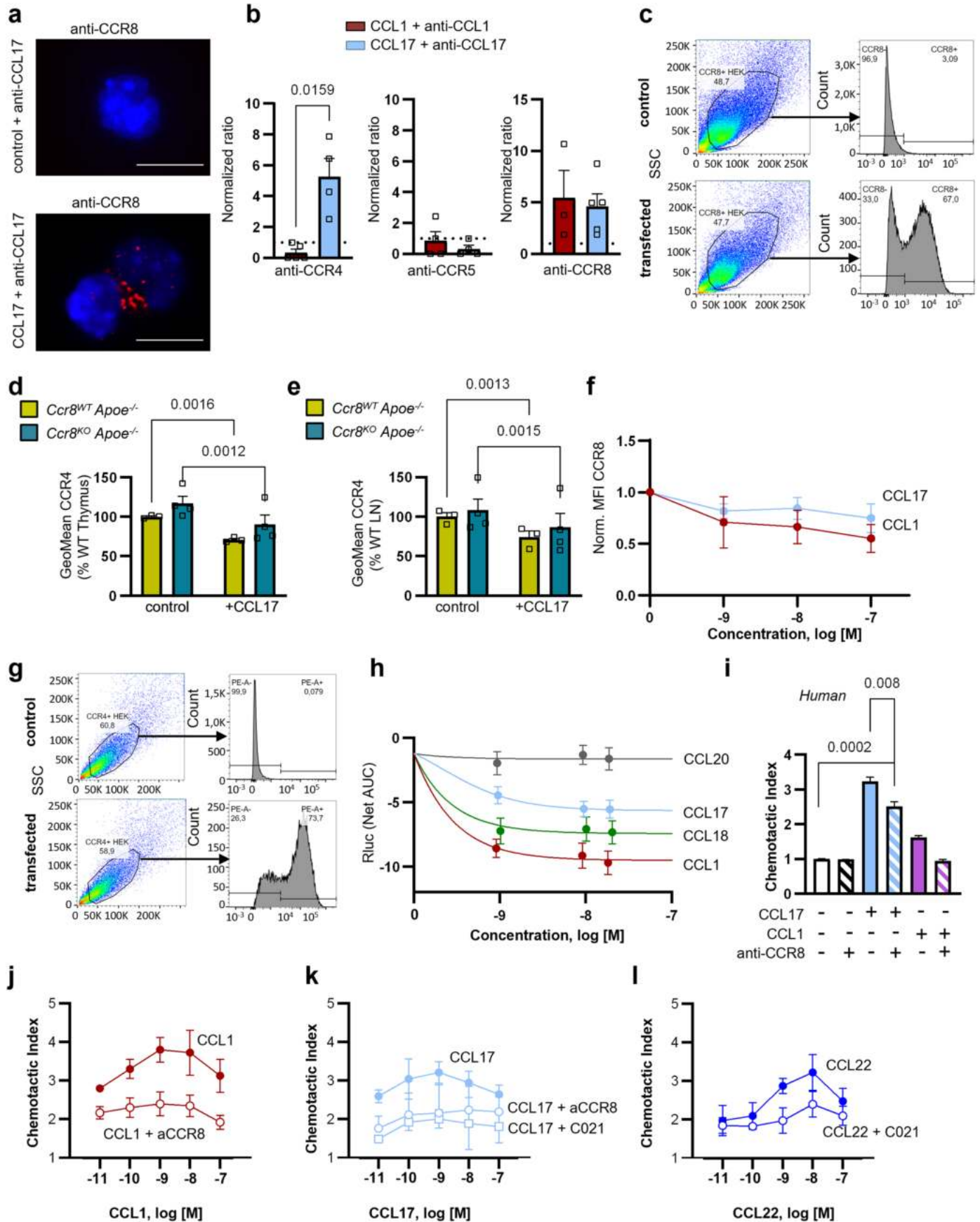
C021 dihydrochloride (0.5 μM), number of replicates in parentheses over number of independent experiments per bar from left to right: n = (40)8, (40)8, (27)6, (27)6, (25)5, (25)5; (i) Transwell migration assay with CD4⁺ T cells (isolated from human blood PBMCs) towards recombinant human CCL17 (100 ng/ml) or CCL22 (50 ng/ml), in the presence or absence of the CCR4 inhibitor C021 dihydrochloride (0.5 μM), number of replicates in parentheses over number of independent experiments per bar from left to right: n = (37)7, (33)7, (31)5, (28)5, (16)4, (16)4; (h, i) All migrated cells were quantified by flow cytometry, chemotactic index calculated as the ratio of chemokine-stimulated and unstimulated migration is depicted; (a-i) Data represent mean ± SEM. Two-sided P values as indicated and analyzed by unpaired Student's t-test, Mann-Whitney U (b-h), or nested ANOVA with Holm-Šidák's post hoc test (h, i).



Extended Data Fig. 3 | See next page for caption.

Extended Data Fig. 3 | Identification of tolerogenic DCs in the LNs of *Apoe*^{-/-} *Ccl17*^{wt/e} or *Apoe*^{-/-} *Ccl17*^{el/e} mice. (a) UMAP projection of 4,731 single cells, colored by inferred cell types, in sorted cells (viable CD45⁺CD3⁻CD11c⁺) from LNs of *Apoe*^{-/-} *Ccl17*^{wt/e} or *Apoe*^{-/-} *Ccl17*^{el/e} mice; (b) UMAP visualization overlaid with the expression of eGFP⁺ *Apoe*^{-/-} *Ccl17*^{wt/e} (left panels) or *Apoe*^{-/-} *Ccl17*^{el/e} (right panel); (c) Heat map of the top 20 marker genes from each cluster and cell type assignment of each cluster; (d-f) UMAP visualization overlaid with the expression of *Aldh1a2* (d), *Cd83* (e) and *Cd274* (f) in 7 distinct DC clusters of sorted cells (viable CD45⁺CD3⁻CD11c⁺) from LNs of *Apoe*^{-/-} *Ccl17*^{wt/e} (left panel) or *Apoe*^{-/-} *Ccl17*^{el/e} (right panel) mice; (g) UMAP projection of single cells, colored by inferred cell types including tolerogenic DCs and other DCs, in sorted cells (viable CD45⁺CD3⁻CD11c⁺) from LNs of *Apoe*^{-/-} *Ccl17*^{wt/e} or *Apoe*^{-/-} *Ccl17*^{el/e} mice; (h-j) Representative dot plots and flow cytometric quantification of CD83⁺ (h), CCR7⁺ (i) and CD83⁺CCR7⁺ (j) tolerogenic DCs among CD45⁺CD11c⁺ MHCII⁺ cDCs

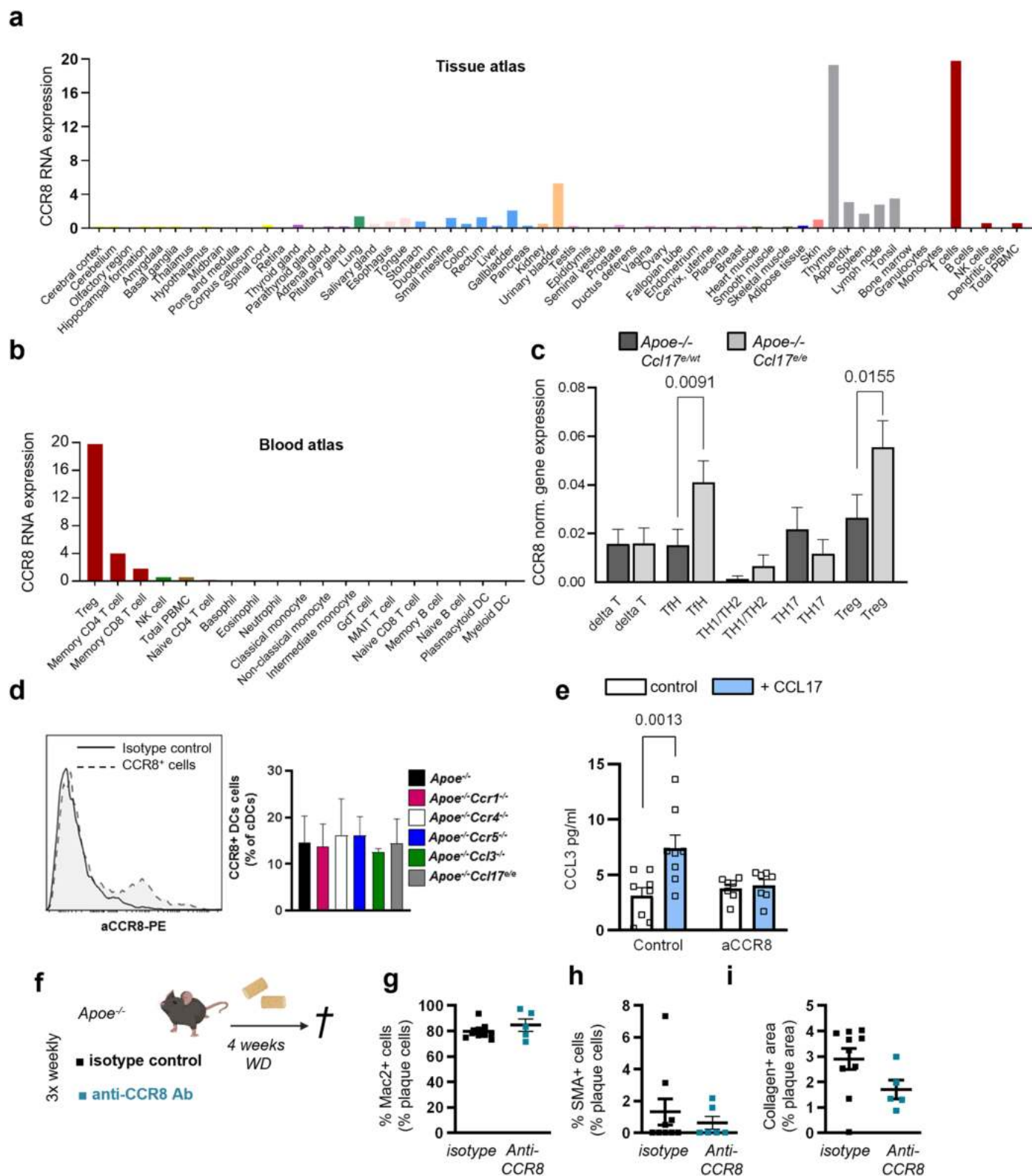
in aortic LNs of *Apoe*^{-/-} or *Apoe*^{-/-} *Ccl17*^{el/e} mice (h-j; each bar n = 7); (k-m) GSVA score was calculated in GO term CCR chemokine receptor binding (k), myeloid leukocyte migration (l) and positive regulation of acute inflammatory response (m) in n = 172 eGFP-expressing CCL17-deficient cells from tolerogenic DCs of *Apoe*^{-/-} *Ccl17*^{el/e} mice or n = 92 CCL17-expressing cells from tolerogenic DCs of *Apoe*^{-/-} *Ccl17*^{wt/e} mice fed on a chow diet; (n) Sorted CD19⁺B220⁺ B cells from lymph nodes (LNs), isolated CD115⁺ monocytes and Ly6G⁺ neutrophils from spleen and bone marrow were cultured for 4 hours in the presence or absence of recombinant mouse CCL17 (100 ng/ml). CCL3 concentrations in the supernatant were measured by multiplex bead array (each condition n = 3); (a-n) Data represent mean ± SEM. Two-sided *P* values as indicated and analyzed compared to control by Mann-Whitney *U*-test (h-j), unpaired Student's *t*-test (k-m), or two-way ANOVA with Holm-Sídák's post hoc test (n).



Extended Data Fig. 4 | See next page for caption.

Extended Data Fig. 4 | Analysis of CCR8 ligand binding, internalization and migration capacities. (a, b) Interactions between mouse CCL17 or CCL1 and CCR4, CCR5 or CCR8 were assessed on the surface of adherent cDCs isolated from LNs of *ApoE*^{-/-} mice using Duolink proximity-ligation assay after incubation with recombinant mouse CCL17, CCL1 (100 ng/ml) or PBS (control) and respective antibodies to CCR4, CCR5 and CCR8, as indicated. **(a)** Shown are representative images recorded with a Leica SP8 confocal microscope for anti-CCR8 and anti-CCL17 after PBS and CCL17 treatment (scale bar = 10 μ m); **(b)** Signals generated by interactions between ligands and receptors on the cDC surface were quantified and normalized to untreated controls (dotted line); number of independent experiments per bar from left to right: n = 5, 4, 4, 4, 3, 5; **(c)** Representative histograms displaying CCR8 expression in HEK293 CCR8-transfectants and controls; **(d, e)** CCR4 internalization in CCR8-deficient or CCR8-competent CD4⁺ T cells from thymus **(d, e)**, number of independent experiments per bar from left to right: n = 3, 4, 3, 4) and LNs **(e, e)**, number of independent experiments per bar from left to right: n = 3, 4, 3, 4) stimulated with CCL17 (100 ng/ml) or vehicle and analyzed by flow cytometry; **(f)** Dose-response curve to compare CCR8 internalization by CCL1 and CCL17 at indicated concentrations in primary CCR8-expressing human T cells; **(g)** Representative

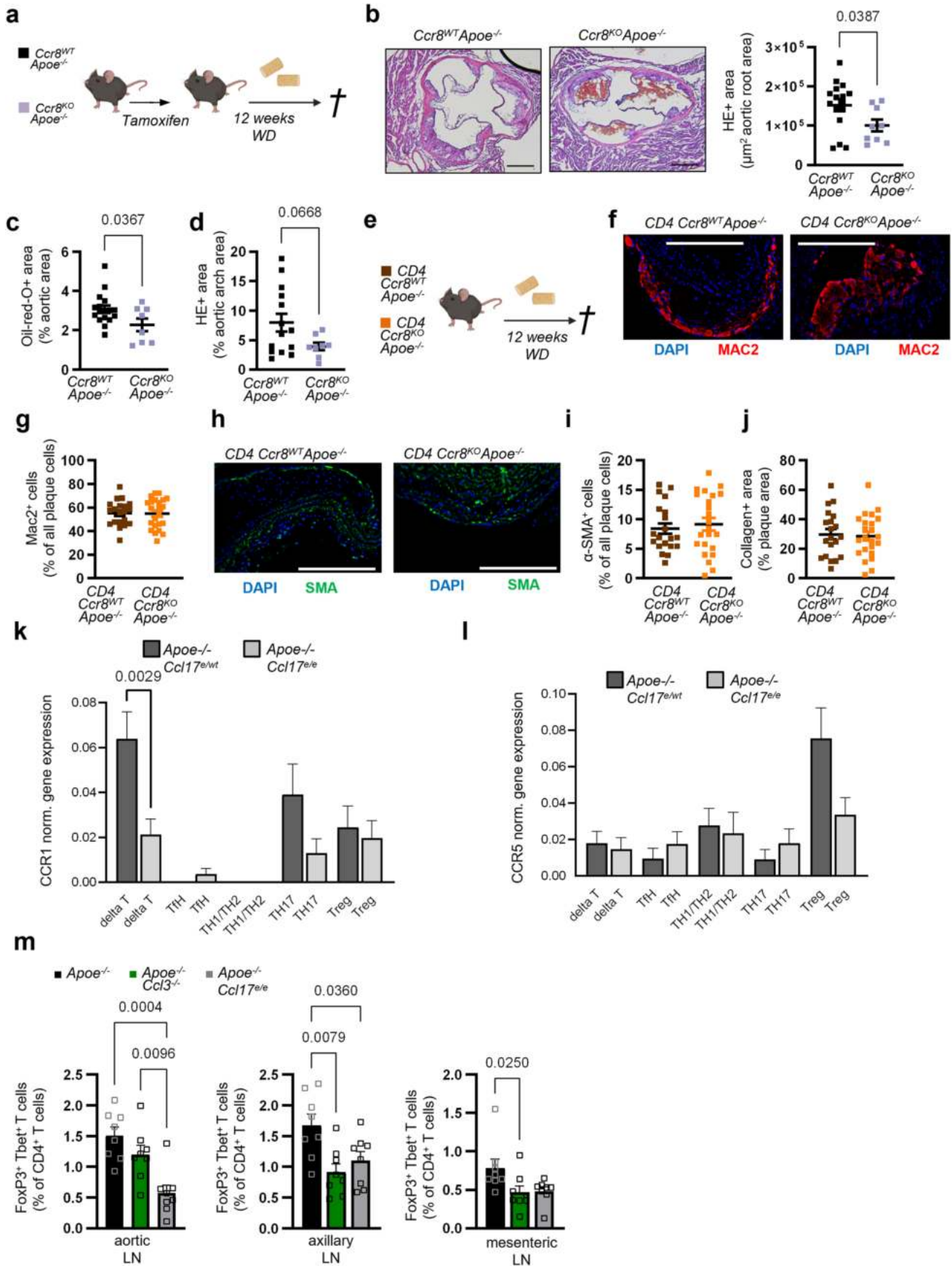
histograms displaying CCR4 expression in HEK293 CCR4-transfectants and controls; **(h)** Area under the curve (AUC) for RLuc in Glosensor assays monitoring cAMP levels in HEK293 CCR8-transfectants to obtain dose-response curves for CCL1, CCL17, CCL18 or irrelevant CCL20 using indicated concentrations (CCL1, CCL18, CCL20, n = 6 independent experiments; CCL17, n = 3 independent experiments); **(i)** Transwell migration assay with human CD4⁺ T cells towards recombinant human CCL17 (100 ng/ml) or CCL1 (50 ng/ml) in the presence or absence of a blocking antibody to CCR8 (2 μ g/ml). Migrated cells were quantified by flow cytometry; number of replicates in parentheses over number of independent experiments per bar from left to right: n = (40)8, (16)5, (46)8, (21)5, (18)5, (18)5; **(j-l)** Transwell migration assays depicted as dose-response curves of *ApoE*^{-/-} CD4⁺ T cell migration induced by CCL1 **(j)**, CCL17 **(k)** or CCL22 **(l)** at indicated concentrations in the presence or absence of anti-CCR8 antibody (2 μ g/ml) or CO21 (0.5 μ M) **(j-l)**, n = 4 independent experiments; CCL17+anti-CCR8, n = 3 independent experiments). **(a-l)** Data represent mean \pm SEM. Two-sided *P* values as indicated and analyzed by Mann-Whitney *U*-test or unpaired Student's *t*-test **(b)**, two-way ANOVA **(d, e)** or nested ANOVA **(i)** with Holm-Šidák's post hoc test **(d, e)**, generalized linear model **(f)**.



Extended Data Fig. 5 | See next page for caption.

Extended Data Fig. 5 | Analysis of CCR8 transcript expression across tissues and cell types and consequences of CCR8 blocking. (a) *CCR8* mRNA expression in different tissues of consensus datasets from *The Human Protein Atlas*. Tissues of the same system (nervous system, endocrine system, digestion system, etc.) are depicted in the same color; (b) *CCR8* mRNA expression in different blood cell types of consensus datasets from *The Human Protein Atlas*; (c) *Ccr8* mRNA expression in different T cell populations of the para-aortic LNs from *ApoE*^{-/-} *Ccl17*^{wt/wt} and *ApoE*^{-/-} *Ccl17*^{fl/e} mice fed a WD for 6 weeks; (d) Flow cytometric quantification of CCR8 expression on DCs from LN of the indicated mouse strains (n = 5 per strain); (e) CCL3 titers in supernatants of CD4⁺ T cells from *ApoE*^{-/-} mice stimulated with CCL17 or vehicle for 4 hours in the presence or absence

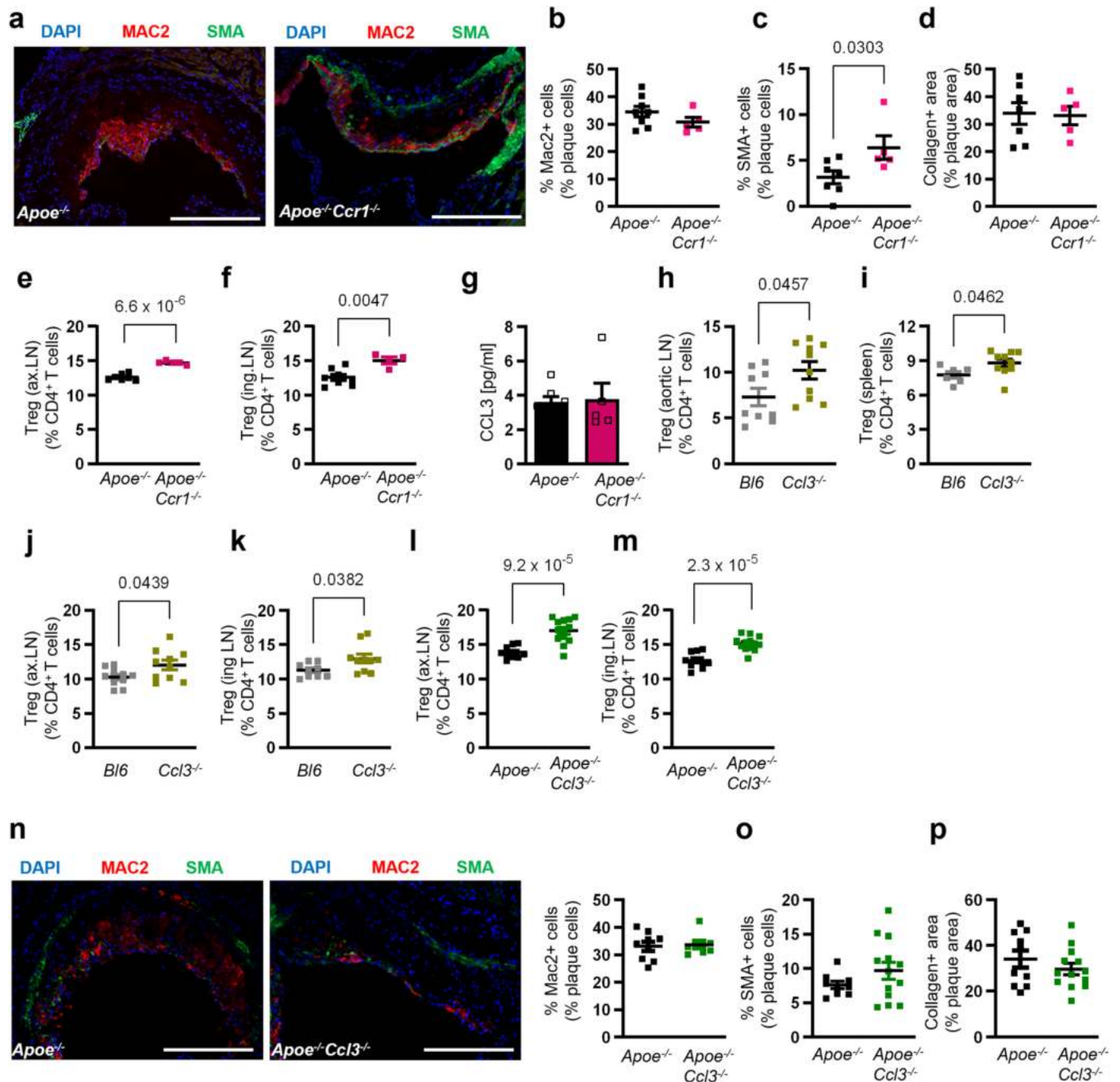
of an antibody to CCR8 (number of replicates in parentheses over number of independent experiments per bar from left to right: n = 8, 8, 7, 7); (f) Experimental scheme of *ApoE*^{-/-} mice injected with isotype control or CCR8-blocking antibody during WD feeding for 4 weeks. (g-i) Quantification of the percentage of lesional Mac2⁺ macrophages (g, isotype, n = 9; anti-CCR8, n = 5), SMA⁺ SMCs (h, isotype, n = 9; anti-CCR8, n = 6) and collagen content (i, isotype, n = 10; anti-CCR8, n = 5) of *ApoE*^{-/-} mice receiving an isotype or CCR8 blocking antibody during WD feeding for 4 weeks. (a-i) Data represent mean ± SEM. Two-sided *P* values as indicated and analyzed by Mann-Whitney *U*-test or unpaired Student's *t*-test (c, g-i) or two-way ANOVA with Holm-Šidák's post hoc test (e).



Extended Data Fig. 6 | See next page for caption.

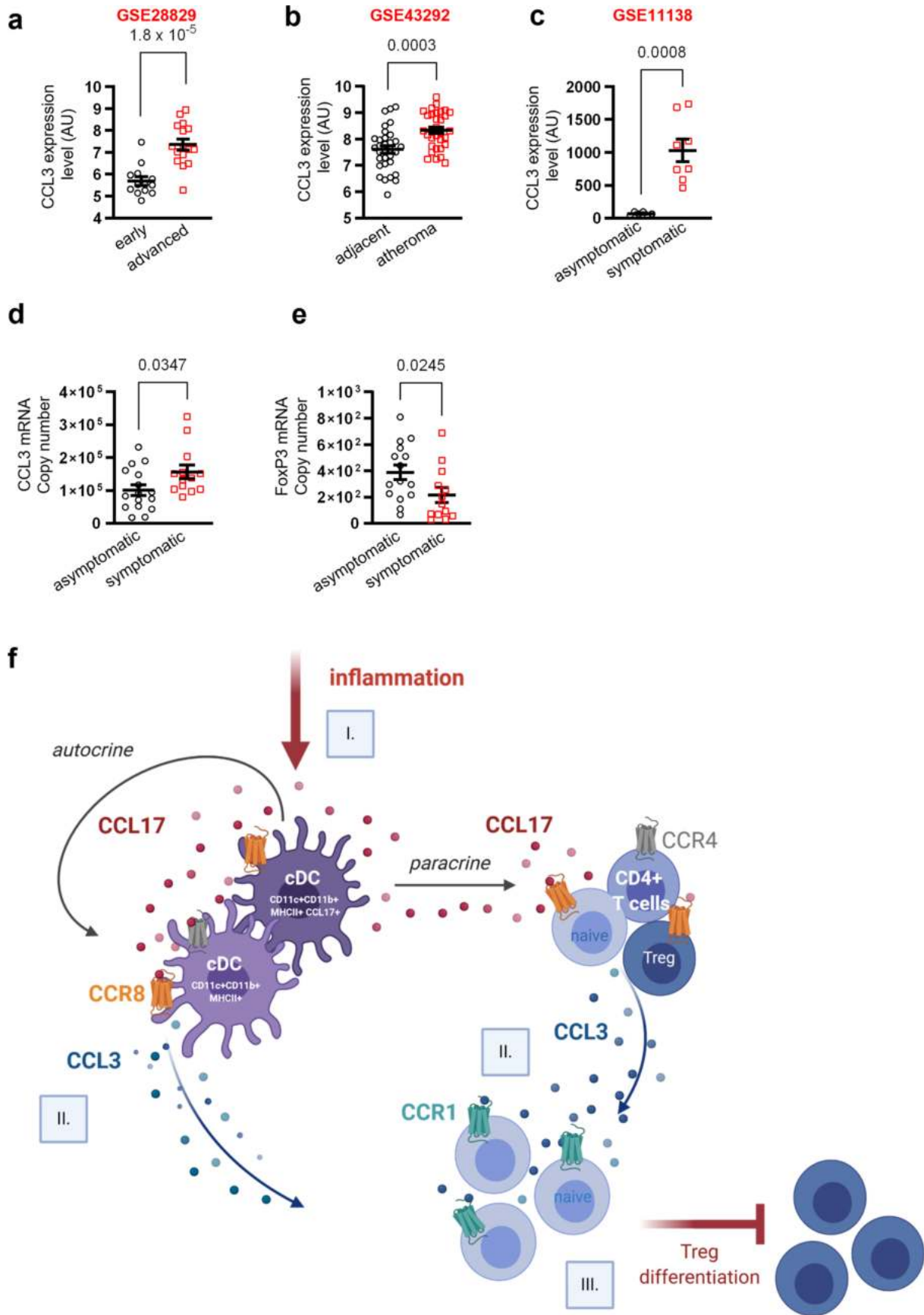
Extended Data Fig. 6 | Effect of systemic and T cell-specific CCR8 deficiency on atherosclerosis and analysis of CCR1 and CCR5 expression in different T cell subsets. (a) Experimental scheme of $CD4^{Cre} Ccr8^{flax/flax} ApoE^{-/-}$ ($CD4Ccr8^{WT} ApoE^{-/-}$) and $CD4^{Cre} Ccr8^{flax/flax} ApoE^{-/-} (CD4Ccr8^{KO} ApoE^{-/-})$ mice fed a WD for 12 weeks; (b) Representative images and quantification of lesion area measured after HE-staining in the aortic root of $CD4Ccr8^{WT} ApoE^{-/-}$ (n = 16) or $CD4Ccr8^{KO} ApoE^{-/-}$ (n = 9) mice. Scale bar = 500 μ m; (c) Quantification of lesion area measured after Oil-Red-O staining for lipid deposits in the thoraco-abdominal aorta of $CD4Ccr8^{WT} ApoE^{-/-}$ (n = 17) or $CD4Ccr8^{KO} ApoE^{-/-}$ (n = 8) mice. (d) Atherosclerotic lesion size in the aortic arch, as quantified after H&E staining in $CD4Ccr8^{WT} ApoE^{-/-}$ (n = 14) or $CD4Ccr8^{KO} ApoE^{-/-}$ (n = 8) mice. (e) Experimental scheme of $CD4Ccr8^{WT} ApoE^{-/-}$ or $CD4Ccr8^{KO} ApoE^{-/-}$ mice fed a WD for 12 weeks; (f-j) Representative images and quantification of the percentage of lesional

Mac2⁺ macrophages (f,g) or SMA⁺ SMCs (h,i) and collagen content (j) in aortic arch sections of $CD4Ccr8^{WT} ApoE^{-/-}$ (g,i,j all n = 20) or $CD4Ccr8^{KO} ApoE^{-/-}$ (g,i,j all n = 23) mice fed a WD for 12 weeks. Scale bar = 250 μ m; (k,l) *Ccr1* and *Ccr5* mRNA expression in different T cell populations of the para-aortic LNs from $ApoE^{-/-} Ccl17^{+/wt}$ and $ApoE^{-/-} Ccl17^{+/e}$ mice fed a WD for 6 weeks; (m) Flow cytometric quantification of CD45⁺CD3⁺CD4⁺FoxP3⁺Tbet⁺ cells in aortic, axillary and mesenteric LNs of $ApoE^{-/-}$, $ApoE^{-/-} Ccl3^{-/-}$ or $ApoE^{-/-} Ccl17^{+/e}$ mice (all n = 8). (a-m). Data represent mean \pm SEM. Two-sided *P* values as indicated and analyzed by by Mann-Whitney *U* test or unpaired Student's *t*-test (b-j), multiple Mann-Whitney *U* test with false discovery rate (FDR) (k,l), one-way ANOVA with Holm-Šidák's post hoc test (aortic and axillary LNs) or Kruskal-Wallis *H* with Dunn's post hoc test (mesenteric LNs) (m).



Extended Data Fig. 7 | Effect of CCR1 and CCL3 on lesional characteristics and Treg numbers. (a) Representative images of staining for Mac2⁺ macrophages, SMA⁺ SMCs and DAPI (nuclei) in aortic root sections of *Apoe*^{-/-} or *Apoe*^{-/-} *Ccr1*^{-/-} mice after 12 weeks of WD. Scale bar = 250 μm; (b-d) Quantification of the percentage of lesional Mac2⁺ macrophages (b), SMA⁺ SMCs (c) and collagen content (d) in *Apoe*^{-/-} (b, n = 8; c, n = 7; d, n = 7) or *Apoe*^{-/-} *Ccr1*^{-/-} (b-d, n = 5 each) mice after 12 weeks of WD; (e-f) Quantification of Tregs (CD45⁺CD3⁺CD4⁺CD25⁺FoxP3⁺) in axillary (e) and inguinal LNs (f) of *Apoe*^{-/-} (e, n = 7; f, n = 8) *Apoe*^{-/-} *Ccr1*^{-/-} (e, n = 5; f, n = 4) mice after 12 weeks of WD; (g) Plasma concentrations of CCL3 in *Apoe*^{-/-} (n = 7) or *Apoe*^{-/-} *Ccr1*^{-/-} (n = 5) mice after 12 weeks of WD, as measured by ELISA; (h-k) Quantification of Tregs (CD45⁺CD3⁺CD4⁺CD25⁺FoxP3⁺) in aortic LN (h), spleen (i), axillary (j) and inguinal LNs (k) of *C57Bl6* (h, n = 9; i, n = 6; j,

n = 10; k, n = 9) or *Ccl3*^{-/-} (h-k, n = 10 each) mice; (l,m) Quantification of Tregs (CD45⁺CD3⁺CD4⁺CD25⁺FoxP3⁺) in axillary (l) and inguinal LNs (m) of *Apoe*^{-/-} (l, n = 9; m, n = 10) or *Apoe*^{-/-} *Ccl3*^{-/-} (l,m, n = 13 each) mice, after 12 weeks of WD; (n) Representative images of staining for Mac2⁺ macrophages, SMA⁺ SMCs and DAPI (nuclei) in aortic root sections of *Apoe*^{-/-} or *Apoe*^{-/-} *Ccl3*^{-/-} mice after 12 weeks of WD. Scale bar = 250 μm. (n-p) Quantification of the percentage of lesional Mac2⁺ macrophages (n), SMA⁺ SMCs (o) and collagen content (p) in aortic root sections of *Apoe*^{-/-} (n, n = 9; o, n = 9; p, n = 10) or *Apoe*^{-/-} *Ccl3*^{-/-} (n, n = 8; o, n = 13; p, n = 13) mice after 12 weeks of WD. (a-p). Data represent mean ± SEM. Two-sided *P* values as indicated and compared to *Apoe*^{-/-} or Bl6 control mice analyzed by unpaired Student's *t*-test or Mann Whitney *U* test (b-p).



Extended Data Fig. 8 | See next page for caption.

Extended Data Fig. 8 | *CCL3* and *FOXP3* mRNA expression in human plaques and synopsis of the proposed pathway. (a) mRNA expression of *CCL3* in advanced atherosclerotic plaques (n = 16) or early (n = 13) lesions derived from GSE28829 dataset; (b) mRNA expression of *CCL3* in human atheroma plaque (atheroma) or paired distant macroscopically intact tissue (adjacent) derived from GSE43292 dataset (n = 32 each); (c) *CCL3* mRNA expression in symptomatic (n = 8) or asymptomatic (n = 6) patients with carotid and coronary plaques derived from GSE11138 dataset; (d,e) Quantification of *CCL3* (d) and *FOXP3* (e) mRNA copy numbers normalized to housekeeping mRNA (10^5 GAPDH or β -actin mRNA copies, respectively) in atherosclerotic lesions of carotid atherectomy

specimens from symptomatic (d, e n = 13) or asymptomatic (d, n = 16; e, n = 15) patients using real-time PCR; (a-e) Data represent mean \pm SEM. Two-sided *P* values as indicated versus corresponding controls, as analyzed by unpaired Student's *t*-test (a-c), or Mann Whitney *U* test (d, e); (f) Pathway synopsis (I.) Sterile inflammation triggers the activation of a subset of cDCs, which respond by releasing CCL17. (II.) In turn, CCL17 binds to CCR8 on cDCs (autocrine) and on CD4⁺ T cells (paracrine) to stimulate an upregulation of *CCL3* expression and release. (III.) Subsequently, *CCL3* interacts with CCR1 on naive T cells, thereby blocking the differentiation and expansion of Tregs.

Extended Data Table 1 | Overview of plasma cytokine/chemokine concentrations from *Apoe*^{-/-} or *Apoe*^{-/-} *Ccl17*^{ex/e} mice

Cytokine/ Chemokine	<i>Apoe</i> ^{-/-} pg/ml		<i>Apoe</i> ^{-/-} <i>Ccl17</i> ^{ex/e} pg/ml		P-value
		n=		n=	
IL-1 β	b.t.	6	b.t.	8	-
IL-2	b.t.	6	b.t.	8	-
IL-4	0.03 \pm 0.03	6	0.9 \pm 0.3	8	0.0536
IL-5	5.7 \pm 1.1	6	9.9 \pm 1.6	8	0.0517
IL-6	2.5 \pm 1.2	6	8.2 \pm 2.9	8	0.0999
IL-9	4.1 \pm 1.3	5	3.3 \pm 0.2	7	0.4040
IL-10	b.t.	6	b.t.	8	-
IL-12p70	0.1 \pm 0.1	6	0.3 \pm 0.1	7	0.1930
IL-13	1.9 \pm 0.4	6	2.3 \pm 0.9	8	0.9485
IL-17A	b.t.	6	b.t.	8	-
IL-22	169.1 \pm 94.4	6	37.6 \pm 8.3	8	0.6903
IL-23	17.4 \pm 11.1	6	22.1 \pm 11.6	7	0.4901
IL-27	24.7 \pm 15.5	6	21.7 \pm 3.1	8	0.2284
CCL1#	3.5 \pm 0.6	12	3.0 \pm 0.5	10	0.8212
CCL2	64.9 \pm 13.5	6	50.6 \pm 3.3	8	0.3458
CCL3	6.5 \pm 0.6	11	4.8 \pm 0.4	13	*0.0406
CCL4	2.9 \pm 0.5	6	3.4 \pm 0.3	8	0.3812
CCL5	21.3 \pm 2.0	6	22.6 \pm 2.4	8	1.0000
CCL7	149.7 \pm 33.2	6	124 \pm 14.0	8	0.9497
CCL11	113.1 \pm 71.7	6	307.5 \pm 110.0	8	0.1119
CXCL1	18.8 \pm 3.8	6	29.9 \pm 2.8	7	0.0423
CXCL2	10.4 \pm 1.3	6	12.2 \pm 0.6	8	0.2302
CXCL10	24.8 \pm 1.8	6	26.6 \pm 1.9	8	0.5084
TNF α	1.3 \pm 0.6	6	1.6 \pm 0.4	8	0.6760
GM-CSF	b.t.	6	b.t.	8	-
IFN γ	0.13 \pm 0.2	6	1.3 \pm 0.6	8	0.3124

Shown are cytokine and chemokine concentrations (pg/ml) measured by multiplex bead array in plasma samples from *Apoe*^{-/-} or *Apoe*^{-/-} *Ccl17*^{ex/e} mice after 12 weeks of WD; b.t. = below threshold, *CCL1 was not included in the multiplex bead array and therefore measured by ELISA. Data represent mean \pm SEM; number of mice per test (n) as indicated in the table for each measurement, Two-sided P values as listed and analyzed unpaired Student's t-test or Mann-Whitney U test.

Extended Data Table 2 | Patient characteristics

	Asymptomatic	n	Symptomatic	n
Male-to-female ratio (male/female)	12/4	16	9/4	13
Age (yr)	70.1 ± 8.7	16	69.7 ± 9.2	13
Weight (kg)	74.8 ± 9.4	14	78.7 ± 10.0	10
Height (cm)	168.8 ± 8.2	14	168.6 ± 6.2	10
BMI (kg m ⁻²)	26.3 ± 2.9	14	27.8 ± 3.9	10
Systolic BP (mm Hg)	149.8 ± 13.1	15	148.8 ± 18.7	11
Diastolic BP (mm Hg)	68.7 ± 8.4	15	78.7 ± 8.1	11
Diabetes mellitus	43.8%	16	53.8%	13
Smoking	18.8%	16	15.4%	13
ASA	93.8%	16	92.3%	13
Clopidogrel	6.3%	16	7.7%	13
Beta-blockers	68.8%	16	69.2%	13
Statins	75.0%	16	76.9%	13

Shown are characteristics of asymptomatic and symptomatic patients, from which the atherosclerotic lesions of carotid atherectomy specimens were analyzed. Data represent mean ± SEM; number of participants per parameter (n) as indicated in the table for each measurement, Two-sided P values as listed. BMI: body mass index; BP: blood pressure; ASA: acetylsalicylic acid.

Reporting Summary

Nature Portfolio wishes to improve the reproducibility of the work that we publish. This form provides structure for consistency and transparency in reporting. For further information on Nature Portfolio policies, see our [Editorial Policies](#) and the [Editorial Policy Checklist](#).

Statistics

For all statistical analyses, confirm that the following items are present in the figure legend, table legend, main text, or Methods section.

n/a Confirmed

- The exact sample size (n) for each experimental group/condition, given as a discrete number and unit of measurement
- A statement on whether measurements were taken from distinct samples or whether the same sample was measured repeatedly
- The statistical test(s) used AND whether they are one- or two-sided
Only common tests should be described solely by name; describe more complex techniques in the Methods section.
- A description of all covariates tested
- A description of any assumptions or corrections, such as tests of normality and adjustment for multiple comparisons
- A full description of the statistical parameters including central tendency (e.g. means) or other basic estimates (e.g. regression coefficient) AND variation (e.g. standard deviation) or associated estimates of uncertainty (e.g. confidence intervals)
- For null hypothesis testing, the test statistic (e.g. F , t , r) with confidence intervals, effect sizes, degrees of freedom and P value noted
Give P values as exact values whenever suitable.
- For Bayesian analysis, information on the choice of priors and Markov chain Monte Carlo settings
- For hierarchical and complex designs, identification of the appropriate level for tests and full reporting of outcomes
- Estimates of effect sizes (e.g. Cohen's d , Pearson's r), indicating how they were calculated

Our web collection on [statistics for biologists](#) contains articles on many of the points above.

Software and code

Policy information about [availability of computer code](#)

Data collection

Flow cytometry data were collected using the FACS CANTO II and FACS Aria III together with FACS DIVA software v. 8.0 (BD Biosciences). Histology and Immunofluorescence pictures were collected using Leica DM4000B LED fluorescence microscope and charge-coupled device (CCD) camera. Non-fluorescent and immunofluorescence images were acquired using the Leica Application Suite X (LAS X) software v3.4.2.18368 and v3.5.2.18963. Multiplex-bead-array ELISA experiment data were collected using the software xPONENT v.4.2 (Thermo Fisher Scientific, Luminox). Blood cell and thrombocyte counts were determined using a Celltac Automated Hematology Analyzer (Nihon Kohden). Cholesterol and triglyceride levels were analyzed using mouse EDTA-buffered plasma and quantified using enzymatic assays (c.f.a.s. cobas, Roche Diagnostics). SPR was performed on a Biacore X100 Plus Package Software v. 2.0.2 (Cytiva Europe GmbH). Real time PCR was performed in a QuantStudio 6 Real-Time-PCR system (Thermo Fisher Scientific) and data were collected with the Design & Analysis software v.2.5 (Thermo Fisher Scientific). For scRNAseq, cell suspensions were loaded into a 10x Genomics Chromium Next GEM Chips and encapsulated with Single Cell 3' v3.1 barcoded gel bead using the 10x Genomics Chromium controller. Libraries from individual samples were sequenced on an Illumina NovaSeq 6000 platform. Sequencing depth was set to be around 50,000 reads per cell for pooled lymph nodes from various positions and around 65,000 reads per cell for paraaortic lymph nodes.

Data analysis

GraphPad Prism v.10 (GraphPad Inc.) software was used to test data distribution (e.g., Gaussian) and to perform statistical analysis such as Student's t , Mann-Whitney U , and univariate, nested or factorial ANOVA with post hoc test for pairwise comparisons, as indicated in figure legends and material and methods. For general-linear (including mixed-effect) models and analysis of the main effects or pairwise contrasts we used SPSS v.29.0.1 (IBM Corp). ProcartaPlex Analyst software v1.0 (Thermo Fisher Scientific) was used to analyze Multiplex ELISA experiments. FlowJo software v.10 (Tree Star Inc.) was used to analyze flow cytometry data. Blinded image analysis was performed using Diskus v.4.8 (Hilgers Technisches Büro), Leica Qwin Imaging v. 3 (Leica Lt.), or ImageJ v.1.53 (NIH) software. Fastq files of sorted CD45+CD11c+CD3-CD19- cells from lymph nodes of Ccl17wt/eApoe-/- and Ccl17e/eApoe-/- mice on a chow diet were aligned to the customized reference genome (eGFP were added to mm10 reference) individually using CellRanger Software v.3.0.0 (10x Genomics). The aggregated dataset was

then analyzed using the R package Seurat v 3.1.4. To generate GSVA enrichment score of each eGFP-expressing Ccl17-deficient cell from tolerogenic DCs of Apoe^{-/-} Ccl17e/e mice and each Ccl17-expressing cell from tolerogenic DCs of Apoe^{-/-} Ccl17wt/e mice fed on chow diet, the ontology gene sets v.7.1 were provided in MSigDB (<https://www.gsea-msigdb.org/gsea/msigdb>). The analysis was implemented using the R package gsva v.1.50.

For manuscripts utilizing custom algorithms or software that are central to the research but not yet described in published literature, software must be made available to editors and reviewers. We strongly encourage code deposition in a community repository (e.g. GitHub). See the Nature Portfolio [guidelines for submitting code & software](#) for further information.

Data

Policy information about [availability of data](#)

All manuscripts must include a [data availability statement](#). This statement should provide the following information, where applicable:

- Accession codes, unique identifiers, or web links for publicly available datasets
- A description of any restrictions on data availability
- For clinical datasets or third party data, please ensure that the statement adheres to our [policy](#)

All data associated with this study are present in the main text or the Supplementary Materials. The scRNA-seq data of Ccl17wt/eApoe^{-/-} and Ccl17e/eApoe^{-/-} mice fed on a chow diet or a WD for 6 weeks have been deposited in Gene Expression Omnibus (GEO) and are available at the accession code GSE200862. The following publicly available datasets for human atherosclerosis were included: GSE28829 (advanced atherosclerotic plaques or early lesions), GSE43292 (human atheroma or paired distant macroscopically intact tissue), and GSE11138 (symptomatic or asymptomatic patients with carotid and coronary plaques).

Field-specific reporting

Please select the one below that is the best fit for your research. If you are not sure, read the appropriate sections before making your selection.

Life sciences Behavioural & social sciences Ecological, evolutionary & environmental sciences

For a reference copy of the document with all sections, see [nature.com/documents/nr-reporting-summary-flat.pdf](https://www.nature.com/documents/nr-reporting-summary-flat.pdf)

Life sciences study design

All studies must disclose on these points even when the disclosure is negative.

Sample size	For animal experiments, a priori calculation of power based on a two-sample t test design and previous data or pilot experiments was performed with the software Java Applets for Power and Sample Size (available at: http://www.stat.uiowa.edu/~rlenth/Power) and aimed at 80% statistical power for detecting biological relevant changes (30%) with a two-tailed α -value of 5%. For in vitro experiments, group sample sizes were determined empirically based on pilot experiments.
Data exclusions	The ROUT outlier function was used to exclude statistical outliers (Q=1%). Such exclusion criteria were pre-established. Otherwise, no data were excluded.
Replication	All the experiments were independently repeated at least three times and experimental findings were successfully replicated. Figure legends of each figure/panel indicate the total number (n) of biological replicates/independent individual samples/animals from the independent experiments.
Randomization	The large majority of in vivo experiments on animal models required a specific genetic background, therefore randomization was not possible. Mice were included in experiments as soon as they reached adulthood. Age and sex-matched controls were used to minimize confounding factors. For in vitro experiments, cells were randomly allocated to specific treatments or co-culture experiments. The sequence of the experimental data acquisition was randomly determined.
Blinding	Investigators were blinded to group allocation during data collection and analysis.

Reporting for specific materials, systems and methods

We require information from authors about some types of materials, experimental systems and methods used in many studies. Here, indicate whether each material, system or method listed is relevant to your study. If you are not sure if a list item applies to your research, read the appropriate section before selecting a response.

Materials & experimental systems

n/a	Involved in the study
<input type="checkbox"/>	<input checked="" type="checkbox"/> Antibodies
<input type="checkbox"/>	<input checked="" type="checkbox"/> Eukaryotic cell lines
<input checked="" type="checkbox"/>	<input type="checkbox"/> Palaeontology and archaeology
<input type="checkbox"/>	<input checked="" type="checkbox"/> Animals and other organisms
<input checked="" type="checkbox"/>	<input type="checkbox"/> Human research participants
<input checked="" type="checkbox"/>	<input type="checkbox"/> Clinical data
<input checked="" type="checkbox"/>	<input type="checkbox"/> Dual use research of concern

Methods

n/a	Involved in the study
<input checked="" type="checkbox"/>	<input type="checkbox"/> ChIP-seq
<input type="checkbox"/>	<input checked="" type="checkbox"/> Flow cytometry
<input checked="" type="checkbox"/>	<input type="checkbox"/> MRI-based neuroimaging

Antibodies

Antibodies used

Anti-Mac2 (Cedarline, Cat.No. CL8942AP, Lot No. 1842222A, 2.5ug/ml), Anti-Smooth muscle actin (SMA) FITC (Sigma, Cat.No. F3777, Lot No. 086M4820V, 10ug/ml), Anti-Rabbit IgG Cy3 (Dianova, Cat.No. 711-165-152, Lot.No. 135964, 10ug/ml), Anti-Rat IgG FITC (Sigma-Aldrich, Cat.No. F6258, Lot No. SLBN3827V, 2.5 ug/ml), Anti-CD45 mouse APC-Cy7 (ThermoFisher Scientific, Cat. No. 47-0451-82, Lot.No. 2255516, 0.1 µg/50µl), Anti-CD11b mouse PerCp (ThermoFisher Scientific, Cat. No. 45-0112-82, Lot.No. 2102846, 0.1 µg/50µl), Anti-CD11b mouse Pe-Cy7 (ThermoFisher Scientific, Cat. No. 25-0112-82, Lot.No. 2044736, 0.1 µg/50µl), Anti-Mouse CD115 PE (ThermoFisher Scientific, Cat.No. 12-1152-82, Lot.No. 4333599, 0.1 µg/50µl), Anti-Mouse Gr1 APC (ThermoFisher Scientific, Cat.No. 17-5931-82, Lot.No. 1976250, 0.1 µg/50µl), Anti-Mouse B220 PerCp (ThermoFisher Scientific, Cat.No. 45-0452-82, Lot.No. 1933255, 0.1 µg/50µl), Anti-Mouse B220 PE-Cy7 (ThermoFisher Scientific, Cat.No. 25-0452-82, Lot.No. 4317673, 0.1 µg/50µl), Anti-mouse CD3 FITC (ThermoFisher Scientific, Cat.No. 11-0031-85, Lot.No. 2159105, 0.25 µg/50µl), Anti-mouse CD4 V500 (BD Bioscience, Cat.No. 560782, Lot.No. 135109, 0.1 µg/50µl), Anti-mouse CD8 e450 (ThermoFisher Scientific, Cat.No. 48-0081-82, Lot.No. 2093800, 0.1 µg/50µl), Anti-mouse CD25 APC (ThermoFisher Scientific, Cat.No. 17-0251-82, Lot.No. 4276862, 0.1 µg/50µl), Anti-mouse FoxP3 PE (ThermoFisher Scientific, Cat.No. 12-5773-82, Lot.No. 2144983, 1 µg/50µl), Anti-mouse FoxP3 APC (ThermoFisher Scientific, Cat.No. 17-5773-82, Lot.No. 2152040, 1 µg/50µl), Anti-mouse CD11c PE-Cy7 (ThermoFisher Scientific, Cat.No. 25-0114-82, Lot.No. 2011154, 0.1 µg/50µl), Anti-mouse MHC-II V500 (BD Bioscience, Cat.No. 562366, Lot.No. 9297747, 0.1 µg/50µl), Anti-mouse Tbet PE (ThermoFisher Scientific, Cat.No. 12-5825-82, Lot.No. 4313524, 1 µg/50µl), Anti-mouse CD83 FITC (ThermoFisher Scientific, Cat.No. 11-0831-82, Lot.No. 4348501, 0.25 µg/50µl), Anti-mouse CCR7 Per-Cp (ThermoFisher Scientific, Cat.No. 12-1971-82, Lot.No. 2194303, 0.1 µg/50µl) Anti-mouse CCR7 PE (ThermoFisher Scientific, Cat.No. 12-1972-82, Lot.No. 4290708, 0.1 µg/50µl), Anti-mouse IDO APC (ThermoFisher Scientific, Cat.No. 50-9473-80, Lot.No. 2210927, 0.1 µg/50µl), Anti-mouse CD274 PE (ThermoFisher Scientific, Cat.No. 12-5982-81, Lot.No. 2101993, 0.1 µg/50µl), Anti-mouse CD86 e450 (ThermoFisher Scientific, Cat.No. 48-0862-80, Lot.No. 2185433, 0.1 µg/50µl), Anti-mouse CCR8 PE (Biolegend, Cat.No. 150312, Lot.No. B257398, 0.1 µg/50µl), Rat IgG2b kappa Isotype control PE-Cy7 (Biolegend, Cat.No. 400617, Lot.No. B237979, 0.1 µg/50µl), Rat IgG2b kappa Isotype control PE (Biolegend, Cat.No. 400608, Lot.No. B220932, 0.1 µg/50µl), Rat IgG2b kappa Isotype control APC (Biolegend, Cat.No. 400611, Lot.No. B202122, 0.1 µg/50µl), Rat IgG2b kappa Isotype control e450 (ThermoFisher Scientific, Cat.No. 48-4031-82, Lot.No. E08514-1632, 0.1 µg/50µl), Anti-human CCR4 APC (Biolegend, Cat.No. 359408, Lot.No. B302034, 0.1 µg/50µl), Anti-human CCR8 PE (Biolegend, Cat.No. 360604, Lot.No. B337993, 0.1 µg/50µl), Anti-CD3 mouse uncon. (ThermoFisher Scientific, Cat.No. 16-0032-86, Lot.No. 4328943, 5ug/ml), Anti-mouse CD28 uncon. (ThermoFisher Scientific, Cat.No. 16-0281-86, Lot.No. 1944975, 1ug/ml), Anti-CCR8 uncon. (Biolegend, Cat.No. 150302, Lot.No. B254594, 5ug/ml), Rat IgG2b kappa Isotype control uncon. (Biolegend, Cat.No. 400602, Lot.No. B240744, 5ug/ml), Anti-CCL1 (R&D Systems, Cat.No. AF272, Lot.No. ABA0620011, 2ug/ml), Anti-CCL17 (ThermoFisher Scientific, Cat.No. PA5-116367, Lot.No. WH3357731, 2ug/ml), Anti-CCR4 (ThermoFisher Scientific, Cat.No. PA1-21624, Lot.No. WI3390460F, 8ug/ml), Anti-CCR8 (ThermoFisher Scientific, Cat.No. PA5-23987, Lot.No. WH3357733, 8ug/ml), CCR8 (ThermoFisher Scientific, Cat.No. PA1-21621, Lot.No. WH3348903D, 8ug/ml), Fox P3 (abcam Cat.No. ab253297 Lot.:GR3396881-5 Lot.: GR3396881-9, 1,245 mg/ml); Anti-mouse CD25 (IL-2Ralpha) (Bio-Cell (Biozol) Cat.No. BE0012 Lot: 795321D1, 7.7.28mg/ml);Rat IgG1 isotype control (Bio-Cell (Biozol) Cat.No.BE0088 Lot: 7244921M1, 12.33mg/ml);CCR8: anti-mouse CD198 (Biolegend Cat.No. 150302 Lot: B293708, 0.5mg/ml); T-bet: anti-mouse Tbet (Thermo Fisher Scientific), Cat.No. eBio4B10, Lot: 4313524, 2.5 µg/50µl; GATA3: anti-mouse Gata3 (Thermo Fisher Scientific), Cat.No. 12-9966-42, Lot: 1916093, 0.06 µg/50 µl; RORyt: anti-mouse Roryt (BD), Cat.No. 562607, Lot: 0037076, 1 µg/50 µl; HELIOS: anti-mouse Helios (Thermo Fisher Scientific), Cat.No. 17-9883-42 (clone 22F6), Lot: 2489361, 0.0075 µg/50µl.

Validation

Anti-Mac2 (Cedarline, Cat.No. CL8942AP):
validated for human/mouse and immunofluorescence staining.

Anti-Smooth muscle actin (SMA) FITC (Sigma, Cat.No. F3777):
Validated for human, mouse, rat, chicken, frog, canine, rabbit, guinea pig, goat, bovine, sheep, snake and immunohistochemistry (formalin-fixed, paraffin-embedded sections).

Anti-Rabbit IgG Cy3 (Dianova, Cat.No. 711-165-152):
Validated for rabbit and ELISA, Flow Cytometry, Immunocytochemistry, Immunofluorescence, Immunohistochemistry (frozen sections), Immunohistochemistry (IHC), Immunohistochemistry (Paraffin-embedded Sections).

Anti-Rat IgG FITC (Sigma-Aldrich, Cat.No. F6258):
Validated for rat and immunofluorescence staining.

Anti-CD45 mouse APC-Cy7 (ThermoFisher Scientific, Cat. No. 47-0451-82):
This 30-F11 antibody has been tested by flow cytometric analysis of mouse bone marrow cells. This can be used at less than or equal to 0.125 µg per test. A test is defined as the amount (µg) of antibody that will stain a cell sample in a final volume of 100 µL. Cell number should be determined empirically but can range from 10⁵ to 10⁸ cells/test.

Anti-CD11b mouse PerCp (ThermoFisher Scientific, Cat. No. 45-0112-82):
This M1/70 antibody has been tested by flow cytometric analysis of mouse bone marrow cells. This can be used at less than or equal to 0.25 µg per test. A test is defined as the amount (µg) of antibody that will stain a cell sample in a final volume of 100 µL. Cell number should be determined empirically but can range from 10⁵ to 10⁸ cells/test.

Anti-CD11b mouse Pe-Cy7 (ThermoFisher Scientific, Cat No. 25-0112-82):
This M1/70 antibody has been tested by flow cytometric analysis of mouse splenocytes and bone marrow cells. This can be used at

less than or equal to 0.125 µg per test. A test is defined as the amount (µg) of antibody that will stain a cell sample in a final volume of 100 µL. Cell number should be determined empirically but can range from 10⁵ to 10⁸ cells/test.

Anti-Mouse CD115 PE (ThermoFisher Scientific, Cat.No. 12-1152-82):

The AFS98 antibody has been tested by flow cytometric analysis of peritoneal exudate cells. This can be used at less than or equal to 0.06 µg per test. A test is defined as the amount (µg) of antibody that will stain a cell sample in a final volume of 100 µL. Cell number should be determined empirically but can range from 10⁵ to 10⁸ cells/test.

Anti-Mouse Gr1 APC (ThermoFisher Scientific, Cat.No. 17-5931-82):

The RB6-8C5 antibody has been tested by flow cytometric analysis of mouse bone marrow cells and splenocytes. This can be used at less than or equal to 0.125 µg per test. A test is defined as the amount (µg) of antibody that will stain a cell sample in a final volume of 100 µL. Cell number should be determined empirically but can range from 10⁵ to 10⁸ cells/test.

Anti-Mouse B220 PerCP (ThermoFisher Scientific, Cat.No. 45-0452-82):

This RA3-6B2 antibody has been tested by flow cytometric analysis of mouse splenocytes. This can be used at less than or equal to 0.5 µg per test. A test is defined as the amount (µg) of antibody that will stain a cell sample in a final volume of 100 µL. Cell number should be determined empirically but can range from 10⁵ to 10⁸ cells/test.

Anti-Mouse B220 PE-Cy7 (ThermoFisher Scientific, Cat.No. 25-0452-82):

This RA3-6B2 antibody has been tested by flow cytometric analysis of mouse splenocytes. This can be used at less than or equal to 0.5 µg per test. A test is defined as the amount (µg) of antibody that will stain a cell sample in a final volume of 100 µL. Cell number should be determined empirically but can range from 10⁵ to 10⁸ cells/test.

Anti-Mouse CD3 FITC (ThermoFisher Scientific, Cat.No. 11-0031-85):

The 145-2C11 antibody has been tested by flow cytometric analysis of mouse thymocytes and splenocytes. This can be used at less than or equal to 0.5 µg per test. A test is defined as the amount (µg) of antibody that will stain a cell sample in a final volume of 100 µL. Cell number should be determined empirically but can range from 10⁵ to 10⁸ cells/test. This 145-2C11 antibody has been tested by immunohistochemistry on frozen mouse spleen and can be used at less than or equal to 10 µg/mL.

Anti-Mouse CD4 V500 (BD Bioscience, Cat.No. 560782):

Validated for mouse and flow cytometry.

Anti-Mouse CD8 e450 (ThermoFisher Scientific, Cat.No. 48-0081-82):

This 53-6.7 antibody has been tested by flow cytometric analysis of mouse splenocytes. This can be used at less than or equal to 0.25 µg per test. A test is defined as the amount (µg) of antibody that will stain a cell sample in a final volume of 100 µL. Cell number should be determined empirically but can range from 10⁵ to 10⁸ cells/test.

Anti-Mouse CD25 APC (ThermoFisher Scientific, Cat.No. 17-0251-82):

The PC61.5 antibody has been tested by flow cytometric analysis of mouse splenocytes. This can be used at less than or equal to 0.125 µg per test. A test is defined as the amount (µg) of antibody that will stain a cell sample in a final volume of 100 µL. Cell number should be determined empirically but can range from 10⁵ to 10⁸ cells/test.

Anti-Mouse FoxP3 PE (ThermoFisher Scientific, Cat.No. 12-5773-82):

This FJK-16s antibody has been tested by intracellular flow cytometric analysis of mouse splenocytes using the Foxp3/Transcription Factor Staining Buffer Set (cat. 00-5523) and protocol. This antibody can be used at less than or equal to 1 µg per test. A test is defined as the amount (µg) of antibody that will stain a cell sample in a final volume of 100 µL. Cell number should be determined empirically but can range from 10⁵ to 10⁸ cells/test.

Anti-Mouse FoxP3 APC (ThermoFisher Scientific, Cat.No. 17-5773-82):

This FJK-16s antibody has been tested by intracellular staining and flow cytometric analysis of mouse splenocytes using the Foxp3/Transcription Factor Buffer Set (cat. 00-5523) and protocol. This antibody can be used at less than or equal to 1 µg per test. A test is defined as the amount (µg) of antibody that will stain a cell sample in a final volume of 100 µL. Cell number should be determined empirically but can range from 10⁵ to 10⁸ cells/test.

Anti-Mouse CD11c PE-Cy7 (ThermoFisher Scientific, Cat.No. 25-0114-82):

This N418 antibody has been tested by flow cytometric analysis of mouse splenocytes. This can be used at less than or equal to 0.5 µg per test. A test is defined as the amount (µg) of antibody that will stain a cell sample in a final volume of 100 µL. Cell number should be determined empirically but can range from 10⁵ to 10⁸ cells/test.

Anti-Mouse MHC-II V500 (BD Bioscience, Cat.No. 562366):

Validated for mouse and flow cytometry.

Anti-Mouse Tbet PE (ThermoFisher Scientific, Cat.No. 12-5825-82):

This eBio4B10 antibody has been tested by intracellular staining and flow cytometric analysis of normal human peripheral blood cells using the Foxp3/Transcription Factor Staining Buffer Set (cat. 00-5523) and protocol. Other validated species are mouse and rhesus monkey. This antibody can be used at less than or equal to 0.5 µg per test. A test is defined as the amount (µg) of antibody that will stain a cell sample in a final volume of 100 µL. Cell number should be determined empirically but can range from 10⁵ to 10⁸ cells/test.

Anti-Mouse CD83 FITC (ThermoFisher Scientific, Cat.No. 11-0831-82):

This Michel-17 (Michel17) antibody has been tested by flow cytometric analysis of LPS-activated mouse splenocytes. This can be used at less than or equal to 0.5 µg per test. A test is defined as the amount (µg) of antibody that will stain a cell sample in a final volume of 100 µL. Cell number should be determined empirically but can range from 10⁵ to 10⁸ cells/test.

Anti-Mouse CCR7 PerCP (ThermoFisher Scientific, Cat.No. 45-1971-82):

This 4B12 antibody has been tested by flow cytometric analysis of mouse splenocytes. This can be used at less than or equal to 1 µg per test. A test is defined as the amount (µg) of antibody that will stain a cell sample in a final volume of 100 µL. Cell number should be determined empirically but can range from 10⁵ to 10⁸ cells/test.

Anti-Mouse CCR7 PE (ThermoFisher Scientific, Cat.No. 12-1971-82):

The 4B12 antibody has been tested by flow cytometric analysis of mouse splenocytes and thymocytes. This can be used at less than or equal to 1 µg per test. A test is defined as the amount (µg) of antibody that will stain a cell sample in a final volume of 100 µL. Cell number should be determined empirically but can range from 10⁵ to 10⁸ cells/test.

Anti-Mouse IDO APC (ThermoFisher Scientific, Cat.No. 50-9473-80):

This mIDO-48 antibody has been tested by intracellular staining and flow cytometric analysis of mouse splenocytes using the Intracellular Fixation & Permeabilization Buffer Set (cat. 88-8824) and protocol. This can be used at less than or equal to 1 µg per test. A test is defined as the amount (µg) of antibody that will stain a cell sample in a final volume of 100 µL. Cell number should be determined empirically but can range from 10⁵ to 10⁸ cells/test.

Anti-Mouse CD274 PE (ThermoFisher Scientific, Cat.No. 12-5982-81):

The MIH5 antibody has been tested by flow cytometric analysis of mouse splenocytes. This can be used at less than or equal to 0.06 µg per test. A test is defined as the amount (µg) of antibody that will stain a cell sample in a final volume of 100 µL. Cell number should be determined empirically but can range from 10⁵ to 10⁸ cells/test.

Anti-Mouse CD86 e450 (ThermoFisher Scientific, Cat.No. 48-0862-80):
This GL1 antibody has been tested by flow cytometric analysis of stimulated mouse splenocytes. This can be used at less than or equal to 0.25 µg per test. A test is defined as the amount (µg) of antibody that will stain a cell sample in a final volume of 100 µL. Cell number should be determined empirically but can range from 10⁵ to 10⁸ cells/test.

Anti-Mouse CCR8 PE (Biolegend, Cat.No. 150312):
Validated for mouse and flowcytometry.

Rat IgG2b kappa Isotype control PE-Cy7 (Biolegend, Cat.No. 400617):
Validated for mouse, rat, human and flow cytometry and immunofluorescent staining.

Rat IgG2b kappa Isotype control PE (Biolegend, Cat.No. 400608):
Validated for mouse, rat, human and flow cytometry and immunofluorescent staining.

Rat IgG2b kappa Isotype control APC (Biolegend, Cat.No. 400611):
Validated for mouse, rat, human and flow cytometry and immunofluorescent staining.

Rat IgG2b kappa Isotype control e450 (ThermoFisher Scientific, Cat.No. 48-4031-82):
eFluor® 450 Rat IgG2b Isotype Control has been tested by flow cytometric analysis of mouse splenocytes.

Anti-human CCR4 APC (Biolegend, Cat.No. 359408):
Validated for human and flow cytometry.

Anti-human CCR8 PE (Biolegend, Cat.No. 360604):
Validated for human and flow cytometry.

Anti-CD3 mouse uncon. (ThermoFisher Scientific, Cat.No. 16-0032-86):
The 17A2 antibody has been tested by flow cytometric analysis of mouse thymocytes and splenocytes. This can be used at less than or equal to 0.25 µg per test. A test is defined as the amount (µg) of antibody that will stain a cell sample in a final volume of 100 µL. Cell number should be determined empirically but can range from 10⁵ to 10⁸ cells/test.

Anti-mouse CD28 uncon. (ThermoFisher Scientific, Cat.No. 16-0281-86):
The 37.51 antibody has been tested by flow cytometric analysis of mouse splenocytes. This can be used at less than or equal to 0.5 µg per test. A test is defined as the amount (µg) of antibody that will stain a cell sample in a final volume of 100 µL. Cell number should be determined empirically but can range from 10⁵ to 10⁸ cells/test.

Anti-CCR8 uncon. (Biolegend, Cat.No. 150302):
Validated for mouse and flow cytometry.

Rat IgG2b kappa Isotype control uncon. (Biolegend, Cat.No. 400602):
Validated for mouse, rat, human and flow cytometry and immunofluorescent staining.

Anti-CCL1 (R&D Systems, Cat.No. AF272):
Validated for human and Western blotting and neutralization. Measured by its ability to neutralize CCL1/I 309/TCA 3-induced chemotaxis in the BaF3 mouse pro B cell line transfected with human CCR8. The Neutralization Dose (ND50) is typically 0.4-2.0 µg/mL in the presence of 0.02 µg/mL Recombinant Human CCL1/I 309/TCA 3.

Anti-CCL17 (ThermoFisher Scientific, Cat.No. PA5-116367):
Validated for human and flow cytometry and Western blotting.

Anti-CCR4 (ThermoFisher Scientific, Cat.No. PA1-21624):
Validated for human and flow cytometry, Western blotting, ELISA and immunohistochemistry.

Anti-CCR8 (ThermoFisher Scientific, Cat.No. PA5-23987):
Validated for human and flow cytometry and Western blotting.

CCR8 (ThermoFisher Scientific, Cat.No. PA1-21621):
Validated for human and flow cytometry, Western blotting, ELISA and immunohistochemistry.

Fox P3 (abcam Cat.No. ab253297):
Validated for mouse and human and Western blotting and immunohistochemistry.

Anti-mouse CD25 (IL-2Ralpha) (Bio-Cell (Biozol) Cat.No. BE0012):
Validated for mouse and flow cytometry and in-vivo regulatory T cell depletion.

Rat IgG1 isotype control (Bio-Cell (Biozol) Cat.No.BE0088):
Validated for mouse, rat, human and flow cytometry and immunofluorescent staining.

CCR8: anti-mouse CD198 (Biolegend Cat. No. 150302):
Validated for mouse and flowcytometry.

T-bet: anti-mouse Tbet (Thermo Fisher Scientific), Cat.No. eBio4B10:
Validated for mouse, human, bat and Rhesus monkey and Western blotting, immunohistochemistry and Flow cytometry.

GATA3: anti-mouse Gata3 (Thermo Fisher Scientific), Cat.No. 12-9966-42:
This TWAJ antibody has been pre-titrated and tested by intracellular staining and flow cytometric analysis of mouse thymocytes using the Foxp3/Transcription Factor Staining Buffer Set (cat. 00-5523) and protocol. This can be used at 5 µL (0.06 µg) per test. A test is defined as the amount (µg) of antibody that will stain a cell sample in a final volume of 100 µL. Cell number should be determined empirically but can range from 10⁵ to 10⁸ cells/test.

RORyt: anti-mouse Roryt (BD), Cat.No. 562607:
Validated for mouse and flowcytometry.

HELIOS: anti-mouse Helios (Thermo Fisher Scientific), Cat.No. 17-9883-42:
This 22F6 antibody has been pre-titrated and tested by intracellular staining and flow cytometric analysis of mouse lymph node cells using the using the Foxp3/Transcription Factor Buffer Set (cat. 00-5523) and protocol. This can be used at 5 µL (0.0075 µg) per test. A test is defined as the amount (µg) of antibody that will stain a cell sample in a final volume of 100 µL. Cell number should be determined empirically but can range from 10⁵ to 10⁸ cells/test.

Eukaryotic cell lines

Policy information about [cell lines](#)

Cell line source(s)

HEK-293 (clone CRL-1573™, ATCC) and Flp-In™ T REX™-293 cell line (derived from HEK-293, Invitrogen, now ThermoFisher), Jurkat T cells (clone E6-1, ATCC)

Authentication

The cell lines were authenticated by the supplier, as follow: HEK293 HEK-293 (clone CRL-1573) STR DNA profiling (D3S1358: 15,17; TH01: 7,9,3; D21S11: 28,30,2; D18S51: 17,18; Penta_E: 7,15; D5S818: 8,9; D13S317: 12,14; D7S820: 11,12; D16S539: 9,13; CSF1PO: 11,12; Penta_D: 9,10 Amelogenin: X; vWA: 16,19; D8S1179: 12,14; TPOX: 11; FGA: 23; D19S433: 15,18;

D2S1338: 19) by ATCC; Flp-In™ T REX™-293 were derived from HEK293 and authenticated by STR DNA profiling (Thermo Fisher Scientific) generated stable lines were authenticated by flow cytometry; Jurkat cells (clone E6-1) were authenticated by STR DNA profiling (D3S1358: 15,17 D21S11: 31.2,33.2; D18S51: 13,21; Penta_E: 10,12; Penta_D: 11,13; D5S818: 9; D13S317: 8,12; D7S820: 8,12; D16S539: 11; CSF1PO: 11,12; Amelogenin: x,y; vWA: 18; D8S1179: 13,14; TPOX: 8,10; FGA: 20,21; D19S433: 14,15.2; D2S1338: 19,23; TH01: 6,9.3) by ATCC.

Mycoplasma contamination

Cell line were tested for mycoplasma contamination and found to be negative.

Commonly misidentified lines
(See [ICLAC](#) register)

No commonly misidentified cell lines were used.

Animals and other organisms

Policy information about [studies involving animals](#); [ARRIVE guidelines](#) recommended for reporting animal research

Laboratory animals

Ccr4^{-/-} mice were kindly provided by K. Pfeffer (Heinrich-Heine-Universität, Düsseldorf, Germany) and Ccl17e/e (GFP reporter knock-in) mice were kindly provided by I. Förster (Universität Bonn, Germany). Ccl3^{-/-} mice were purchased from the Jackson Laboratories (Bar Harbor, USA). Ccr1^{-/-} mice and Ccr5^{-/-} mice were kindly provided by P.M. Murphy and W.A. Kuziel, respectively. Ccr4^{-/-}, Ccr1^{-/-}, Ccr5^{-/-}, Ccl17e/e and Ccl3^{-/-} mice were crossed with Apoe^{-/-} mice purchased from the Jackson Laboratories. Ccr8^{flox/flox} mice were generated at Ozgene, backcrossed into a C57Bl/6 background, and crossed with C57Bl/6 Apoe^{-/-} mice in-house. Apoe^{-/-} CreERT2 (ubiquitous inducible Cre expression) and CD4Cre (purchased from Jackson laboratory) bred to Apoe^{-/-} were crossed in-house with Apoe^{-/-} Ccr8^{flox/flox} mice to generate whole body or T cell-specific Ccr8 knock out mice, respectively. All strains were backcrossed for at least 10 generations to the C57Bl/6 background. All of the mice were housed under specific pathogen-free conditions in 12 h/12h light–dark cycles at 21°C and 50% humidity with ad libitum food and water. For diet-induced atherosclerosis experiments, male and female animals aged 8-10 weeks were used and fed a Western type diet for 4 or 12 weeks before sacrifice. For the rescue experiment using CCL3 injections, male and female mice were injected 3x weekly with 20 µg recombinant mouse CCL3 or PBS control by intraperitoneal injection. For depletion of CD25⁺ cells including Tregs, Apoe^{-/-} or Apoe^{-/-}Ccl3^{-/-} male and female mice were fed a WD for 4 weeks and injected twice (every second week) with isotype control or anti-CD25 antibody (each 250 µg antibody per intraperitoneal injection). For the experiment using anti-CCR8 blocking antibody, male and female mice were injected 3x weekly with 5 µg anti-CCR8 antibody or isotype control by intraperitoneal injection. For single-cell RNA sequencing (scRNA-seq), male Ccl17wt/eApoe^{-/-}, and Ccl17e/eApoe^{-/-} mice were fed a normal chow diet or 6 weeks of WD. All experimental mice were sex- and age-matched. All experiments were approved by local authorities and complied with German animal protection law (Regierung von Oberbayern, Germany).

Wild animals

No wild animals were used in this study.

Field-collected samples

No field-collected samples were applied in this study.

Ethics oversight

All mouse experiments were performed according to European guidelines for Care and Use of Laboratory Animals. Protocols were approved by the Committee on the Ethics of Animal Experiments of the Regierung von Oberbayern (ROB-55.2-2532.Vet_02-14-189, ROB-55.2-2532.Vet_02-18-96, ROB-55.2-2532.Vet_02-20-26)

Note that full information on the approval of the study protocol must also be provided in the manuscript.

Flow Cytometry

Plots

Confirm that:

- The axis labels state the marker and fluorochrome used (e.g. CD4-FITC).
- The axis scales are clearly visible. Include numbers along axes only for bottom left plot of group (a 'group' is an analysis of identical markers).
- All plots are contour plots with outliers or pseudocolor plots.
- A numerical value for number of cells or percentage (with statistics) is provided.

Methodology

Sample preparation

Whole blood from the mice was collected in EDTA-buffered tubes. Afterwards, samples were subjected to red-blood-cell lysis for further analysis using flow cytometry. Spleen and lymph nodes (LNs) were mechanically crushed and passed through a 30 µm cell strainer (Cell-Trics, Partec) using Hank's Medium (Hanks' Balanced Salt Solution + 0.3 mmol/l EDTA + 0.1% BSA; Gibco by life technologies) to obtain single cell suspensions. Leukocyte subsets were analyzed using the following combination of surface markers: neutrophils (CD45+CD11b+CD115-Gr1high), classical monocytes (CD45+CD11b+CD115+Gr1high), non-classical monocytes (CD45+CD11b+CD115+Gr1low), B cells (CD45+B220+), T cells (CD45+CD3+). Regulatory T cells (Tregs) were classified as CD45+CD3+CD4+CD25+Foxp3+ (gating strategy used to identify Treg throughout the manuscript is depicted in Extended Figure 1G) and its subpopulation as CD45+CD3+CD4+FoxP3+Tbet+. Foxp3 transcription factors was stained using the Foxp3/Transcription Factor Staining Buffer Set (eBioscience). Cell populations and marker expression were analyzed using a FACSCanto-II, FACSDiva software (BD Biosciences) and the FlowJo analysis program (Tree Star Inc.).

For the isolation of dendritic cells (DCs), LNs were mechanically crushed and passed through a 30 µm cell strainer (Cell-Trics, Partec) using Hank's Medium (Hanks' Balanced Salt Solution + 0.3 mmol/l EDTA + 0.1% BSA; Gibco by life technologies) to obtain single cell suspensions. Conventional DCs are isolated from this suspension by fluorescence-activated cell sorting (BD FACSAria), by gating for CD45+CD11c+MHCI+ cells. Furthermore, eGFP+Ccl17wt/e and eGFP+Ccl17e/e DCs were isolated by

	<p>gating for the endogenous eGFP signal in the FITC channel (pre-gating: CD45+CD11c+MHCII+).</p> <p>For the isolation of T and B cells, spleens were mechanically crushed and passed through a 30 µm cell strainer (Cell-Trics, Partec) using Hank's Medium (Hanks' Balanced Salt Solution + 0.3 mmol/l EDTA + 0.1% BSA; Gibco by life technologies) to obtain single cell suspensions. Cell subsets are isolated by fluorescence-activated cell sorting (BD FACS Aria), by gating for CD45+CD3+ cells (T cells) or CD45+CD19+ cells (B cells).</p>
Instrument	BD FACS Aria, BD FACS CANTO II
Software	Data was collected using FACS Diva and analysed using FlowJo v.10 software (Tree Star Inc.).
Cell population abundance	Purity of sorted cells was >90% as assessed by confirmatory flow cytometry.
Gating strategy	<p>As a general gating strategy, initial forward-scatter (FSC) vs. side-scatter (SSC) gates were adjusted by size for lymphocytes or total leukocytes in the target population analyzed to exclude debris. Doublets were discriminated and dead cells were excluded by Fixable Viability dye before gating for leukocytes. Gating strategies were based on staining controls (e.g., isotype IgGs and fluorescence minus one, FMO) and were consistent between experiments except for small variations needed to fine-tune gating within each experiment and kept consistent within the experiment. The cell subsets were gated by antibody-guided cell type identification as detailed in the Extended materials and methods section. A gating strategy for regulatory T cells is provided in the supplementary information. The gating strategy for T-cell subsets, and particularly Tregs, is presented in Extended Data Figure 1G.</p>

Tick this box to confirm that a figure exemplifying the gating strategy is provided in the Supplementary Information.